International Scientific-Technical and Production Journal

CONTENTS

50 YEARS AT THE HEAD OF THE NATIONAL ACADEMY OF SCIENCES OF UKRAINE

In February there will be 50 years since Boris E. Paton has been elected the President of the Academy of Sciences of the Ukrainian SSR, now the National Academy of Sciences of Ukraine. Boris Paton is an outstanding scientist in the field of welding, metallurgy and technology of metals and materials science, prominent public figure and talented organiser of science, Active Member of the National Academy of Sciences of Ukraine, Russian Academy of Sciences, Professor, honoured scientist and technologist of the Ukr. SSR, Twice the Hero of the Socialist Labour of the USSR, Hero of Ukraine, participant in the Great Patriotic War, and liquidator of accident at the Chernobyl NPP.

Deep understanding of the role of science in society, its goals and tasks, high international authority of a scientist, devotion to science, inexhaustible energy and high moral qualities, social and political activities, and experience of heading a major scientific team were decisive arguments for electing Boris Paton to this post. A new structure and charter of the Academy aimed at a more rational utilisation of the research efforts and means, their concentration on addressing the critical problems of science and impact on development of the economy of Ukraine were worked out under the leadership of B.E. Paton.

Dozens of new institutions and organisations making research in the most important scientific areas wider and deeper were founded within the system of the Academy of Sciences of the Ukr. SSR on the initiative and with the active support of Boris Paton. He persistently seeks clear definition of the research profile of each institute and takes care that each of them becomes a leader in its area in the republic, state and world.

The Academy of Sciences is the main scientific centre, where research is conducted in an extended front on topical problems of natural and technical sciences and humanities. Institutions of the Academy take worthy positions in such areas as mathematics, theoretical physics, solid-state and low-temperature physics, radio physics and radio astronomy, materials science, cybernetics and computer science, neurophysiology, molecular biology, microbiology and virology, genetic engineering and others. The Academy has high-end experimental-production facilities, and it develops new forms of connection between science and industry.

In different years Boris Paton initiated foundation of the academic research centres in a number of regions of the country, e.g. Donetsk, Lvov, Odessa, Kharkov, Dnepropetrovsk and Simferopol, which function as regional interdisciplinary bodies for coordination of research activities.

Close collaboration of the Academy of Sciences of the Ukr. SSR with the Academy of Sciences of the USSR, State Committee for Science and Technology and academies of sciences of the union republics promoted development of many new research areas in the Ukr. SSR, foundation of new institutions and engineering centres, and strengthening of the international authority of our Academy of Sciences.

Boris Paton initiated formation of major integrated scientific and technical programs in the interests of individual industries, transport, communication and agriculture. Scientists of the Academy made considerable contribution to development of the economy of the country. This form of organisation of the research activity was generally recognised.

Policy speech of B.E. Paton at elections of the President of the Academy of Sciences of the Ukrainian SSR, Kiev, February 1962

Boris Paton was the organiser of a number of scientific councils. In 1966, he was at the head of the USSR Scientific Council on problem «New Welding Processes and Welded Structures». The Council united the USSR scientists and specialists, and was functioning effectively from 1958 till 1991.

In 1972, the International Scientific-and-Technical Council of the COMECON Member-Countries on welding problems was set up by the initiative of Boris Paton. Owing to the activity of the Council, which was successfully functioning till 1992, many scientific and engineering organisations of the COMECON Member-Countries grew to the state-of-the-art research level, and had a great influence on progress of welding in their countries.

B.E. Paton organised the Scientific Council at the Presidium of the Academy of Sciences of the USSR on problem «New Processes of Manufacturing and Treatment of Metallic Materials», which united scientists of academic institutions and specialists of many other departments, and promoted development of materials science in the Academy of Sciences of the USSR, Russian Academy of Sciences and National Academy of Sciences of Ukraine. Many materials scientists and metallurgists, who were active at the Council, were elected into the Academy of Sciences of the USSR and Russian Academy of Sciences with the support of Boris Paton, and made great contribution to development of the materials studies.

Boris Paton has the fundamental understanding of the role and place of science in addressing humanitarian problems of the society. While placing high emphasis on development and commercial application of advanced technologies, he, at the same time, seeks substantiated scientific estimates of their effect on the environment and humans. Led by Boris Paton, big teams of scientists of the Academy made pre-

B.E. Paton with pilot-cosmonaut A.A. Leonov in the orbital station training facility at the Yu.A. Gagarin Cosmonaut Training Centre, Zvyozdny Gorodok, Moscow Region, 1973

dictive estimates of the negative ecological and social-economic consequences of large-scale drainage and irrigation meliorations in Ukraine, intensive chemisation of agriculture, and diversion of part of the runoff of the Danube and Dnieper Rivers.

Boris Paton adhered to his principles also in the issue of construction of a nuclear power plant in the Chernobyl region. Unfortunately, his warnings were fully confirmed by the universally known events of 1986 at the ChNPP. Outstanding capabilities of Boris Paton as a leader, scientist and organiser were fully revealed during the memorable days of the Chernobyl tragedy. Teams of many institutes of the Academy of Sciences of the Ukr. SSR and its Presidium became involved in the activities on liquidation

Delegation from the E.O. Paton Electric Welding Institute at the «Azovstal» Works, Mariupol, 1982

Reception of Helmut Kohl, Chancellor of West Germany, at the E.O. Paton Electric Welding Institute, Kiev, June 1983

of consequences of the accident from its very first days. Hundreds of scientists, specialists of the Academy of Sciences, ministries, departments, and enterprises of Ukraine took part in this work. Boris Paton led the efforts on preparation of proposals for decision-making authorities of Ukraine and the USSR Government Commission. Later on, in September 1997, B.E. Paton headed the Advisory Board of Independent Experts on finding comprehensive solutions to the problems of the Chernobyl Nuclear Power Plant, newly established by the President of Ukraine.

After disintegration of the Soviet Union and formation of the independent Ukraine, under conditions of long-term economic and financial crisis, which did not spare the Academy, its President managed to preserve the Academy and its major scientific schools. The status of the Academy as a supreme governmental research organisation was secured at the legislative level, principles of its academic self-administration were preserved, its restructuring was accomplished in keeping with the new conditions, and

fundamental and applied studies were focused on addressing the urgent problems of formation of the state. New priorities were identified in the field of natural, engineering, social sciences and humanities. A number of new institutes and centres of socio-humanitarian profile were established.

The world level of research was preserved in several areas of mathematics, informatics, mechanics, physics and astronomy, materials science, chemistry, molecular and cell biology, and physiology. The contribution of scientists of the Academy to fundamental and applied research in Ukraine is increasing. New technologies, materials and computer facilities have been developed, and new mineral deposits have been discovered, etc.

The Institute for Economy and Forecasting, Institute for Economic and Legal Research, Institute for Market Problems and Economic-and-Ecological Research, Institute of Regional Research, Institute for Demography and Social Studies, Institutes of Ukrainian Studies, Oriental Studies, Political and Ethnic Studies, Sociology, Ukrainian Archaeography and Source Studies, Ukrainian Language, as well as other departments, institutions and centres have been established and are successfully functioning.

The Institutes of the Academy take an active part in working out of the innovative programs on economic development of Ukraine, investigation of its history, culture and language.

Organisation of fundamental and applied research is being improved, and priorities are being determined in development of individual scientific areas and interdisciplinary studies. Among them are such programs as «Nanosystems, Nanomaterials and Technologies», «Sensing Systems», «Intelligent Information Technologies», «Hydrogen Power Generation», «Power Saving», «Problems of Demography and Development of Mankind», etc.

Boris Paton is continuously concerned about young scientists, attracting talented young people into science, supporting them financially, and trying to improve their living standards. Youth scientific projects are being funded, and dormitories for post-graduates are being built and reconstructed.

B.E. Paton makes a lot of efforts for preservation and development of international scientific cooperation and foreign economic contacts with business partners from foreign countries. Ukrainian scientists participate in many collaborative programs. Project competitions have

At the NASA Research Centre, USA, May 1996

been conducted together with the Science and Technology Centre in Ukraine, Russian Foundation for Fundamental Research, Russian Humanitarian Sciences Foundation and Siberian Division of the Russian Academy of Sciences.

B.E. Paton is one of the initiators of formation and preservation of common scientific space within the Commonwealth of the Independent States. In 1993, the International Association of the Academies of Sciences (IAAS) was established, which united national academies of 15 countries of Europe and Asia. Boris Paton is the permanent President of this Association. The Scientific Council of IAAS on Advanced Materials is functioning under his direction.

Academician Boris Paton is an Honorary President of the International Engineering Academy, member of the Academia Europaea, Honorary Member of the Roman Club, International Academy of Technological Sciences, Honorary Member of the International Academy of Sciences, Education and Arts, International Aeronautical Academy, Foreign Member of the academies and scientific-and-technical societies of many countries. B.E. Paton performed and continues performing extensive public work. He was many times elected a Deputy of the Supreme Soviet of the USSR and Ukr. SSR, Deputy Chairman of the USSR Supreme Soviet, member of the Presidium of the Supreme Soviet of the Ukr. SSR, member of the Central Committees of the Communist Party of the Soviet Union and Communist Party of Ukraine. He was the head and a member of various high committees and commissions. The list of his positions is very impressive. He is successfully working in these positions owing to the deep sense of personal responsibility to the state, people and his own conscience.

In addition, he has such traits as outstanding organisation, efficiency, rare ability of precisely grasping the point, and immediately making the right decision. This heavy load is made easier to bear due to his good physical shape, which he has preserved up to now owing to his active life style and regular sports activities.

For his great services to the science and the state, B.E. Paton was awarded the high titles of the Twice the Hero of Socialist Labour of the USSR and Hero of Ukraine. He is the knight of four Orders of Lenin, Orders of October Revolution, Labour Red Banner, Friendship of Nations, orders of the State, Prince Yaroslav the

Meeting of the Council of the International Association of the Academies of Sciences, Dubna, 21 June 2000

Wise of the 1st, 4th and 5th Degrees, Orders of Freedom, Order «For the Services to Motherland» of the 1st and 2nd Degrees, «Order of Honour» (Russian Federation), Order of Frantsisk Skorina (Republic of Belarus), Order of Honour (Georgia), Order «Dostyk» (Republic of Kazakhstan), and many other awards of the CIS countries. B.E. Paton is a laureate of the Lenin and State Prizes of the USSR and Ukraine in the field of science and technology. He was awarded the M.V. Lomonosov, S.I. Vavilov and S.P. Korolyov Gold Medals, A. Einstein Silver Medal, and many other prizes and decorations.

Boris Paton is utterly devoted to the science, Institute, Academy and Motherland.

His worldly wisdom, tremendous experience and international authority in science and society allowed preserving the scientific potential of Ukraine.

Boris Paton is a leader, fighter, creative personality, deeply decent and kind man, possessing fantastic energy and capacity for work, enormous experience, deep knowledge in many areas, and ability to continually learn. He has a generous nature and quick analytical mind. He is democratic, well-wishing, open for communication, affable, and always ready to support a person in need and help him.

Boris Paton is full of creative ideas, indomitable wish to work and enhance the contribution of science to prosperity of our state — the independent Ukraine. Let us wish him new successes, good health and much happiness with all our hearts.

I.K. Pokhodnya
Academician of the NAS of Ukraine

The Paton WELDING JOURNAL

WELDED STRUCTURES FROM AUSTENITIC STEEL OF 10Kh18N10T TYPE UNDER CONDITIONS OF RADIATION-INDUCED SWELLING

V.I. MAKHNENKO, O.V. MAKHNENKO, S.S. KOZLITINA and **L.I. DZYUBAK**
E.O. Paton Electric Welding Institute, NASU, Kiev, Ukraine

Mathematical modeling of deformation processes in different structural elements from steel 10Kh18N10T under radiation-induced swelling conditions showed peculiarities of their behaviour, allowing for residual welding stresses depending on the radiation dose, temperature and external load.

Austenitic steels of 10Kh18N10T type are characterized by high levels of corrosion crack resistance, cold resistance, are readily weldable, and have high ductile properties, that promotes their wide application in critical structures, also in the field of nuclear engineering, where this steel is the main material of the so-called reactor internals (RI) operating at high radiation exposure doses. Such steels have high physico-mechanical properties, stable structure right up to temperatures of about 800 °C.

The above-mentioned stabilization is not absolutely invulnerable. In particular, long-term heating of austenitic steel in the temperature range of approximately 500–900 °C promotes the so-called $\gamma \rightarrow \alpha$ (austenitic-ferritic) transformation with concurrent formation of carbides, intermetallics, etc., leading to a quite abrupt change of steel properties, particularly in aggressive media, and to brittle fracture susceptibility. Temperature conditions of welding heating can to a certain extent cause sensibilization (increased susceptibility) of austenitic steel to corrosion and brittle fractures [1]. A similar factor lowering stability of austenitic microstructure is irradiation of structural elements from austenitic steel that is extremely typical for RI of modern nuclear reactors [2, 3].

In terms of engineering of RI elements, irradiation changes the mechanical and physical properties of materials of RI elements and hence the hazard of violation of integrity of these elements operating under extreme conditions, that determines the safety of operation of nuclear engineering facilities in many countries, including Ukraine. At present sufficiently reliable data are available as regards the change of mechanical properties of austenitic steels at irradiation. Long-term exposure of these steels involves the physical phenomenon of austenitic steel swelling (an irreversible process of volume increase) that may lead to an essential change of stressed state in structural elements with the respective consequences. It should be kept in mind that the swelling process largely depends not only on the radiation exposure, but also on temperature of material irradiation and non-linearity of stresses and plastic strains associated with material swelling.

Proceeding from experimental studies [4–8] of the respective samples from austenitic steel, it was established that the relative change of volume V at radiation exposure can be presented as

$$S = \frac{\Delta V}{V} = C_D D^n f_1(T) f_2(\sigma) f_3(\omega_p), \quad (1)$$

where $C_D = 1.035 \cdot 10^{-4}$ dpa$^{-1.88}$ (dpa dimension — displacement per atom); D is the dose of irradiation with not more than 0.5 MeV energy; $n = 1.88$ according to [3]; $f_1(T)$ is the correction for material temperature T; $f_2(\sigma)$ is the correction related to the volume invariant of stress tensor. The following dependence is used at irradiation [9]:

$$f_1(T) = \exp\left[-(T - T_{\max})^2 r\right], \quad (2)$$

where $T_{\max}$ is the peak irradiation temperature equal to about 470 °C [6]; $r = 1.1 \cdot 10^{-4}$ °C^{-2} [9] is the experimental constant;

$$\sigma = \frac{\sigma_{xx} + \sigma_{yy} + \sigma_{zz}}{3};$$

$\sigma_{xx}, \sigma_{yy}, \sigma_{zz}$ are the normal components of stress tensor of irradiated material;

$$f_2(\sigma) = 1 + p\sigma \text{ at } 1 + p\sigma \geq 0,$$
$$f_2(\sigma) = 0 \text{ at } 1 + p\sigma < 0; \quad (3)$$

p is the experimental quantity having the value of approximately $4 \cdot 10^{-3}$ 1/MPa^3; $f_3(\omega_p)$ is the correction for the level of plastic strains related to tensor invariant ε_{ij}^p by Odqvist strain hardening parameter

$$\omega_p = \int_0^D d\varepsilon_i^p, \quad (4)$$

where

$$d\varepsilon_i^p = \frac{\sqrt{2}}{3}\sqrt{d\varepsilon_{ij}^p d\varepsilon_{ij}^p} \quad (i, j = x, y, z)$$

is the intensity of plastic strain increment.

The dependence

$$f_3(\omega_p) = \exp(-\eta\omega_p) \qquad (5)$$

is used, where $\eta = 8.75$ for the considered steels [3].

From dependencies (1)–(5) it is seen that swelling level S rather strongly depends on damaging dose of radiation with more than 0.5 MeV energy, on absolute value of temperature difference $|T - T_{\max}|$ of irradiated material, value and sign of spherical stress tensor

$$\delta_{ij}\sigma = \begin{vmatrix} \sigma & 0 & 0 \\ 0 & \sigma & 0 \\ 0 & 0 & \sigma \end{vmatrix},$$

and plastic strain accumulation parameter ω_p.

In terms of ensuring the integrity of RI elements it is important to determine how the swelling process, related to accumulation of dose D in operation, interacts with initial temperature stresses at reactor commissioning or with residual technological (for instance, welding) stresses. It is obvious that at uniform swelling $S(x, y, z) = $ const of a specific RI element, similar to uniform heating $T(x, y, z) = $ const, no stresses develop (except for reactive stresses, related to element fastening).

In [7, 8] it is shown that the process of material swelling is accompanied by lowering of the initial stressed state, as at respective temperature annealing, when reversible elastic strains go to irreversible strains of diffusion ductility through the mechanism of material creep. The term of «radiation creep» [7–9] is associated with this phenomenon. It should be noted that irradiation of a solid does not change the main regularities of deformations of continuum mechanics in terms of the phenomenological approach, except for mechanical properties of the deformed solid, determining the kind of deformation, namely elastic, instant plasticity, diffusion plasticity (creep). In this connection (as long as there are no additional kinds of deformation in the mechanics of solid deformation), the relationships of strains and stresses change qualitatively and quantitatively, their parameters being determined experimentally on the respective samples, depending on the specific conditions and material.

Considering a rather high interest to application of calculated predictions of RI element performance in modern nuclear reactors of WWER-1000 type and certain doubts as to the reality of the mechanisms of «radiation creep» for austenitic steel at temperatures below 450–470 °C after irradiation, significantly increasing the steel yield point, stricter treatment of models of steel deformation at irradiation and swelling

in terms of classical approaches tried out in practice, appears to be important.

Let us write the strain tensor ε_{ij} $(i, j = x, y, z)$ as the sum

$$\varepsilon_{ij} = \varepsilon_{ij}^e + \varepsilon_{ij}^p + \varepsilon_{ij}^c + \delta_{ij}\frac{S}{3}, \qquad (6)$$

where indices e, p, c pertain to elastic strain, instantaneous plasticity and creep.

In the general case for austenitic steels, when the volume of phase changes is small, elastic strain is reversible by definition, i.e. disappearing, if its cause is eliminated, and it is presented in the following form, according to Hooke's law [9]:

$$\varepsilon_{ij}^e = \frac{\sigma_{il} - \delta_{il}\sigma}{2G} + \delta_{il}[k\sigma + \alpha(T - T_0)] \quad (i, j = x, y, z),$$

where $G = E/(2(1 + \nu))$; ν is the Poisson's ratio; E is the modulus of normal elasticity; k is the coefficient of volume compression equal to $(1 - 2\nu)/E$; α is the coefficient of relative thermal expansion in temperature range $T(x, y, z)$ and T_0 (x, y, z, t_0).

For tensor of instantaneous plasticity strains ε_{ij}^p in modern commercial software the plastic flow law is usually used, which is associated with Mises yield condition [10], i.e.

$$d\varepsilon_{ij}^p = d\lambda(\sigma_{ij} - \delta_{ij}\sigma) \quad (i, j = x, y, z), \qquad (7)$$

where $d\lambda$ is the scalar function of x, y, z coordinates and time t, connecting increment of tensor ε_{ij}^p with stress deviator $(\sigma_{ij} - \delta_{ij}\sigma)$ by yield condition of the following form:

$$d\lambda = 0, \text{ if } f = \sigma_{eq}^2 - \sigma_y^2(\omega) < 0 \text{ or } f = 0, \text{ but } df < 0;$$
$$d\lambda > 0, \text{ if } f = 0 \text{ and } df \geq 0 \qquad (8)$$
$$(f > 0 \text{ state is inadmissible}),$$

where σ_{eq} is the equivalent stress or stress intensity

$$\sigma_{eq}^2 = \frac{1}{2}(\sigma_{ij} - \delta_{ij}\sigma)(\sigma_{ij} - \delta_{ij}\sigma); \qquad (9)$$

$\sigma_y(\omega)$ is the material yield point at temperature T, radiation dose D and degree of strain hardening ω_p according to formulas (4) and (5).

For tensor of strains of diffusion plasticity or creep ε_{ij}^c the plastic flow law [10] is usually used in the following form:

$$d\varepsilon_{ij}^c = \Omega dt(\sigma_{ij} - \delta_{ij}\sigma) \quad (i, j = x, y, z), \qquad (10)$$

where Ω is the creep scalar function which is determined by value σ_{eq}^m $(m = 4-6)$ for material at a given temperature and extent of irradiation, i.e.

$$\Omega(\sigma_{eq}, T, D) = \Omega_q(T, D)\sigma_{eq}^m. \qquad (11)$$

In the works by the supporters of «radiation creep» approach the following relationship is used:
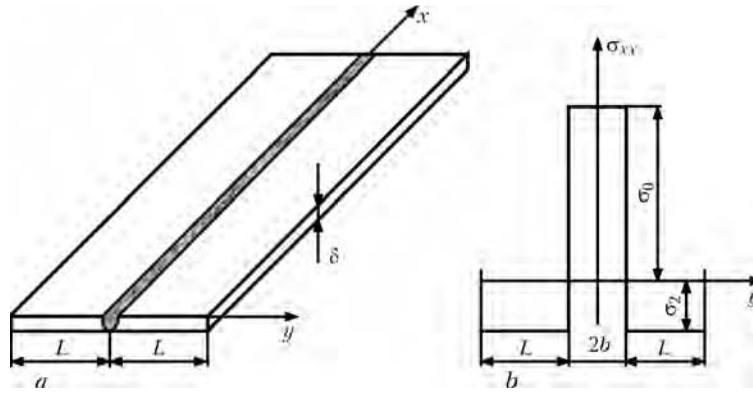
Figure 1. Schematic of austenitic steel strip with a weld (*a*), and distribution of residual stresses σ_{xx} (*b*)

$$\xi_{eq}^c - \left(B_0 \frac{dD}{dt} + \omega_0 \frac{dS_0}{dt}\right)\sigma_{eq}, \qquad (12)$$

where ξ_{eq}^c is the rate of change of equivalent creep strain according to [9], i.e.

$$\xi_{eq}^c = \frac{\sqrt{2}}{3}\sqrt{\frac{d\varepsilon_{ij}^c}{dt}\frac{d\varepsilon_{ij}^c}{dt}}; \qquad (13)$$

B_0, ω_0 are the material characteristics, little dependent on temperature [9]; $S_0 = S$ according to formula (1) at $f_2(\sigma) = 1$ and $f_3(\omega_p) = 1$.

From comparison of expressions (10) and (12) under conditions (9), (13) it follows that identity of equations (10) and (12) is in place at

$$\Omega = \frac{2}{3}\frac{\xi_{eq}^c}{\sigma_{eq}} = \frac{2}{3}\left(B_0 \frac{dD}{dt} + \omega_0 \frac{\partial S_0}{dt}\right) \qquad (14)$$

or taking into account formula (11), provided B_0 and ω_0 are proportional to σ_{eq}^m. In [9], however, it is recommended that $B_0 = 1 \cdot 10^{-6}$ (MPa·dpa)$^{-1}$, $\omega_0 = 6 \cdot 10^{-3}$ MPa^{-1}, i.e. are constant.

Thus, the process of «radiation creep» is based on significant linearization of the connection between

Figure 2. Kinetics of residual stress variation in the strip at $L = 20$ cm, $b = 1$ cm, $Q_x = 0$; $\sigma_0 = 300$ MPa; $\sigma_2 = -300\ b/(L - b)$ (*a*), and change in swelling in zone $y = 0$ (*b*)

strains and stresses that may be acceptable for a narrow range of stress variation, or when direct experiments on determination of creep function of irradiated material confirm that m value in expression (11) is close to zero.

In this connection, it appears to be logical to apply a more conservative approach based on the assumption that at temperatures of RI element irradiation $T \le T_{\max} = 470$ °C austenitic material is characterized by a high creep resistance, i.e. in formula (10) creep function is equal to zero. The conservatism of this approach consists in higher risk of appearance of stresses close in their value to material yield point, considering the radiation and strain hardening [9].

The process of austenitic steel swelling is accompanied to a certain extent by relaxation of already formed stresses. It can be shown that instantaneous plasticity can well be the relaxation mechanism. The above phenomenon is readily modelled on such a simple example, as austenitic steel plate with a weld (Figure 1). Longitudinal residual stresses σ_{xx} are approximately described by the relationships

$$0 < |y| \le b, \quad \sigma_{xx} = \sigma_0, \quad b < |y| < L, \quad \sigma_{xx} = -\frac{\sigma_0 b}{L - b}.$$

Plate temperature is constant and equal to 470 °C. Edges $y = \pm L$ are free, edge $x = 0$ is restrained, i.e. displacement $U_x(0, y) = 0$; edge $x = L_{x_L}$ is loaded by distributed forces q_x so that $\delta\int_0^L q_x dy = 2Q_x$, where δ is the plate thickness. Let us assume that $Q_x = q_x 2\delta$. Yield point of plate material, depending on strain hardening ω_p and radiation hardening, changes by a dependence given in [6]:

$$\sigma_y = 202 + 239\varepsilon\xi\pi\left[-2.22 \cdot 10^{-3}(T + 273\ °C)\right] + 400\left[1 - \exp\left(-0.47D/D_0\right)\right]^{0.5},$$

where $D_0 = 10/2.22$ dpa.

Figures 2–4 give the results of swelling distribution across the welded joint at $b = 1$ cm, $L = 20$ cm and different Q_x values, as well as the respective changes of stresses in zones $0 < |y| < b$ and $b < |y| < L$, depending on plate radiation dose and different
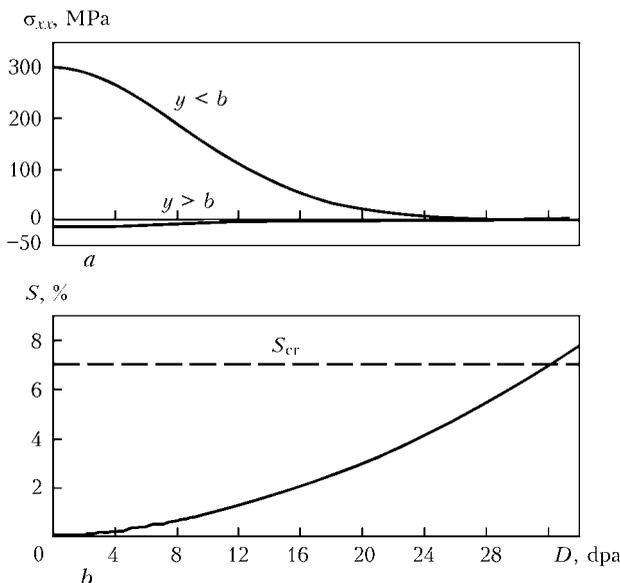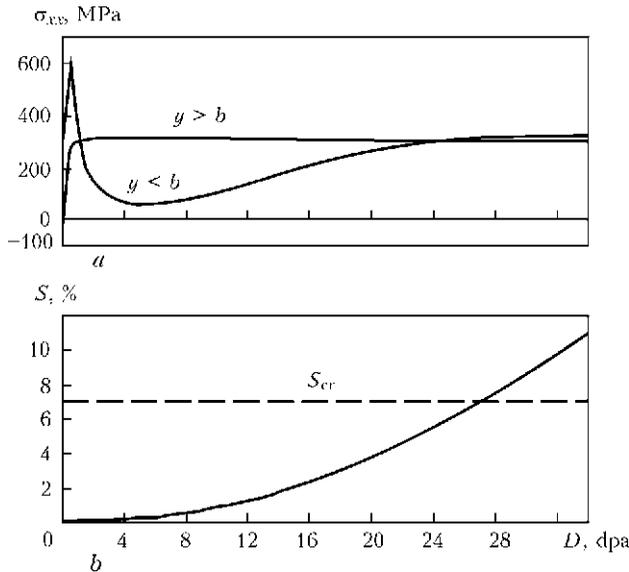
Figure 3. Kinetics of the change of residual stresses in the strip at $L = 20$ cm, $b = 1$ cm, $Q_x = 300L\delta H$; $\delta = 1$ cm; $\sigma_0 = 300$ MPa; $\sigma_2 = -300\,b/(L-b)$ (*a*), and change in swelling in zone $y = 0$ (*b*)
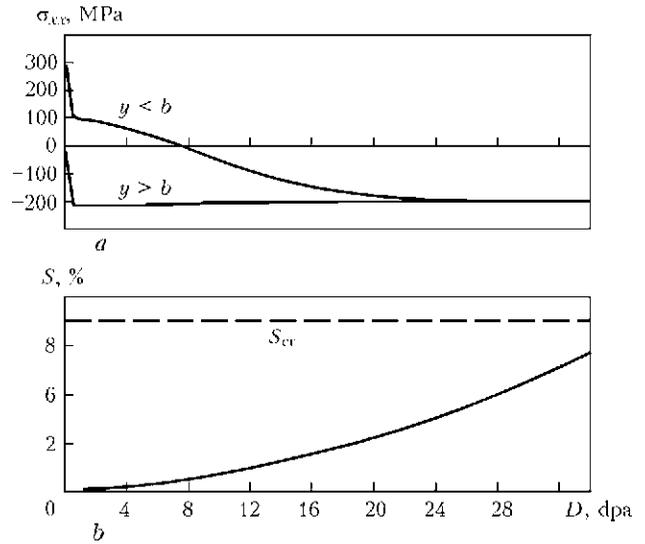
Figure 4. Kinetics of the change of residual stresses in the strip at $L = 20$ cm, $b = 1$ cm, $Q_x = -200L\delta H$; $\delta = 1$ cm; $\sigma_0 = 300$ MPa; $\sigma_2 = -300\,b/(L-b)$ (*a*), and change in swelling in zone $y = 0$ (*b*)

Q_x values. It is seen that for an unrestrained plate at $Q_x = 0$ and radiation dose of more than 14 dpa the initial residual stresses are completely relaxed (forgotten). The same is noted also at $Q_x > 0$ (Figure 3). In case of a compressive external load (Figure 4) deceleration of this process occurs at the expense of correction $f_2(\sigma)$, which nonetheless proceeds owing to plastic flow by the mechanism of instantaneous plasticity without «radiation creep».

Note that the critical level of swelling, corresponding to 7 % [9], is achieved at favourable tension (see Figure 3) approximately during 35 years of operation of reflection shield elements, and at unfavourable compression (see Figure 4) — during a period of not less than 60 years (within the reflection shield of WWER-1000 reactor the average radiation dose after 30 years corresponds to 20 dpa).

Let us consider a more complex example of RI element of WWER-1000 reactor, when considerable gradients of radiation dose and respective gradients of swelling level are preserved in the element body for a long time (Figure 5). It should be noted that the data in Figure 5, *a* can to a certain extent be postulated for the shaft wall in the core. Shaft wall thickness is 60 mm, average exposure dose (point $z = 30$ mm) by the data of [11] is equal to about 0.20 dpa per year. On the shaft inner surface $z = 0$, this value is close to average irradiance of the reflection shield, i.e. $D = 1.5$ dpa per year, and in point $z = 60$ mm radiation dose is equal to approximately 0.03 dpa after 30 years, i.e. approximately 0.001 dpa per year [11].

Here, the initial stressed state, connected with reaching the thermal conditions at reactor commissioning, was not taken into account. It was assumed that $T = 470$ °C ($z = 0$), $T = 300$ °C ($z = 60$ mm). As the temperature fields, determining this stressed state, become stationary after several days, temperature

stresses related to them are also stationary of the type of initial (residual) ones, considered in Figures 2–4. Their interaction with swelling at developed plastic flow (high radiation dose) leads to the respective relaxation.

At reactor cooling (temperature homogenizing) new fields of residual stresses are formed, which are largely compensated at subsequent heating of the reactor. For postulated irradiation field (see Figure 5, *a*) dependence (1) was used to calculate the fields of volume strain of swelling. Their connection to the stressed state and accumulated plastic strain (corrections $f_2(\sigma)$ and $f_3(w_p)$) was taken into account. For this purpose an approach was used, which is based on successive tracing (depending on the field of radiation dose $D(x, y, z)$) of evolution of the field of swelling $S(x, y, z)$ (see Figure 5, *b*), displacements $U_j(x, y, z)$, strains $\varepsilon_{ij}(x, y, z)$ and stresses $\sigma_{ij}(x, y, z)$.
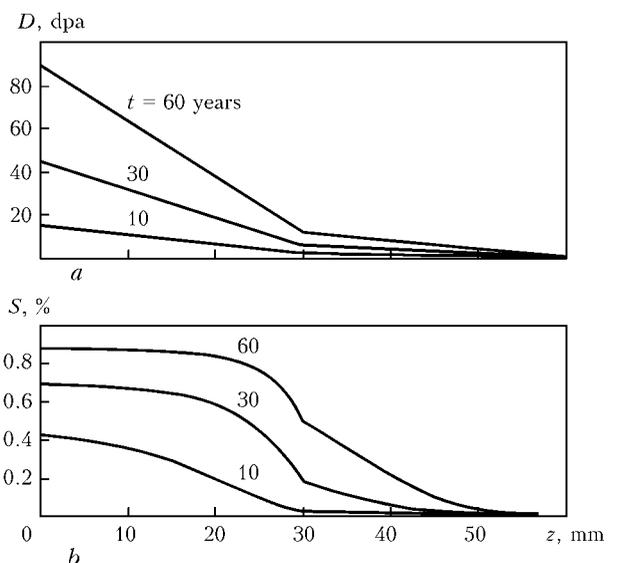
Figure 5. Distribution of radiation dose D (*a*) and swelling S (*b*) across wall thickness in different moments of time t

σ, MPa
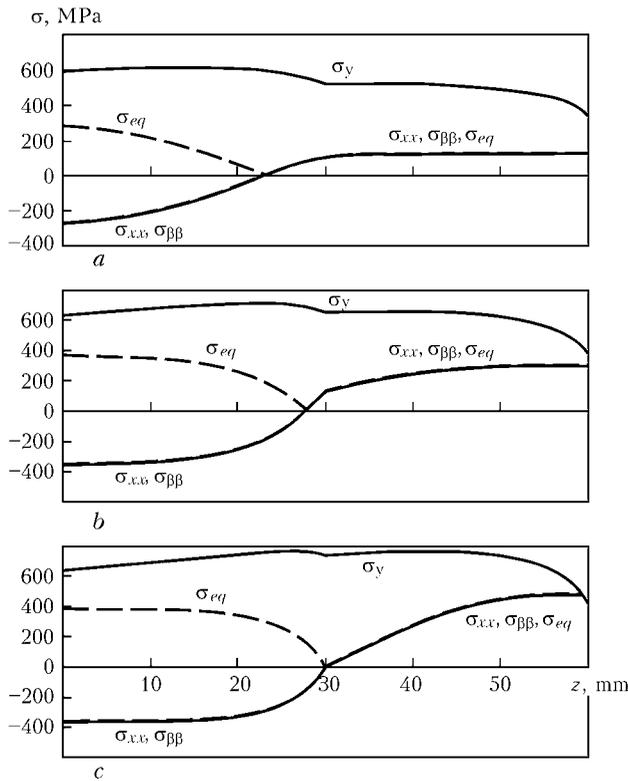
Figure 6. Distribution of stresses σ_{xx} (axial), $\sigma_{\beta\beta}$ (tangential), σ_{eq} (equivalent), yield point σ_y across wall thickness at $t = 10$ (a), 30 (b) and 60 (c) years

It follows from the data in Figures 5, 6 that the zone of the most intensive irradiation (see Figure 5, b) adjacent to the shaft inner surface is in the compressed state by x and β, that, however, leads to a rather significant swelling (on the level of 0.3 %). Value of σ is small. Zone $30 < z < 60$ mm has a relatively low radiation dose and small swelling, respectively, that determines the respective distribution of stresses σ_{xx} and $\sigma_{\beta\beta}$. Nature of plastic strain development across the wall thickness related to swelling kinetics is quite specific. In fact, mainly elastic deformation occurs during 60 years. Plastic flow after 60 years arises in zone $x \approx 60$ mm, because of the low level of σ_y (small radiation dose).

CONCLUSIONS

1. Calculation methods, based on modern models of nonisothermal elastoplastic deformation of material, allow prediction of the stress-strain state of RI welded elements in nuclear power reactors of WWER-1000 type under the conditions of intensive irradiation, taking into account the process of material swelling.

2. Specific examples were used to show the possibility of predictive estimation of the residual safe operating life for individual RI elements based on the conditions of local critical swelling of material.

An implicit schematic of allowing for swelling from average normal stress σ was used. For this purpose dependence (6) was presented in the following form:

$$\varepsilon_{ij} = \varepsilon_{ij}^e + \varepsilon_{ij}^p + \frac{S_0}{3}(1 + p\sigma)\delta_{ij} = \overline{\varepsilon}_{ij}^e + \varepsilon_{ij}^p + \delta_{ij}\frac{S_0}{3}p, \quad (15)$$

where

$$\overline{\varepsilon}_{ij}^e = +\varepsilon_{ij}^e + \frac{S_0}{3}p\sigma\delta_{ij} =$$

$$= \frac{\delta_{ij} - \delta_{ij}\sigma}{2g} + \delta_{ij}\left[\left(K + \frac{S_0}{3}p\right)\sigma + \alpha(T - T_0)\right](i, j = x, y, z),$$

which is equivalent to expression (15), if $\left(K + \frac{S_0}{3}p\right)\overline{K}$ is used instead of K, that eliminates the need for S iterations.

Respective elastoplastic problems in each tracing step were solved in terms of ideology of «Weldpredictions» software package developed at the E.O. Paton Electric Welding Institute of NASU, i.e. with involvement of elastoplastic flow theory of Plandtl–Reuss, associated with Mises yield condition, i.e. with application of relationships (5)–(8), (14) and finite element method. Figure 6 gives fragments of the above tracing of stress-strain states in the shaft wall across its thickness, allowing for axial symmetry and in terms of shell hypotheses of Kirchhoff–Love in the core midheight part.

1. Makhnenko, V.I., Kozlitina, S.S., Dzyubak, L.I. et al. (2010) Risk of formation of carbides and σ-phase in welding of high-alloy chrome-nickel steels. *The Paton Welding J.*, **12**, 5–8.
2. Kursevich, I.P., Margolin, B.Z., Prokoshev, O.Yu. et al. (2006) Mechanical properties of austenitic steels in neutron irradiation, effect of different factors. *Voprosy Materialovedeniya*, **4**, 55–56.
3. *PNAE G-7002–86*: Codes of design on strength of equipment and pipelines of nuclear power plants. Moscow: Energoatomizdat.
4. Margolin, B.Z., Kursevich, I.P., Sorokin, A.A. et al. (2009) To problem of irradiation-induced swelling and embrittlement of austenitic steels. Pt 1. Experimental results. *Voprosy Materialovedeniya*, **2**, 89–98.
5. Vilmaz, G., Harsan, V.A., Porter, D.Y. (2003) Dependence of mechanical properties on swelling in austenite steels. In: *Proc. of 2nd Conf. on Nuclear Engineering* (Tokyo, Apr. 2003), 109–122.
6. Applady, W.K. (1977) Swelling in neutron-irradiated 300-series stainless steels. In: *Proc. of Int. Conf. on Rad. Effects in Breeder Structural Materials* (Scottsdate, AZ, USA, May 1977), 509.
7. Garner, F.A. (1984) Recent insights on the swelling and creep of irradiated austenite alloys. *Nuclears Mater.*, 122/123(1/3), 459–471.
8. Garner, F.A., Porter, D.L., Hadman, G.L. (1990) Irradiation creep and swelling of annealed type 3041 stainless steel at 390 °C and high neutron fluence. In: *Proc. of Int. Conf. of Rad. Materials Science* (Krakov, Ukraine, Sept. 1990), Vol. 1, 68–74.
9. Margolin, B.Z., Kursevich, I.P., Sorokin, A.A. et al. (2009) To problem of irradiation-induced swelling and embrittlement of austenitic steels. Pt 2. Physical and mechanical principles of embrittlement. *Voprosy Materialovedeniya*, **2**, 99–111.
10. Makhnenko, V.I. (1976) *Calculation methods in examinations of kinetics of welding stresses and strains*. Kiev: Naukova Dumka.
11. (2000) *Nuclear reactor WWER-1000*: Manual of UTTs ZaporozhAES, Ch. 6, 51–80.

INVESTIGATION OF FACTORS INFLUENCING THE FORMATION OF WELD DEFECTS IN NON-VACUUM ELECTRON BEAM WELDING[*]

U. REISGEN[1], **M. SCHLESER**[1], **A. ABDURAKHMANOV**[1], **G. TURICHIN**[2], **E. VALDAITSEVA**[2], **F.-W. BACH**[3], **T. HASSEL**[3] and **A. BENIYASH**[3]

[1]Aachen University, Welding and Joining Institute, Aachen, Germany
[2]Saint-Petersburg State Polytechnic University, Institute of Welding and Laser Technology, RF
[3]Leibniz University of Hannover, Institute of Materials Science, Garbsen, Germany

The influence of welding condition parameters and properties of material on formation of defects, such as humping and undercuts, in non-vacuum electron beam welding was investigated. The influence of separate welding parameters on the quality of welds was determined.

K e y w o r d s : *non-vacuum electron beam welding, welding speed, power density, shielding gas, weld defects, humping, undercuts*

Nowadays the modern technologies of electron beam welding (EBW) are a very widespread tool for treatment of materials. One of the unique types of EBW is the EBW in the open atmosphere (non-vacuum EBW — NV-EBW), developed more than 50 years ago [1] and basically applied in mass production of light structures [2], in particular in automobile industry in welding of exhaust systems, transmission parts and other components [3, 4]. This process is also applied in production of welded pipes, in welding of hot-rolled strips and structural steels [5]. The basic advantages of NV-EBW as compared to conventional EBW in vacuum are the absence of need in creation of vacuum in working chamber, high speed of welding, small working cycle, good overlapping of gap of welded edges by a beam, high efficiency factor of the equipment. The disadvantages of the process can be small working distance, formation of X-ray radiation and ozone which require facilities with ventilation system protected from radiation.

Due to a large reserve of power the very high speeds of NV-EBW of thin-sheet metals can be theo-retically achieved. However, as works [6, 7] show, the intensive dynamics of weld pool at high speed of welding leads to formation of surface weld defects, especially to humping (Figure 1, *a*) and undercuts (Figure 1, *b*). These defects are observed in welding of steel at the speeds of more than 8 m/min, and for aluminium alloys — more than 15 m/min. These phenomena restrict the application of a full potential of power and economic efficiency of NV-EBW technologies.

Experimental installation. For experimental research at the Institute of Materials Science the installation of the type NV-EBW 25-175 TU of the company «PTR-Precision Technology» was used (Figure 2, *b*). The maximum beam power of this system is 25 kW at accelerating voltage U_{acc} = 175 kV and maximum welding speed v_w = 20 m/min. The installation can function both in pulsed and also in continuous conditions. The inclination angle of EB gun can vary from 0 to 90° [5]. At the Welding and Joining Institute of Aachen the «Steigerwald» company equipment was used (Figure 2, *a*). The maximal power of electron beam of this system is 30 kW at accelerating voltage U_{acc} = 150 kW, beam current I_b = 200 mA, maximal reached speed v_w = 57 m/min [4].
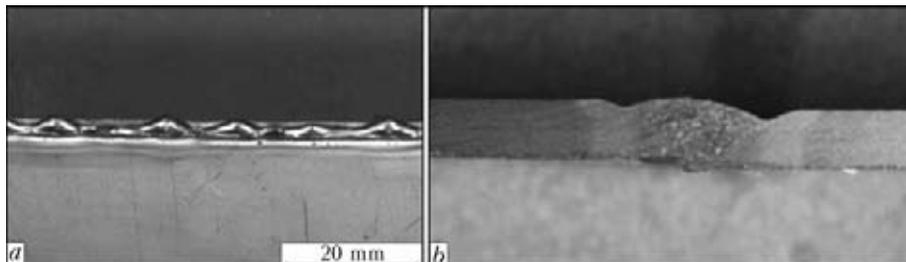
Figure 1. Dynamic defects of welds: *a* — humping (v_w = 10 m/min); *b* — undercut (v_w = 12 m/min)
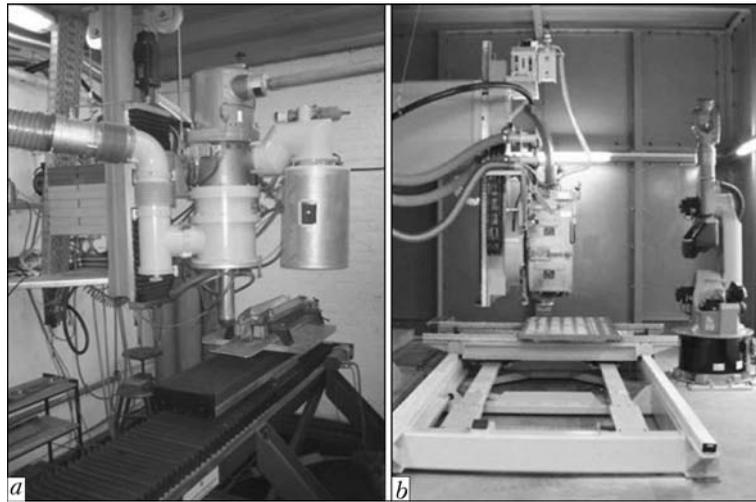
Figure 2. Experimental installations for EBW in open air: *a* — Anlage Type IGM G 150 K («Steigerwald»); *b* — 25-175 TU («PTR-Precision Technology»)

Investigation and modeling of surface dynamics of weld pool. *Shape of free surface of weld pool.* Basing on the equation of Navier–Stokes for the flow of a melt, the equations of continuity of flowing of a melt and conditions of balance of pressures on the free surface, as is shown in [8], the equation was derived describing the shape of a surface of weld pool:

$$\frac{\partial^3 \zeta}{\partial x^3} + \left(\frac{\rho v_0^2}{\sigma H} - \frac{2}{b^2}\right)\frac{\partial \zeta}{\partial x} = -\frac{3}{2LH} + 3\nu\,\frac{\rho v_0}{\sigma H^2}. \quad (1)$$

The designations of parameters are presented in Figure 3.

After solution of the equation (1) it is possible to determine the higher level of a melt above the surface of specimen in the tail of weld pool:

$$\zeta\,|_{x=L} = \frac{-\dfrac{3}{2}\dfrac{H}{L} + 3\dfrac{G}{\mathrm{Re}}}{G - 2\dfrac{H^2}{b^2}} \times$$

$$\times \left(L - 2H\,\frac{1 - \cos\left(G - 2\dfrac{H^2}{b^2}\right)^{1/2}\dfrac{L}{H}}{\left(G - 2\dfrac{H^2}{b^2}\right)^{1/2}\,\sin\left(G - 2\dfrac{H^2}{b^2}\right)^{1/2}\dfrac{L}{H}}\right), \quad (2)$$

where $G = (\rho v_0^2)/(\sigma/H)$ is the relation of high-speed pressure of flow of a melt to capillary pressure; v_0 is
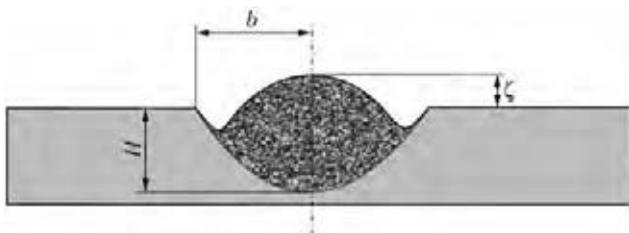
the speed of a melt relatively to a solid phase, connected with melt flowing round the crater formed under the beam, and can be evaluated in accepted one-dimensional approximation as $v_0 = v_{\mathrm{w}}\dfrac{h}{H}$, where h is the crater depth.

The equation (2) allows evaluation of the influence of material properties and geometry of weld pool on reinforcement of a weld.

Let us consider the case of «shallow» and «wide» weld pool, when $G > (2H^2)/b^2$, i.e. when the depth of penetration is less than the width of weld pool. In this case the waves at $(G - (2H^2)/b^2)L/H > 2\pi$ can be formed on the melt surface. Moreover, the middle line of the surface is lowered in direction to the pool tail. In case of a «deep» weld pool, when $G < (2H^2/b^2)$ (depth reaches one third of the width and more), the situation changes radically. The lowering of middle line is changed to its lifting to the end of the pool, the maximal height of which can reach $\dfrac{3}{2}\dfrac{b^2}{H}$. One should pay attention to the case when $G \approx (2H^2/b^2)$. Then the height level can be even sufficiently higher. These conditions are the most dangerous from the point of view of unstable formation of surface, but it is impossible to analyze this using accepted approximations of «boundary layer».

This model describes the shape of weld pool at relatively low speeds of welding (welding speed before formation of humping and low weld reinforcements ζ). For experimental verification the welding experiment with relative parameters was carried out. On the produced weld a long-wave profile of the welding bead is observed (Figure 4).

In principle, the given analysis is a theoretical description of process of formation of «stationary» lowering and lifting of weld surface, i.e. formation of undercuts. To analyze the quite non-stationary phenomena, such as humping, it is necessary to preserve

Figure 3. Designation of parameters of weld pool section
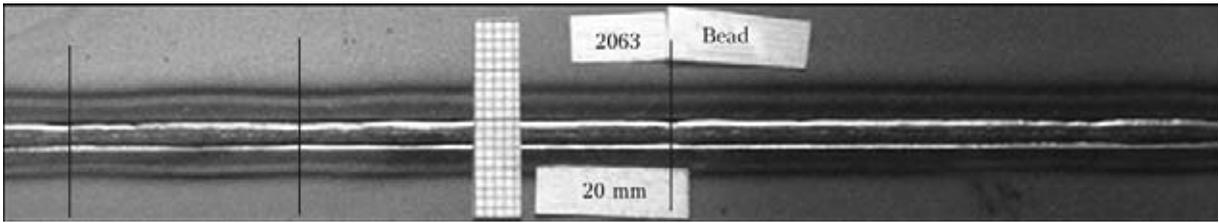
Figure 4. Surface of weld at welding speed before formation of humps (DC05 1.5 mm thick, v_w = 10 m/min, I_b = 70 mA, A = 15 mm)

«non-stationary» members with temporary derivatives and to analyze the stability of «quasi-stationary» behavior, described above.

Stability of weld pool surface. To analyze the stability of weld pool surface, the equation for local lifting of its surface above the surface of specimen was used, derived on the basis of the non-stationary equation of Navier−Stokes, equation of discontinuity and balance of pressures

$$\frac{\partial^2 \zeta}{\partial t^2} = -\frac{\sigma H \partial^4 \zeta}{\rho \partial x^4} + \frac{2\sigma H \partial^2 \zeta}{\rho b^2 \partial x^2} + \frac{3\sigma \partial \zeta}{2\rho L H \partial x}. \tag{3}$$

The designations used in the equation (3) are shown in Figure 5. The analysis of stability of solution of this equation by Lyapunov (stability of flat surface of weld pool) showed that on the surface of weld pool the waves are developed, described by the expression

$$\zeta = \zeta_0 e^{i(\omega t - kx)},$$

where $\omega = \pm\Omega \pm i\gamma$ is the angular frequency. The frequency of waves is preset by expression

$$\Omega = \sqrt{\frac{\sigma H}{\rho}} \left[\left(k^4 + \frac{2k^2}{b^2} \right)^2 + \frac{9k^2}{4L^2 H^4} \right]^{1/4} \times$$
$$\times \cos\left(\frac{1}{2} \operatorname{arctg} \frac{3b^2}{2L H^2 k(k^2 b^2 + 2)} \right). \tag{4}$$

The increment of waves γ is determined by expression

$$\gamma = \sqrt{\frac{\sigma H}{\rho}} \left[\left(k^4 + \frac{2k^2}{b^2} \right)^2 + \frac{9k^4}{4L^2 H^4} \right]^{1/4} \times$$
$$\times \sin\left(\frac{1}{2} \operatorname{arctg} \frac{3b^2}{2L H^2 k(k^2 b^2 + 2)} \right). \tag{5}$$
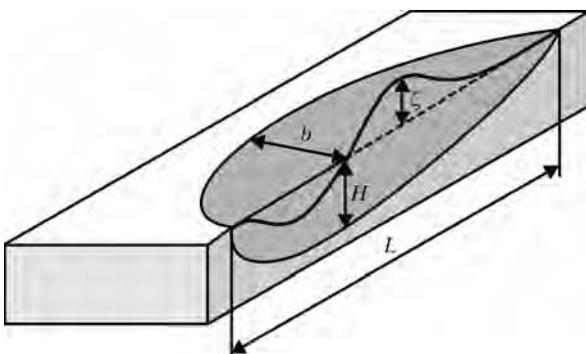
The expressions (4) and (5) determine the conditions and speed of humps growth. As far as the solution of equation (3) contains always the members of the type $e^{\gamma t}$ and $e^{-\gamma t}$, then at any character of γ there is a solution, increasing with time. This means that the presence of Marangoni flow at the surface leads to originating of oscillating instability on it which becomes a reason of humping. The parameters of humping, such as distance between humps and their size, are determined by wave number k (length of exciting waves), which in its turn determines the maximal value of increment γ (maximal speed of growth of disturbances). Thus, humps grow with such wave number which corresponds to maximal speed of growth (humps at a low speed grow also, but they are not seen as far as big humps absorb the small ones). In view of finiteness of length of weld pool L should be selected from the values $k = 2\pi n / L$, where n = 1, 2, 3, ..., m. It is obvious that maximal k value exist on the real axis, which does determine the parameters of humping.

The analysis of expression for increment of wave growth shows that k value providing maximum of increment γ, at made assumptions, depends only on length, width and depth of the weld pool.

As an example let us analyze the process of development of humping with increase of welding speed. The possible lengths of waves on the surface of weld pool are shown in Figure 6 in a form of vertical lines (markers). The speeds of growth of these waves are determined by corresponding values of waves increment. With increase of welding speed, leading to elongation of weld pool, all markers are shifted in the plot to the left, here the speeds of waves growth of different length change and after transition by marker of the longest wave through the maximum its speed begins

Figure 5. Designations of parameters to the model of weld humping
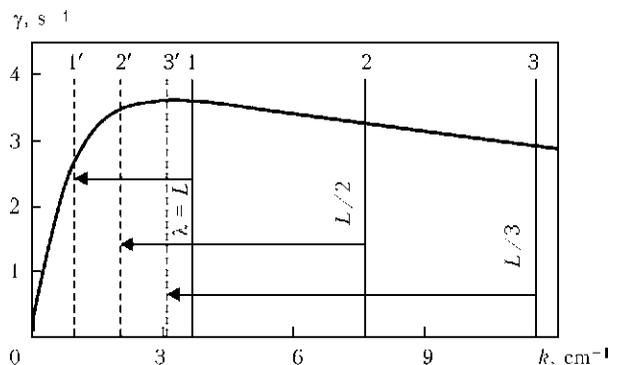
Figure 6. Dependence of increment of wave growth on wave number (for description see the text)
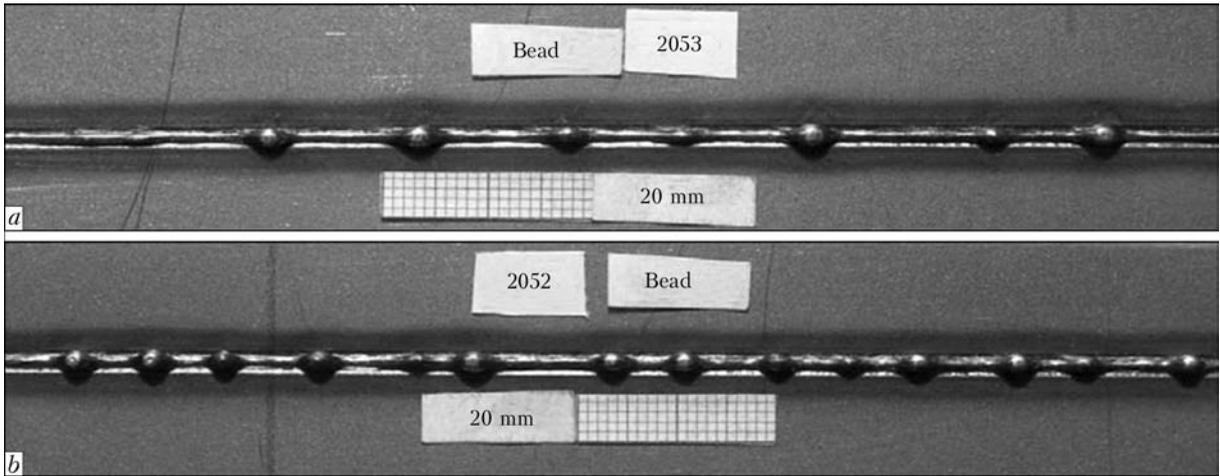
Figure 7. Dependence of humps formation on welding speed (respectively, on weld pool length) at $A = 10$ mm: a — $v_w = 12$ m/min, $I_b = 65$ mA; b — $v_w = 15$ m/min, $I_b = 5$ mA

to decrease, which with further increase of welding speed leads to replacement of long-wave humping to short-wave one, i.e. to multifold decrease of distance between the humps. The solid vertical lines in Figure 6 show wave number for short weld pools and dash lines — for long pools. In the long weld pool the short waves are growing quicker, while the long ones are growing in the short pool.

The constructed model can be illustrated by a real example. The growth increment is changed with increase in length of weld pool according to Figure 6. During experiments with a short weld pool (Figure 7, a) a wave with $\lambda = L$ is located on the right to the maximum on the plot, therefore it grows faster. At a long weld pool the waves with $\lambda = L$ (Figure 7, b) are shifted to the left part from maximum function $\gamma(k)$, i.e. increment of hump growth at wave length L is lower than for waves of length $L/2$.

Experimental investigations. In accordance with the theory given above the basic parameters influencing formation of defects, such as humping and undercut, are length, depth and width of the weld pool. Their values determine threshold speed of welding, at which defects connected with dynamics of pool are still not observed.

Determination of critical speed of welding at different parameters. The results of experiments, carried out on low-carbon steel DC05, showed that with in-

crease of welding speed first the undercuts appear, and achieving the certain critical speed for given parameters of welding the first large humps are formed with non-regular distances between them. With increase of welding speed the number of humps per weld length grows, i.e. frequency of their appearance is increased, the distance between them decreases and sizes of the humps themselves decrease (Figure 8).

The next important parameter is a working distance A, which influences the power density in heating spot. With increase of working distance the density of power sharply increases [9]. The results of experiment show that with decrease of working distance it is necessary to decrease the beam current to maintain the required depth of metal penetration. Here, a weld is already produced and threshold of humping changes not considerably.

The determination of boundary of formation of humps for different materials was carried out similarly to the methods applied for the steel DC05. The experiments showed that there is a certain dependence of critical speed of welding on material being welded (Table 1).

Whereas the threshold of speed of formation of humps for steels is within the limits of 10–12 m/min and depends inconsiderably on chemical composition, even at 20 m/min no humps were observed in welding of aluminium alloy and lead. It is obvious that the
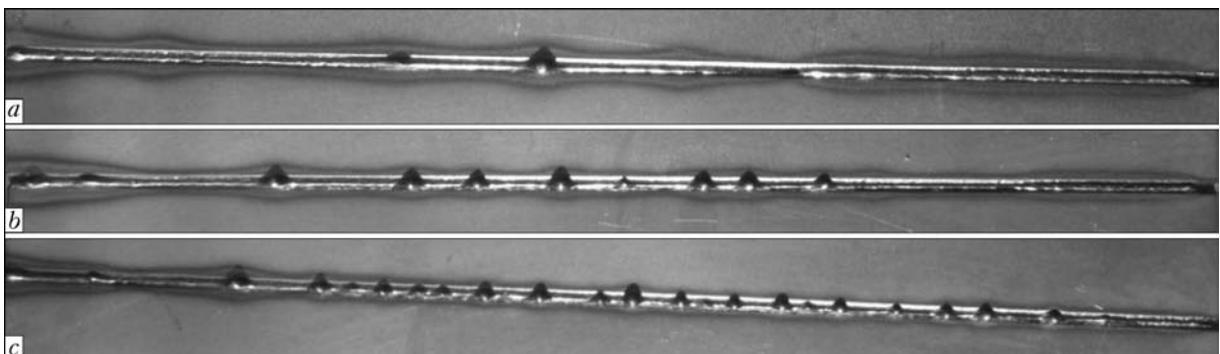
Figure 8. Formation of humps and undercuts at different speed of welding of steel DC05 at $U_{acc} = 150$ kV, $I_b = 100$ mA, A = 10 mm: a — $v_w = 14$; b — 16; c — 18 m/min

Table 1. Influence of material type on critical speed of humps formation

Material	d, mm	v_w, m/min	ρ, J/cm^3	I_b, mA	σ^*, mN/m	Notes
Steel DC05	1.5	12	7.874	80	1800	Beginning of humping
Steel TRIP 700	1.5	12	7.874	75	1800	Same
Cu	1.5	15	8.920	68	1250	»
AlMg$_3$	1.7	20	2.660	40	865	Humping was not obtained
Pb	1.0	20	11.340	12.5	451	Same

*Surface tension of pure materials (Fe, Cu, Al, Pb).

Table 2. Influence of material thickness on threshold of speed of formation of weld humping (A = 15 mm, consumption of helium — 90 min^{-1})

Material	d, mm	I_b, mA	v_w, m/min	Notes
DC05	0.7	57	20	Normal weld
DC05	1.5	80	12	Undercut, humping
DC05	3.5	75	6	Same
AlMg$_3$	1.5	40	20	Small undercuts
AlMg$_3$	4.0	70	10	Undercut, humping
Pb	1.0	12.5	20	Small undercuts
Pb	5.5	40	15	Undercut, humping

threshold of speed of humps formation depends on physical properties of material itself and, first of all, on surface tension. It is seen from Table 1 that with decrease of surface tension the threshold of humping is shifted to the region of high speeds of welding which confirms the abovementioned conclusion about leading role of thermal capillary effect at formation of humping in a shallow weld pool. It is indirectly confirmed by dependence of threshold of humping on thickness of material. The results of experiments on determination of influence of thickness of metal on dynamics of weld pool are presented in Table 2.

It was established that threshold of speed of formation of humps drops with increase in thickness of material. It can be explained by change of mechanism of heat conductivity in metallic sheet during transition from two to three dimensional case. The dynamics of weld pool is changed on which, despite surface thermal capillary effect, the convection flows from the bottom of pool to surface influence.

The surface-active substances, such as oxygen in welding of steels, are acting as element decreasing forces of surface tension, moreover, according to Rayleigh theory [10] the critical length of a pool increases ($\lambda > 2\pi R$) and formation of humps can be avoided or their formation shifted to high speeds of welding. At decrease of surface tension the radius is increased and also the critical length, i.e. pool will freeze earlier than a wave will occur. Figure 9 shows the example of influence of Ar + 4 % O_2 gas on formation of humping in the overlap joint.

The investigations showed that application of shielding gas allows increasing the welding speed by 2 m/min earlier than humping is formed.

The conclusion about the fact that Marangoni effect is a decisive factor for dynamics of weld pool is proved also by the following experiment. It is known that sulphur and carbon considerably influence the surface tension of weld pool [11]. Coming from it, a graphite sprayer was used for experiments to cover the half of a metal plate. After welding pass it was revealed that on the part of the plate not covered with graphite the humps were formed, whereas on the part of a plate, treated with graphite, the humps were not observed (Figure 10). As far as the time typical of NV-EBW is very short, one can neglect the influence of diffusive processes and come simply from surface effects.

High-speed video record of weld pool. Using the high-speed video record of weld pool carried out in

Figure 9. Influence of shielding gas on hamps formation in overlap joint (steel S420MC 2 mm thick, v_w = 10 m/min, shots behind the welding process): *a*, *b* — without shielding gas; *c*, *d* — with Ar + O_2 gas
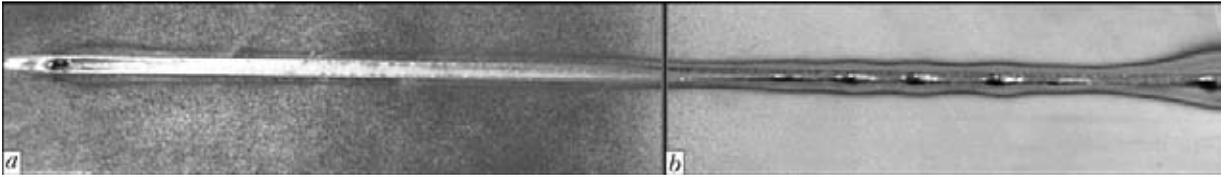
Figure 10. Influence of surface-active substance on dynamics of weld pool (DC05 1.5 mm thick, v_w = 14 m/min) with (*a*) and without (*b*) graphite
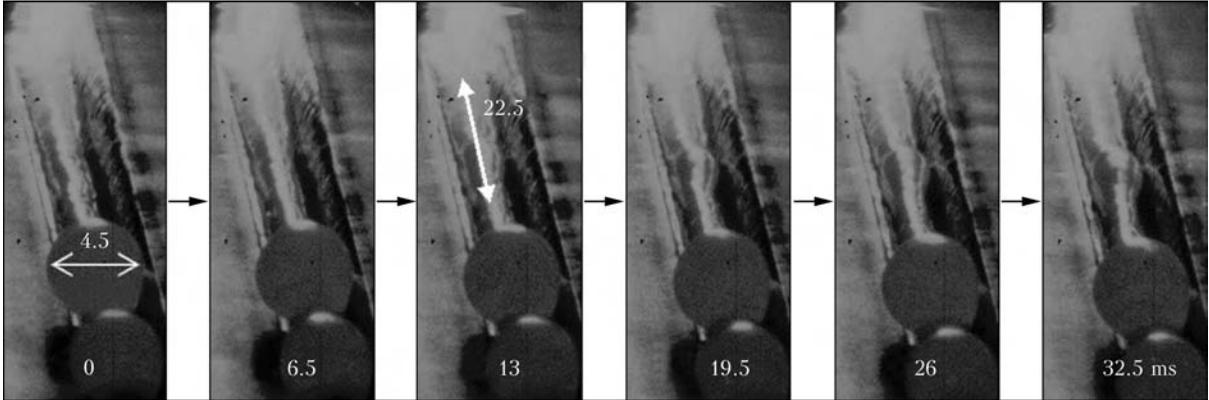
Figure 11. Dynamics of humps growth (high-speed video record of weld pool)

the scopes of investigations during welding process (Figure 11) the flow of melt was fixed in the direction to the tail of weld pool. Besides, one can observe the dynamics of development of single humps, their sizes and speed of growth (Figure 12).

It was observed that humps have definite speed of movement relative to the surface of metal plate being welded. The speed of movement of humps decreased as they grow from the order of five speeds of welding to speed of welding. The average speed of melt flow in the middle of weld pool was about 40 m/min relative to the surface of a plate. As the measurements showed, the humps grow fast at first. With increase of sizes the speed of their growth sharply decreases.
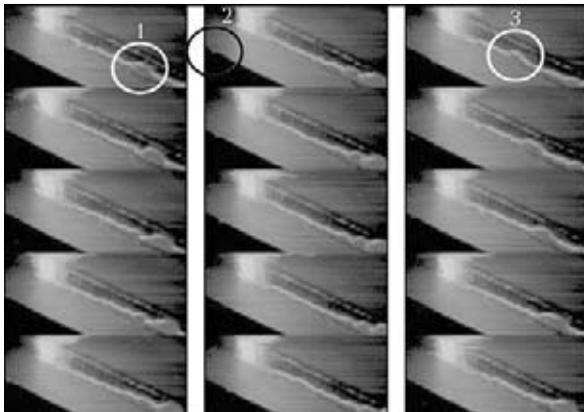
Figure 12. Dynamics of humps growth of weld pool (filming during welding process)
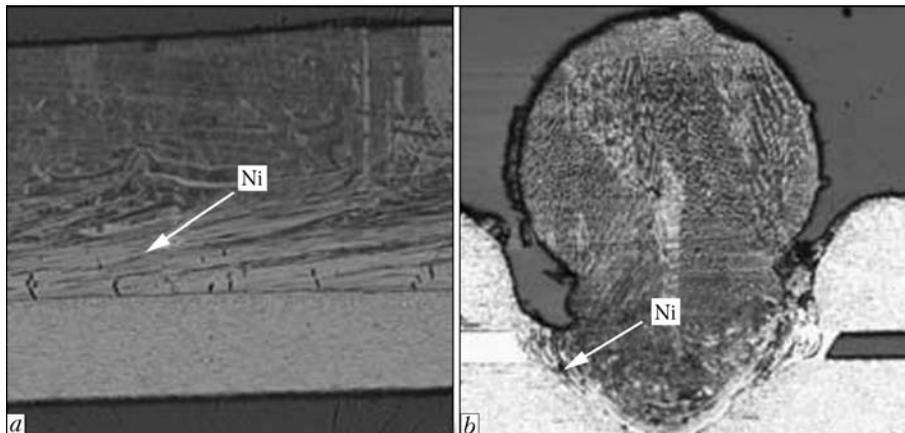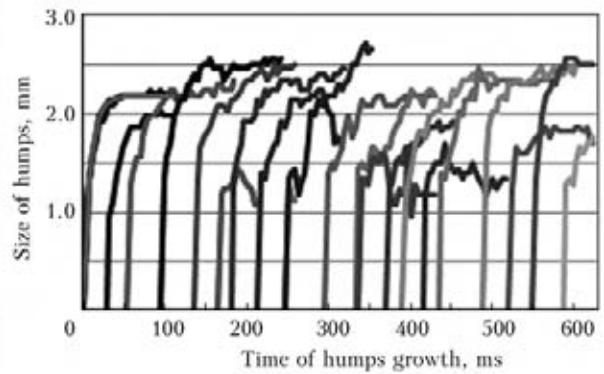
Figure 13. Distribution of nickel in weld in reflected electrons: *a* — longitudinal; *b* — transversal section of hump
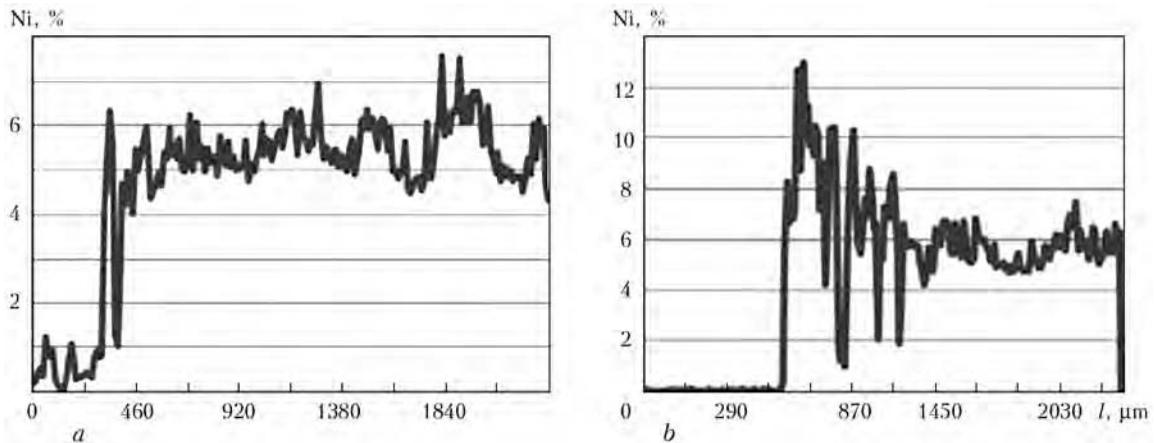
Figure 14. Distribution of nickel in a hump in horizontal (*a*) and vertical (*b*)

The measured data were numerically imposed on exponential function $\Delta\gamma = ae^{-\gamma t}$. As an average value for damping growth of humps the parameter $\gamma = 90 \text{ s}^{-1}$ was used. Further, on some curves under investigation the sharp deviation from constant damping growth is observed. There are single humps which stop their growth at the initial stage and are dispersed in the weld pool volume. The absorption of the small humps by large ones does also take place.

Experimental determination of melt flows in weld pool. For visualization of melt movement in weld pool the specimen was used which represented two overlap metal plates of 1 mm thickness with a thin nickel strip between them, the thickness of which was 100 μm. The similar experiments were carried out earlier on thick materials [12] where vertical flows of liquid in weld pool were observed. In our experiments the similar vertical flows were not revealed, but horizontal flows of indicator material in weld root were fixed (Figure 13).

Except of optical and metallographic investigation the microprobe power disperse analysis was carried out (Figure 14) the results of which did not reveal the gradient in concentration of nickel in the section of a hump both in longitudinal and also in transverse direction.

The given results represent the principally different dynamics of formation of weld pool surface and evidence of the fact that driving force in formation of humps in welding of thin-sheet materials is not vertical convection flows, but surface effects, first of all, the Marangoni effect.

CONCLUSIONS

1. Basing on the joint investigation of stability of hydrodynamic and thermal processes in weld pool, the model of formation of undercuts and humps on the surface of welds in NV-EBW was developed. Theoretical analysis and results of modeling showed that the cause of formation of undercuts is the surface phenomenon, and the cause of humps occurrence is the developing of instability of thermal capillary flow of melt in the weld pool.

2. The thresholds of speed of humps and undercuts formation are determined depending on beam current and working distance. It was established that with increase of beam current the instability of weld pool is increased. With decrease of working distance the intensity of beam is increased, therefore, it is necessary to decrease beam current to maintain the required penetration depth. The weld profile in this case becomes narrower and the threshold of speed of humping formation is changed negligibly.

3. The thresholds of speed of humps formation were experimentally determined for different materials. With increase of material thickness the threshold of speed of humps formation is decreased. The reason is the change in conditions of heat-mass transfer of a melt. It was established that the leading role is played by the Marangoni effect.

4. The application of surface-active substances allows suppressing of humps formation due to change of coefficient of surface tension.

5. High-speed video record allowed estimation of speed of melt flowing in weld pool, dynamics of growth and sizes of separate humps.

6. Due to application of the nickel indicator in weld pool the horizontal flows and lack of vertical ones were revealed, which was proved by results of microprobe analysis of sections in longitudinal and transverse directions.

1. (1962) *Introduction to electron beam technology*. Ed. by R. Bakish. NY; London: John Wiley & Sons.
2. Bach, Fr.-W., Szelagowski, A., Versemann, R. et al. (2002) Non vacuum electron beam welding of light sheet metals and steel sheets. *IIW Doc. 823−02*.
3. Powers, D.E., Schumacher, B.W. (1989) Using the electron beam in air to weld conventionally produced sheet metal parts. *Welding J.*, 68(**2**), 48–53.
4. Dilthey, U., Masny, H. (2005) *Hochgeschwindigkeitssch-weissen mit dem Elektronenstrahl an Atmosphaere − Fer-*

tigung von Karosseriekomponenten: DVS-Berichte, Vol. 237. Duesseldorf: DVS.

5. Bach, Fr.-W., Beniyash, A., Lau, K. et al. (2009) Non-vacuum electron beam welding of structural steels. *The Paton Welding J.*, **5**, 22–26.

6. Albright, C.E., Chiang, S. (1988) High speed laser welding discontinuities. In: *Proc. of 7th ICALEO* (Santa Clara, CA, USA, 1988), 207–213.

7. Wei, P.S. (2011) Thermal science of weld bead defects: A review. *J. Heat Transfer*, 133.

8. Turichin, G., Valdaytseva, E., Bach, Fr.-W. et al. (2010) Dynamic processes at high speed laser and electron beam treatment of materials. In: *25th Ann. of Cooperation: Transactions of St. Petersburg State Polytechnic University and Leibniz University of Hannover*, 91--101.

9. Reisgen, U., Schleser, M., Abdurakhmanov, A. et al. (2010) Messung der Strahlqualitaet einer Elektronenstrahlanlage in Umgebungsatmosphaere. *Materialwissenschaft und Werkstofftechnik*, 41(**1**), 45–52.

10. Rayleigh, J. (1945) *The theory of sound*. NY: Dover.

11. Czerner, St. (2005) *Schmelzbaddynamik beim Laserstrahl — Waermeleitungsschweissen von Eisenwerkstoffen*: Diss. Hannover.

12. Sievers, E.-R. (2006) Schmelzbadinstabilitaeten beim Elektronstrahlschweissen von Grobblechen. *Schweissen und Schneiden*, 58(**6**), 288–295.

APPLICATION OF TITANIUM ALLOYS WITH SUBMICROCRYSTALLINE STRUCTURE FOR RECONDITIONING OF GTE ROTOR PARTS

A.V. OVCHINNIKOV

Zaporozhie National Technical University, Zaporozhie, Ukraine

Influence of structural condition of filler materials on the structure and properties of welds in welded joints of high-temperature titanium alloy VT8 is considered for the case of repair of aircraft engine parts. It is established that application of filler materials with submicrocrystalline structure allows ensuring an increase of the level of the joint mechanical properties.

Application of welding in manufacturing and repair of products from complex-alloyed titanium alloys is related to a whole number of problems. The most complex of them is welding of two-phase titanium alloys used in gas-turbine engines (GTE), as they are applied in different structural states, ensuring the required level of mechanical and service properties of material [1]. Weldability problems are related to a change of the structure of weld and HAZ metal, as well as formation of defects of weld structure (porosity, nonmetallic inclusions, chemical and structural inhomogeneity). One of the main defects is weld porosity responsible for up to 56 % of the general number of defects [2]. Weld properties and appearance of such defects as pores, nonmetallic inclusions, chemical and structural inhomogeneity in its structure directly depend on the composition and quality of filler materials. Issues related to filler material quality have gained special importance over the recent years, as complex-alloyed high-temperature titanium alloys are applied for thin-walled parts (blades, blisks, etc.) operating at the limit of material strength margin. Therefore, presence of microdefects in filler materials can lead to a complete loss of performance of the reconditioned parts. Several works describe the methods to reduce the number of defects in filler materials [3, 4]. The proposed solutions, however, pertain to surface defects and do not solve the problems of volume structural state of the fillers.

Thus, in welding of critical parts from high-temperature titanium alloys applied for GTE rotor parts, it is necessary for filler materials to provide a stable high quality of the weld. The present work deals with the influence of structural state of filler materials on the structure and properties of welds in welded joints of high-temperature titanium alloys.

Materials and investigation procedure. Welded joints of two-phase high-temperature titanium alloy VT8 were selected as an object of investigations. This alloy is used for monowheels (blisks) of high-pressure compressor (HPC) of D27 turbofan. 2 mm plates from VT8 alloy were welded by argon-arc welding by 1.8 mm nonconsumable tungsten electron in the following modes: $I_w = 180$ A, $U_w = 10$ V. VD302 power source, U6872-5306 chamber with controllable atmosphere (argon), filler materials of standard compositions (VT2 alloy wire and VT8 alloy rod) were used. 2 mm rods of the same composition, but with submicrocrystalline (SMC) structure were used as experimental filler materials. Blanks for rods with SMC structure were produced at realization of intensive plastic deformation by the method of helical extrusion with simultaneous application of normal and tangential stresses at temperatures of 400–800 °C [5, 6].

Chemical composition was studied by means of chemical analysis to GOST 19863.1-19863.13 and microanalysis in the JEOL scanning electron microscope JSM-T300. Microstructure was studied in optical microscope «Neophot-32» and transmission electron microscope JEM-100CXII at accelerating voltage of 100 kV, as well as in scanning electron microscopes JSM-T300 and REM-106I with energy dispersive
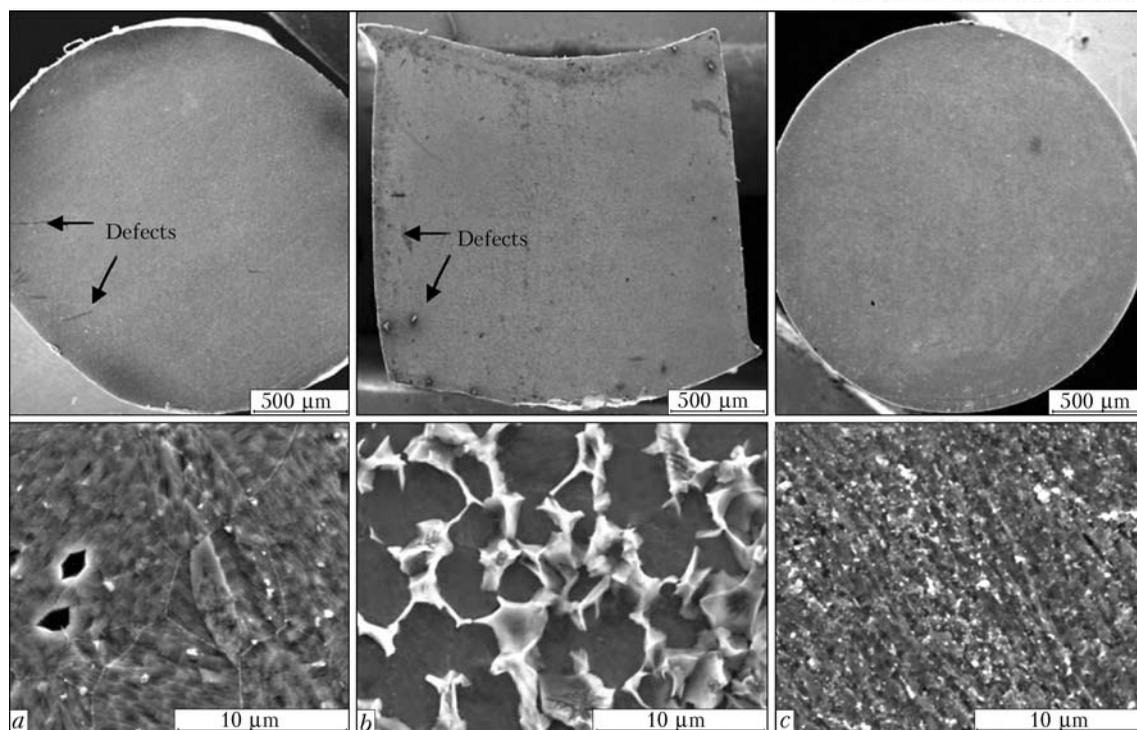
Figure 1. Macro- and microstructure of filler materials: *a* — VT2 alloy wire; *b* — VT8 alloy rod; *c* — VT2 alloy rod with SMC structure

analysis along a line and in a point. Mechanical properties were determined in the INSTRON tensile testing machine. Static strength and bend angle ψ of welded joints were determined according to GOST 6996−66 «Welded joints. Methods of determination of mechanical properties» and GOST 14019−2003 «Metallic materials. Method of bend testing», and pore quantity — by quantitative metallography methods [7]. At analysis of the surface of sample fracture in the weld, the number and size of pores per 1 mm^2 were recorded. Microhardness was studied in the BUEHLER microhardness meter MM7T (by the procedure to GOST 9450−76).

Investigation results and their analysis. As was noted above, the main causes for weld porosity are defects in the filler material structure. Analysis of the results of investigation of macro- and microstructure of standard filler materials revealed the presence of pores and discontinuities in the wire of VT2 alloy (Figure 1, *a*). These defects were technological, characteristic for wrought alloys.

The second drawback concerning the chemical and structural inhomogeneity of filler materials is characteristic for complex-alloyed titanium alloys (Figure 1, *b*). Investigations of standard filler materials applied in welding of VT8 alloy showed their chemical inhomogeneity (Figure 2).

Microanalysis of structural components demonstrated a significant difference in the content of the main alloying elements in α- and β-phases for an alloy of the following average composition, wt.%: Ti — base; 5.8 Al; 3.1 Mo; 0.3 Si; 0.5 Zr. In α-phase the content of α-stabilizing aluminium was equal to about 5.24 %, its minimum content in β-phase was within

2 % (Table 1). An inverse regularity was found in distribution of β-stabilizing elements, that is the most clearly manifested in molybdenum content (more than 10 times).

Presence of chemical inhomogeneity determined the difference in mechanical properties. Investigation of microhardness of structural components of VT8 alloy demonstrated that α-phase on average had microhardness of 3932·10^6, and β-phase — 2215·10^6 MPa. Difference in microhardness between α- and β-phases was more than 70 %. In welding and surfacing of thin-walled critical items of up to 1 mm thickness (blades, monowheels, etc.), such a difference in phase composition and properties in standard fillers can lead to a significant change in weld properties.

To eliminate the above defects, a new approach to formation of filler material structure was defined. It was proposed to apply filler materials with nano- or SMC structure. This, according to results of earlier research, will allow achieving a uniform distribution of alloying elements in the filler material volume.

Experimental material rods were produced by a specially developed technology, which was based on

Table 1. Alloying element content in structural components of VT8 alloy, wt.%*

Analysis section (phase)	Al	Mo	Zr	Fe	Si
001 (α-phase)	5.24	0.51	−	−	0.11
002 (β-phase)	4.08	3.55	0.80	1.08	0.28
003 (β-phase)	2.02	7.08	1.10	1.15	0.08
*Ti — base.					
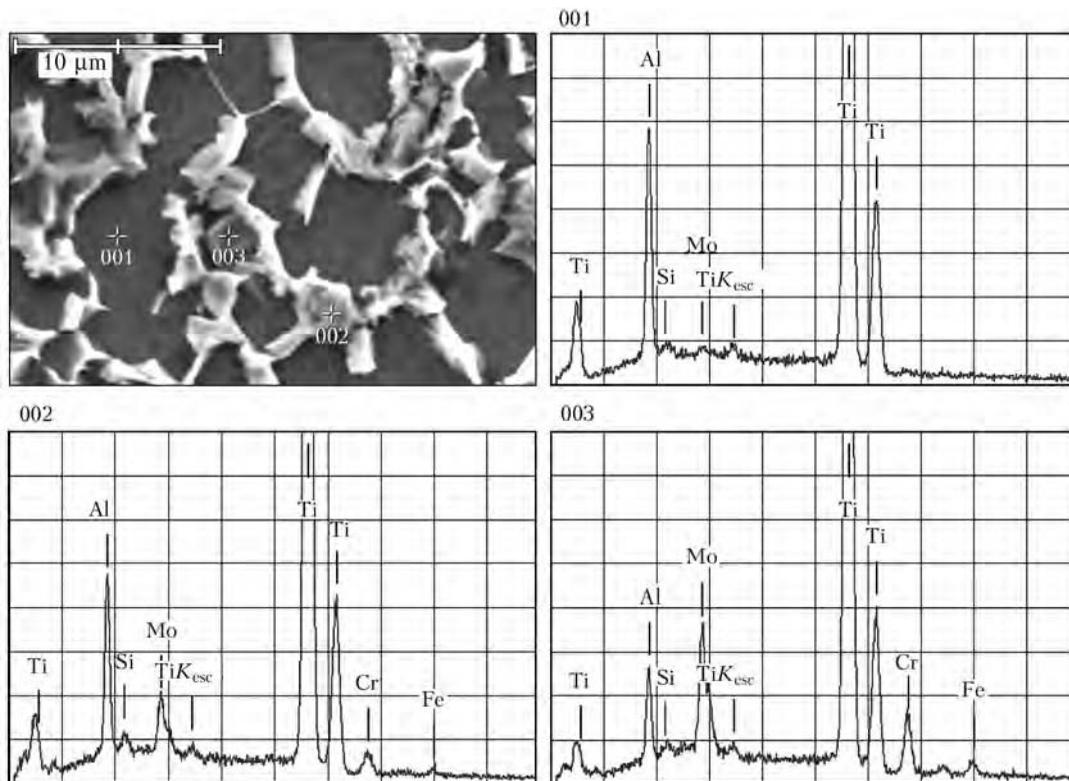
Figure 2. Energy-dispersion spectra in structural components of filler material from VT8 alloy

the method of helical extrusion [5, 6]. Application of intensive plastic deformation method for complex-alloyed titanium alloys ensured a more uniform distribution of alloying elements that is quite comprehensively described in [8, 9]. As a result, alloying elements were uniformly distributed through the entire alloy volume, and chemical and structural inhomogeneity in filler materials with SMC structure was practically absent. Filler materials with SMC structure did not have any pores, discontinuities or other defects, noted for standard alloys, that is readily seen on macro- and microsections (see Figure 1, c). Absence of the above defects, obviously, was the consequence of «healing» of pores under the impact of high pressures and higher temperature. A similar effect is used in treatment of cast titanium alloys in a gasostat [10, 11].
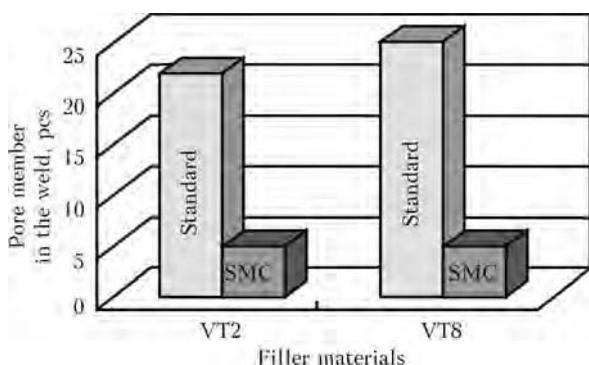
Figure 3. Number of pores on fracture surface of the weld in welded joints of VT8 alloy produced with application of standard and test filler materials with SMC structure

Comparative investigations of welded joints of plates from high-temperature titanium alloy VT8, produced with application of standard filler materials or those with SMC structure, showed that in the second case an increase of the level of welded joint mechanical properties was observed (Table 2).

As follows from analysis of the presented data, the level of mechanical properties of welded joints, produced with application of SMC filler materials, increased in terms of both strength and ductility, compared to standard fillers. Application of fillers with SMC structure allowed improving the stability of welded joint properties. Average value of ultimate strength for welded joints with application of fillers with SMC structure, made of VT2 titanium, was equal to 948 MPa, and for standard fillers it was not higher than 890 MPa. Difference in the value of ultimate strength between the joints made with fillers with SMC structure and standard fillers from VT8 alloy was equal to 65 MPa.

Table 2. Mechanical properties of welded joints on plates from VT8 titanium alloy produced using various filler materials

Filler	Fracture site	σ_t, MPa	$\sigma_{0.2}$, MPa	δ, %	ψ, %
VT2	Weld	888.0	476.7	5.9	61.5
VT2 (SMC)	Same	948.3	520.0	6.5	72.0
VT8	HAZ, weld	1083.2	656.3	4.7	23.0
VT8 (SMC)	HAZ	1148.3	705.7	5.4	31.3
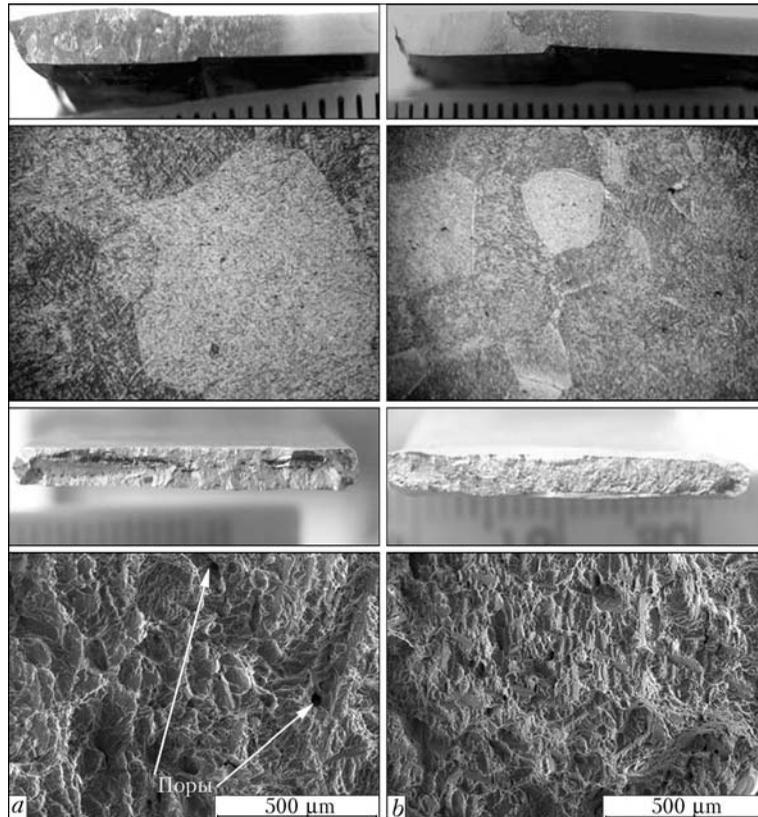
Figure 4. Characteristic view of fracture surface and microstructure of weld metal of welded joints on VT8 alloy at application of standard (*a*) and test filler materials with SMC structure from VT2 alloy (*b*)

A similar tendency was established also for ductility indices. For welds made with application of fillers with SMC structure, average value of bend angle was by 14.58 % for VT2 filler and by 26.4 % for VT8 filler higher than for welds made with fillers with a standard structure.

An important aspect is improvement of stability of test joint properties. So, maximum scatter of properties was found for joints produced with application of standard fillers. As to strength indices, scatter of properties was equal to: for σ_t — about 15, for σ_y — about 19 %. Here, the sample failed in the weld, and, therefore, fracture was caused by structural defects. For welded joints made with fillers with SMC structure, scatter of strength properties did not exceed 3 %, and for bend angle — 12 %. For standard fillers the difference in bend angle of welded joints was about 33 %. The established regularity is characteristic also for relative elongation. On the whole, welded joints, obtained with application of fillers with SCM structure, had higher values of mechanical properties: ultimate strength — by 6.32 and 5.66 %, yield point — by 8.14 and 7 %, relative elongation by 8 and 15 %, bend angle — by 14.5 and 26.4 % for unalloyed and alloyed fillers, respectively.

Higher and more stable properties of welded joints, produced with application of fillers with SMC structure, can be attributed to the fact that welded joint structure contains a much smaller number of defects. This was confirmed by the results of investigation of weld defects. Pores on weld fracture surface of more than 20 μm size were regarded as defects. Investigation results are given in Figure 3.

As follows from analysis of the presented data, in welded joints made with fillers with SMC structure pore number is 4—5 times smaller than that for joints produced by standard technology. Reduction of the number of defects in the weld of test joints led to an increase of weld metal fracture toughness, as follows from the appearance of welded joint fracture surface (Figure 4).

Pores of 20 to 80 μm size were found on fracture surface of welded joint produced by the standard technology. Mode of sample fracture leads to the conclusion about the connection between the found pores and formation of initial cracks and their subsequent propagation. In joints made with application of alloys with SMC structure, pores were practically absent, that, apparently, also ensured a higher level of mechanical properties of these joints compared to standards ones.

CONCLUSION

Application of filler materials with SMC structure instead of standard fillers allows:

• eliminating pores and discontinuities in filler material structure as a result of «healing» of the latter under the impact of volume deformation at elevated temperature by the principle similar to gasostatic treatment;

• lowering the chemical and structural inhomogeneity, characteristic for fillers from two-phase titanium alloys;

• increasing the energy intensity of fracture of welded joints on high-temperature titanium alloys due to reduction of the number of defects in the weld structure;

• increasing the values of mechanical properties of welded joints from VT8 alloy, compared to joints made with application of standard fillers.

1. Kolachev, B.A., Malkov, A.V. (1983) *Physical principles of fracture of titanium*. Moscow: Metallurgiya.
2. Muraviov, V.I. (2005) Problems of pore formation in titanium alloy welds. *Metallovedenie i Termich. Obrab. Metallow*, **7**, 30−37.
3. (1979) *Metallurgy and technology of welding of titanium and its alloys*. Ed. by S.M. Gurevich. Kiev: Naukova Dumka.
4. Dolotov, B.I., Merkulov, V.I. *Method of argon-arc welding*. Pat. 2201320 Russia. Int. Cl. B23K9/16. Publ. 27.03.2003.
5. Bejgelzimer, Ya.E., Varyukhin, V.N., Orlov, D.V. et al. (2003) *Spiral extrusion as a process of strain accumulation*. Donetsk: TEAN.
6. Synkov, S.G., Varyukhin, V.N., Synkov, V.G. et al. *Method of reinforcement of materials and device for its implementation*. Pat. 46999 Ukraine. Fil. 12.04.2001. Publ. 15.05.2001.
7. *MR 149-36−81*: Quantitative metallographic analysis of two-phase titanium alloys. Introd. 20.01.81.
8. Pavlenko, D.V., Ovchinnikov, A.V., Kachan, A.Ya. et al. (2007) Application of spiral extrusion for producing of submicroscopic structure and homogenizing of titanium alloy VT3-1. *Vestnik Dvigatelestroeniya*, **2**, 185−188.
9. Ovchinnikov, A.V., Pavlenko, D.V., Kachan, A.Ya. et al. (2007) Evaluation of efficiency in application of intensive plastic deformation for producing of nanocrystalline structure in titanium alloy VT3-1. *Novi Mater. i Tekhnol. v Metallurgii ta Mashinobud.*, **1**, 27−31.
10. Padalko, A.G. (2007) *Practice of hot isostatic pressing of inorganic materials*. Moscow: IKTs.
11. Garibov, G.F. (2006) Development of high-temperature gas-static treatment of titanium alloys. *Tekhnologiya Lyog. Splavov*, **1/2**, 120−130.

EFFECT OF HIGH-TEMPERATURE THERMAL CYCLING ON DEPOSITED METAL OF THE TYPE OF HEAT-RESISTANT DIE STEELS

I.A. RYABTSEV, I.A. KONDRATIEV, A.A. BABINETS, G.N. GORDAN, T.V. KAJDA and **I.L. BOGAJCHUK**

E.O. Paton Electric Welding Institute, NASU, Kiev, Ukraine

The effect of high-temperature cyclic loads on thermal stability, structure and microscopic chemical heterogeneity of deposited metal of the type of heat-resistant die steels was investigated. It was shown that, despite the fact that no diffusion of main alloying elements was detected during the tests, structure of the deposited metal experienced changes leading to its weakening.

One of the main types of wear of working surfaces of forming rolls, dies and other tools used for hot deformation of metals is thermal fatigue, i.e. formation of a network of fire cracks caused by high-temperature cyclic loads [1−4]. The thermal fatigue cracks form on the surfaces of parts after some (relatively small) quantity of thermal cycles. They result from the effect of cyclic thermal stresses induced by constraint changes in size of isolated regions of a part in periodic fluctuations of temperatures [5−8].

A combination of cyclic temperatures and elasto-plastic deformations is a characteristic feature of anisothermic cyclic fatigue. The type of anisothermic cyclic fracture, at which the maximal temperature of a thermal cycle corresponds to compression in a cycle of elasto-plastic deformation, was called the thermal fatigue [5, 6]. The quantity of the heating−cooling cycles to formation of cracks usually serves as a characteristic of resistance of materials to thermal fatigue [2, 3].

Depending on the test procedure that meets service conditions of parts to this or other extent, the quantity of thermal cycles leading to formation of the thermal fatigue cracks for the majority of materials does not exceed several hundreds or thousands of the heating−cooling cycles [2−3].

In addition to thermal stresses, when investigating thermal stability of the deposited metal it is necessary

Table 1. Chemical composition and hardness of deposited metal

Flux-cored wire grade	Content of elements, wt.%							Hardness *HRC*
	C	Mn	Si	Cr	W	Mo	V	
PP-Np-30Kh4V2M2FS	0.35	0.72	1.1	3.97	2.52	1.88	0.44	50
PP-Np-35V9Kh3GSF	0.34	0.6	1.0	3.0	9.3	−	0.71	54

to take into account also the structural changes that may occur in it as a result of high-temperature cyclic effects. Irreversible changes in structure and properties of the deposited metal during operation determine in many respects the serviceability and reliability of the clad tools used for hot deformation of metals and alloys. The purpose of this study was to investigate structural transformations taking place in the deposited metal of the type of heat-resistant die steels as a result of its thermal stability tests.

Experimental flux-cored wires were used for cladding of billets preheated to 300 °C. After cladding the billets were subjected to slow cooling. Actual composition of the deposited metal and its hardness are given in Table 1. Specimens measuring 40 × 40 × 40 mm were made from the clad billets to determine thermal stability of the deposited metal.

Investigations of thermal stability were carried out by using a modular rig for testing of different properties of the deposited metal [9] by the following procedure: heating of the polished surface of a clad specimen to 680–700 °C, and rapid water quenching to 70–90 °C. Thermal stability was evaluated from the quantity of heating–cooling cycles to formation of fire cracks.

Results of the thermal stability tests of the deposited metal, as well as thermal stability values for widely applied die steel 5KhNM quenched and tempered to hardness HRC 50 are given in Table 2. Figure 1 shows surface of the clad specimens after the thermal stability tests.

Table 2. Results of thermal stability tests of deposited metal

Type of deposited metal	Formation of cracks		
	First cracks	Crack network	Developed crack network
30Kh4V2M2FS	45	80	120
35V9Kh3GSF	30	70	100
Steel 5KhNM	15	50	70
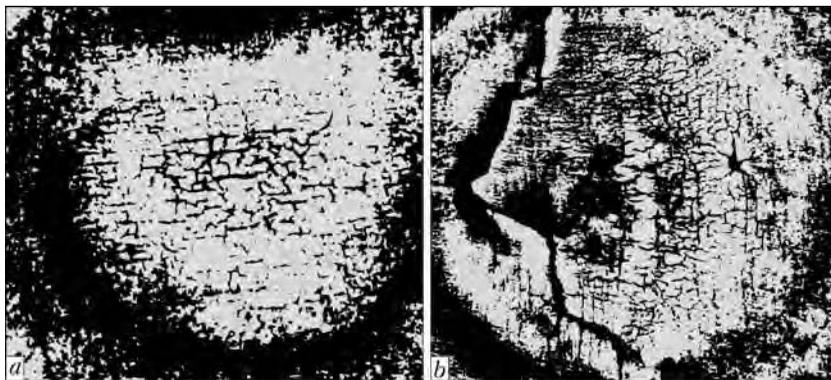
Figure 1. Appearance of specimens after thermal stability tests of deposited metal: a — 30Kh4V2M2FS; b — 35V9Kh3GSF
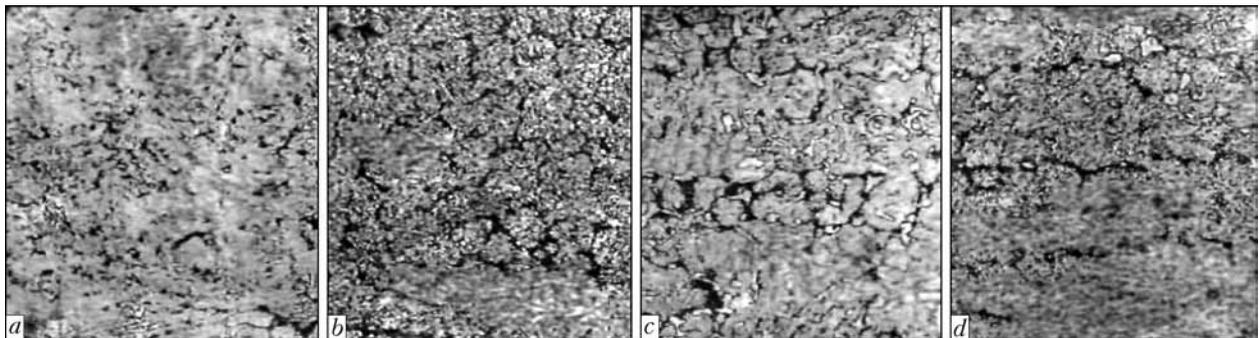
Figure 2. Microstructures (×400) of deposited metal 30Kh4V2M2FS (a, b) and 35V9Kh3GSF (c, d) before (a, c) and after (b, d) thermal stability tests
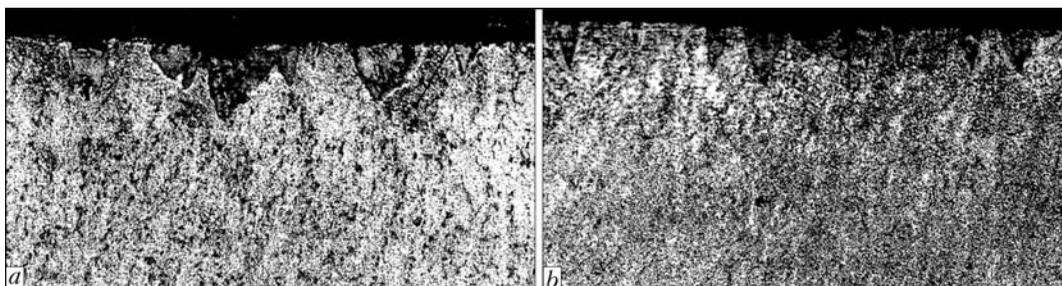
Figure 3. Microstructures (×100) of deposited metals 30Kh4V2M2FS (a) and 35V9Kh3GSF (b) in thermal cycling zone
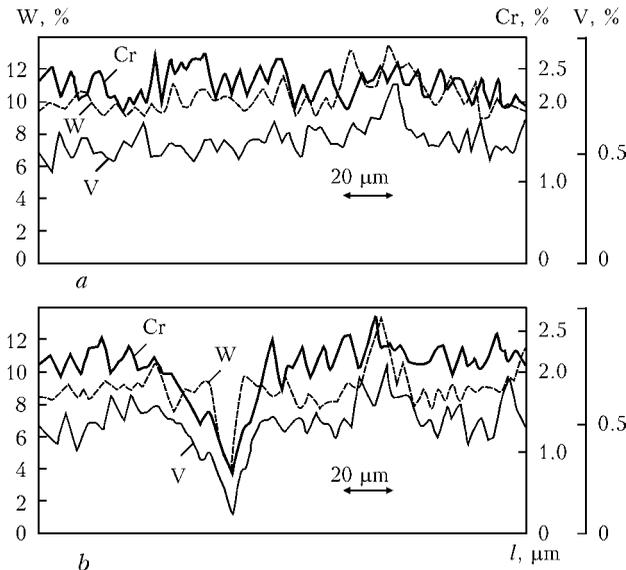
Figure 4. Distribution of alloying elements in deposited metal 35V9Kh3GSF before (*a*) and after (*b*) thermal stability tests

The best thermal stability values were exhibited by the deposited metal of the type of Cr−W−Mo steel, having a comparatively low content of tungsten.

Microstructure of the deposited metal was examined before and after the thermal stability tests. Up to 200 heating−cooling cycles were applied to provide a more complete development of fire cracks. Microstructure of the as-clad metal was examined in the last deposited layer, while after the thermal stability tests the examinations were carried out within the thermal cycling zone (location of fire cracks) at a distance of about 10−20 μm from the surface of the deposited layer.

Microstructure of both types of the deposited metal before and after the tests is shown in Figure 2, and that within the fire cracks zone at low magnification − in Figure 3.

Metal 30Kh4V2M2FS in the as-clad condition had fine-acicular martensitic-bainitic structure with hardness HV 5140−6060 MPa. Precipitates of retained austenite and an insignificant amount of eutectic were fixed along the polygonisation boundaries (see Figure 2, *a*). Cracks (see Figure 3) and structural changes evidencing coagulation and spheroidisation of carbides (Figure 2, *b*), as well as decomposition of martensite and partial decomposition of eutectic along the polygonisation boundaries, which led to decrease in hardness to HV 3830−4010 MPa, were detected after thermal cycling in the wear zone.

Approximately the same picture was fixed for deposited metal 35V9Kh3GSF. The martensitic structure with microhardness HV 5140 MPa was fixed in the matrix, while precipitates of retained austenite and an insignificant amount of eutectic were detected along the polygonisation boundaries (see Figure 2, *c*) after cladding. Decomposition of the martensite component (HV 3090 MPa) was fixed after the thermal

stability tests, small regions of retained austenite being preserved (see Figure 2, *d*).

As shown by the examinations of microstructure, multiple heating and cooling cycles (thermal cycling) resulted in structural changes taking place in surface layer of the deposited metal, leading to its weakening. Also, this was proved by the results of X-ray diffraction analysis of phase composition. For instance, the content of the α-phase in metal of the 35V9Kh3GSF type after thermal cycling increased from 84 to 87 % because of formation of the ferrite component. Compressive stress of the second kind grew from −0.27 to −0.44 GPa.

X-ray spectral microanalysis of distribution of main alloying elements in structure of the clad specimens before and after the thermal stability tests at a depth of down to 20 μm from the cladding surface in parallel to it in the automatic mode with an interval of 2−99 μm along the fire crack network front was carried out by using analyser CAMEBAX SX-50. Figure 4 shows results of examinations of the 35V9Kh3GSF type deposited metal. Distribution of the main alloying elements in the deposited metal was practically uniform (Figure 4, *a*) and remained almost unchanged after the thermal stability tests, except for one point − dramatic decrease in the content of alloying elements was fixed in the thermal fatigue crack zone (Figure 4, *b*), which probably was caused by their oxidation.

Approximately identical character of distribution of alloying elements (before and after the tests) was noted in the 30Kh4V2M2FS type deposited metal.

It is likely that the temperature-time parameters of the chosen procedure for testing the deposited metal to thermal stability do not lead to diffusion of the main alloying elements in the investigated types of the deposited metal.

Therefore, though no diffusion of the main alloying elements was fixed in surface layer of the deposited metal of the die tool steel type, the changes in structure leading to its weakening were detected after multiple heating and cooling cycles.

1. Frumin, I.I. (1961) *Automatic electric arc surfacing.* Kharkov: Metallurgizdat.
2. Tylkin, M.A. (1971) *Improvement of service life of metallurgical equipment parts.* Moscow: Metallurgiya.
3. Ryabtsev, I.A., Kondratiev, I.A. (1999) *Mechanised electric arc surfacing of metallurgical equipment parts.* Kiev: Ekotekhnologiya.
4. Ryabtsev, I.A. (2004) *Surfacing of machine and mechanism parts.* Kiev: Ekotekhnologiya.
5. Dulnev, R.A., Kotov, P.I. (1980) *Thermal fatigue of metals.* Moscow: Mashinostroenie.
6. Balandin, Yu.F. (1967) *Thermal fatigue of metals in ship power machine building.* Leningrad: Sudostroenie.
7. Tylkin, M.A., Yalovoj, N.I., Polukhin, P.T. (1970) *Temperature and stresses in parts of metallurgical equipment.* Moscow: Vysshaya Shkola.
8. Birger, I.A., Shorr, B.F., Demianushko, I.V. et al. (1975) *Thermal strength of machine parts.* Moscow: Mashinostroenie.
9. Ryabtsev, I.I., Chernyak, Ya.P., Osin, V.V. (2004) Modular unit for testing of deposited metal. *Svarshchik*, **1**, 18−20.

FORMATION OF STRUCTURE AND PROPERTIES OF 316 TYPE STEEL AT SUCCESSIVE CIRCUMFERENTIAL ELECTROSLAG SURFACING WITH LIQUID METAL

A.A. POLISHKO, L.B. MEDOVAR, V.Ya. SAENKO, S.I. STEPANYUK, A.Yu. TUNIK, I.N. KLOCHKOV and **I.V. BEREZIN**

E.O. Paton Electric Welding Institute, NASU, Kiev, Ukraine

The paper gives the results of metallographic investigations of structure, chemical composition and physical-mechanical properties of high-alloy 316 type steel (AISI) model ingot, produced under laboratory conditions by a method of enlargement using a successive circumferential electroslag surfacing with liquid metal.

The reliability and service life of modern machines and mechanisms are defined mainly by the quality of their separate parts. Special requirements are specified to the critical machine parts, operated under severe and extremely severe conditions at elevated and high temperatures (rotors and discs of steam and gas turbines). Fulfillment of these requirements leads to the complication of the chemical composition of metals and alloys, causes the need in improving the quality of the billet metal. Strength and ductile properties of the cast metal are of a special importance today [1].

Using the traditional methods it is not always possible to produce products of the required quality, it refers in particular to large ingots of high-alloy steels and alloys, as there are the significant limitations in ingot diameter due to the risk of formation of defects of liquation origin [2].

In this case the electroslag technology has a clear advantage, allowing producing metal with high values of density, physical and chemical homogeneity, isotropy of properties, uniform distribution of non-metallic inclusions, characterized by high level of purity and fine-dispersed structure. All this is important for critical parts, operated under severe conditions, when the stable high values of physical and mechanical properties are required.

Wide opportunities for the formation of the required structure and properties of large ingots of 316 type high-alloy steels are opened by the application of one of the varieties of electroslag technologies, namely the successive circumferential electroslag surfacing with liquid metal (ESS LM) for the enlargement of ingots. Application of ESS LM allows decreasing greatly the section and volume of solidifying metal, successively deposited on the ingot being enlarged and, thus, preventing the developing of liquation processes in each deposited layer [3–5].

The present work presents the results of metallographic investigations of structure and properties of two-layer model 110–180 mm diameter ingot of high-alloy steel of 316 type (10Kh17N14M2), produced
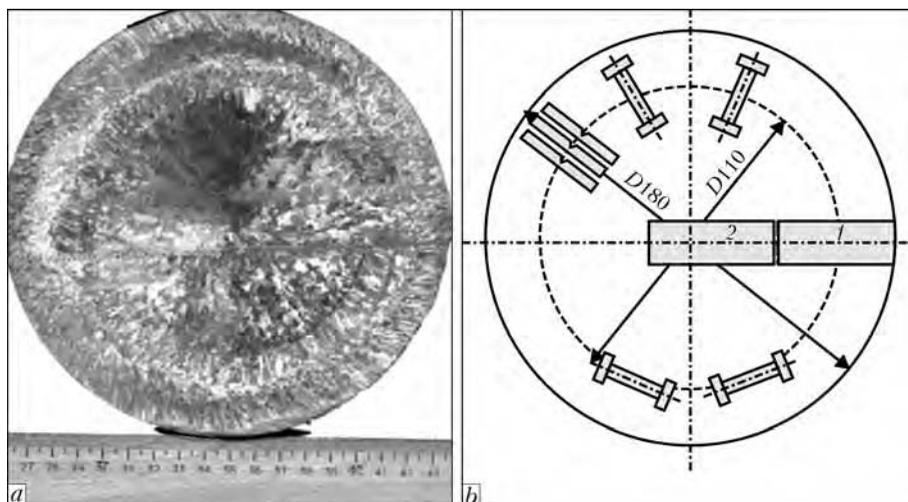
Figure 1. Macrostructure of transverse template of model two-layer ingot of steel 316 + steel 316 after ESS LM (*a*), and scheme of cutting out of specimens *1* and *2* for further investigations (*b*)

Table 1. Chemical composition of model two-layer ingot in the zone of layers fusion, wt.%

Object of investigation	C	Mn	Si	Cr	Ni	Cu	Mo	Nb	P	S
Deposited layer	0.059	1.13	0.31	15.6	11.9	0.20	2.2	0.20	0.027	0.006
	0.069	1.02	0.15	15.5	12.0	0.21	2.2	0.23	0.029	0.005
	0.058	1.13	0.32	15.5	11.6	0.21	2.2	0.20	0.027	0.006
	0.065	1.00	0.15	15.3	11.7	0.21	2.2	0.22	0.033	0.005
Central ingot	0.052	1.20	0.43	16.3	11.7	0.21	2.2	0.19	0.022	0.011
	0.073	1.03	0.16	15.9	12.1	0.23	2.2	0.23	0.029	0.005
	0.044	1.17	0.41	16.3	11.4	0.21	2.2	0.19	0.023	0.010
	0.069	1.01	0.15	15.6	12.1	0.21	2.2	0.23	0.028	0.005

under laboratory conditions using a successive circumferential ESS LM.

After melting the model ingot for further investigations, a transverse template was cut out of it (Figure 1, *a*).

The macrostructure of the transverse template was characterized by a homogeneous and dense structure (Figure 1, *a*) without defects of a shrinkage and liquation nature. Thickness of deposited layer in a transverse section of the ESS LM model ingot was almost similar.

The chemical composition of metal was determined by the method of a spectral analysis (GOST 9717−75). Using the emission spectral analysis in the diffraction photometric spectrometer, the distribution of elements in the transverse section of the model ingot in the zone of fusion of metal layers of similar chemical composition was studied. Zones were examined on the side of the deposited layer and central ingot in four points

on each side. The obtained results are presented in Table 1.

As is seen from the Table, the distribution of elements in the transverse section of a model two-layer ingot is almost uniform with a slight scattering within the ranges of allowable error in measurements of up to 2 %.

The metallographic examinations using the metallographic microscope «Neophot-32», equipped with an attachment for digital photographing of etched sections (solution of chromic acid H_2CrO_4) in accordance with the scheme of cut out (see Figure 1, *b*), showed that the microstructure of fusion zone metal of the two-layer model ingot is austenitic with orientation of crystallites, typical of polycrystalline materials with a dendritic shape of crystals both on the side of a central ingot (along fusion line) and also in the deposited layer (Figure 2).

Specimens for investigation of physical and mechanical properties were cut out of metal of the model
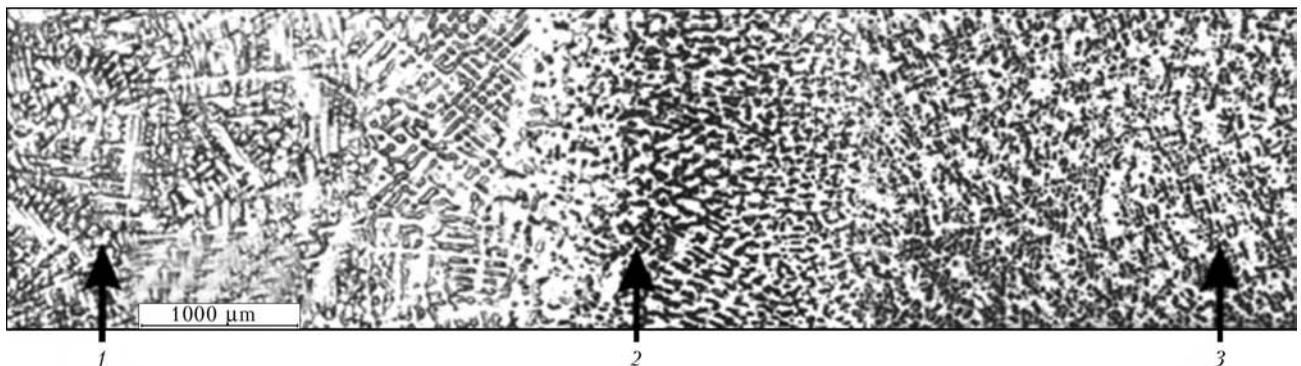
Figure 2. Microstructure of fusion zone of metal of model two-layer ingot: *1* — deposited layer; *2* — fusion zone; *3* — central ingot
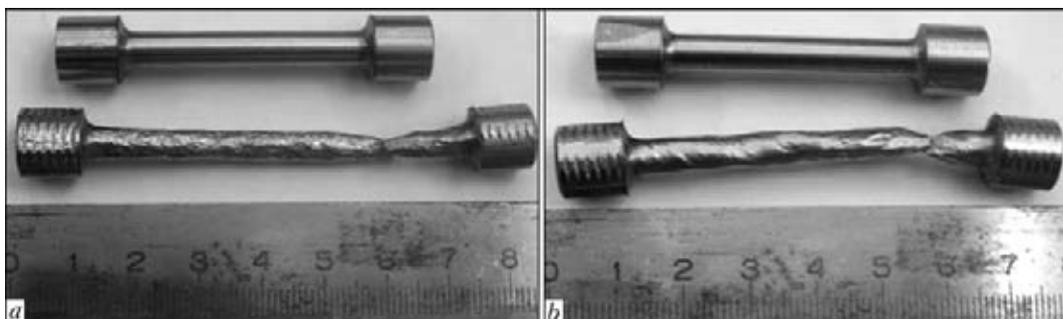
Figure 3. Specimens of metal of model ingot of 316 type steel before and after static (short-time) tensile tests in tangential (*a*) and radial (*b*) directions

Table 2. Physical-mechanical characteristics of metal of transverse specimens of model two-layer ingot of 316 type steel

Direction of specimens cutting out from ingot	σ_t, MPa	σ_y, MPa	δ, %	KCV, J/cm^2	k_{σ_t}	k_{σ_y}	k_δ
Tangential	491.0	201.5	55.0	−	0.98	1.01	1.05
Radial	502.4	198.8	52.5	240−298[*]	0.98	1.01	1.05
Requirements of Metals Handbook (9th ed.) of American Society for Metals for wrought metal	480.0	170.0	40.0	182−312	−	−	−

Notes. 1. Mean values of σ_t, σ_y, δ are given. 2. Coefficients of anisotropy k_{σ_t}, k_{σ_y}, k_δ are equal to ratio of values of characteristics of specimens cut out in tangential and radial directions. 3. Values of KCV are obtained for specimens after testing the cast metal with a notch in the HAZ at the distance of 2 mm from the fusion line.

two-layer ingot after ESS LM in transverse section at two levels in ingot height in radial and tangential directions (see Figure 1, *b*).

Static (short-time) tensile tests were performed according to requirements of GOST 1497−84 in servo-hydraulic test machine MTS 318.25 (USA) at maximum force 250 kN. The results were processed using the software TestWorks4 of MTS company. The error in obtained results was ±0.5 %, while it is allowable up to 1 % according to the GOST 1497−84.

Bend impact tests for determination of impact toughness KCV were performed according to requirements of GOST 9454−78 on specimens with a sharp notch (stress raiser) in the middle using one impact of a pendulum hammer. The notch on the specimens was made at the 2 mm distance from fusion line in the HAZ. Experiments were carried out using a pneumatic pendulum hammer of 2130-KM-03 type at a rated potential energy of pendulum of 300 J at 20 °C temperature (Table 2, Figures 3 and 4). Results of investigations showed the stable high level of strength characteristics of fusion zone metal of model ingot, and also homogeneity of metal properties both in section in tangential and radial directions and also in height at two levels.

It should be noted that the authors of this article studied the physical and mechanical properties on cast metal of the model two-layer ingot of 316 type steel, while in all the handbooks of steels and alloys the data are given for the wrought metal. Therefore, it is important for us to compare the obtained results for cast and wrought metals.
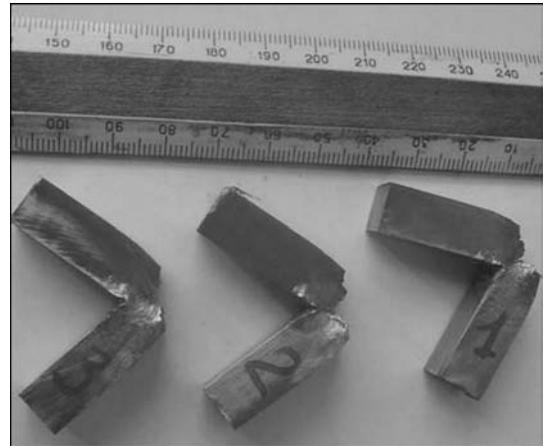
Figure 4. Specimens of metal of model two-layer ingot of 316 type steel after bend impact tests

The specimen fracture surfaces were investigated after static tensile and impact bend tests using the JEOL scanning electron microscope JSM-35CF and the Oxford Instruments X-ray spectrometer with a dispersion in energy of X-ray quanta (model INCA Energy-350, UK).

The fractographic analysis (Figure 5) showed a pit fracture, confirming a tough character of fracture, thus proving the high quality of fusion zone metal of the model two-layer ingot after ESS LM.

Structural homogeneity of fusion zone metal of the two-layer ingot, the absence of defects of shrinkage and liquation natures, as well as formation of homogeneous structure were revealed. Isotropy of strength characteristics and high level of impact toughness KCV of cast metal (240−298 J/cm^2) is typical, while
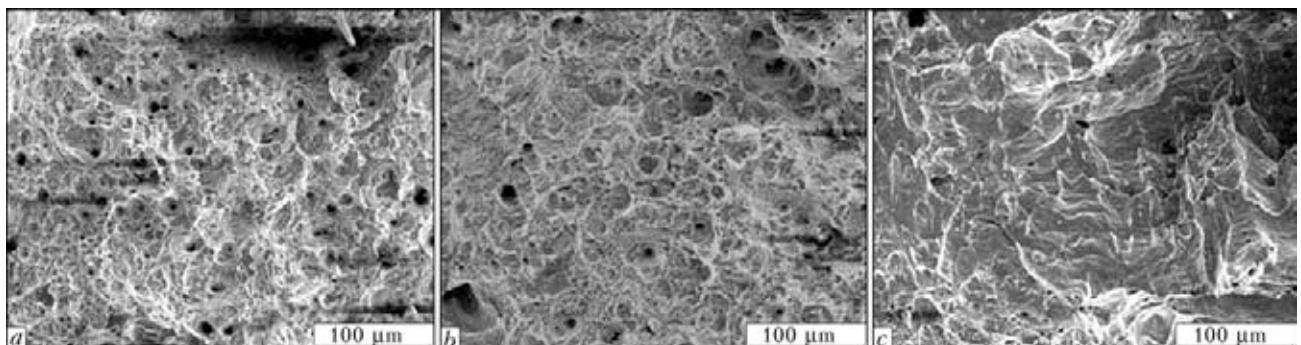
Figure 5. Fractograms of fracture surfaces of specimens cut out in radial (*a*) and tangential (*b*) directions after static (short-time) tensile and impact bend tests (*c*)

for the wrought metal the standard level of *KCV* amounts to 182−312 J/cm^2.

The obtained results of investigation of peculiarities of formation of structure and properties of high-alloy steel show the high level and isotropy of physical and mechanical properties of cast metal of the model ingot after the successive circumferential ESS LM without post high-temperature heat treatment, usually used after the electroslag welding. This shows the challenges in application of the described method for the enlargement of ingots of high-alloy steels and alloys.

1. (1981) *Electroslag metal*. Ed. by B.E. Paton, B.I. Medovar. Kiev: Naukova Dumka.
2. Volkov, S.E., Volkov, A.E., Zabaluev, Yu.I. et al. (1979) *Nonmetallic inclusions and defects in electroslag ingot*. Moscow: Metallurgiya.
3. Polishko, G.O., Remezov, O.G., Shevchenko, M.T. et al. (2007) Assessment of possibility to produce the steel ingots of 60 t weight on the base of 20 tons ESR furnace. In: *Coll. of reports of students and graduates of chair FKhOTM «Special Metallurgy: Yesterday, Today, Tomorrow», dedicated to 30th anniversary of chair of FKhOTM IFF of NTUU KPI*. Kiev: Politekhnika.
4. Paton, B.E., Medovar, L.B., Saenko, V.Ya. et al. (2007) New technological process of producing of super-large steel ingots by ESC LM method. *Advances in Electrometallurgy*, **1**, 2−5.
5. Medovar, L.B., Stovpchenko, G.P., Saenko, V.Ya. et al. *Method of production of large-tonnage metal ingot*. Pat. 94333 Ukraine. Int. Cl. B 22 D 19/16, C 22 B 9/18, B 23 K 25/00 C 6/00. Publ. 26.04.2011.

EFFICIENCY OF THE USE OF PROTECTIVE EXTENSION IN PLASMA SPRAYING

A.P. MURASHOV, A.P. GRISHCHENKO, N.V. VIGILYANSKAYA, A.N. BURLACHENKO and **I.A. DEMIANOV**
E.O. Paton Electric Welding Institute, NASU, Kiev, Ukraine

It was established that the use of the protective extension provides a 25 % increase in average velocity of spraying particles, improves heating of the particles, and decreases the required specific energy of the spraying process by 20 % due to increase in size of the high-temperature zone of the plasma jet. The content of oxides in coatings deposited by using the extension is 10 % lower, the content of pores in them is 4 times lower, and the coating to substrate adhesion strength is 20 % higher.

Keywords: *plasma spraying, plasma jet, extension, properties of coatings, material utilisation factor, experimental design*

In deposition of coatings by the plasma jet in open atmosphere, formation of a coating is affected by an admixture of ambient gases to the jet. The initial region of the jet measured from the plasmatron nozzle with diameter d_0 to boundary $I-I$ is characterised by the constant values of velocity u_0 and temperature of the flow, as well as by their equality to the initial values up to x_0 (Figure 1) [1]. In addition, the ionisation and dissociation energies are intensively released in the initial region of the plasma jet. Efflux of the electric current, additional release of the energy and turbulisation of the flow caused by the processes of large- and small-scale shunting of the arc take place sometimes. Static pressure in the initial region is not equal to zero because of electromagnetic compression

of the ionised gas in the electric arc. That is why, depending on the shape of the outlet part of the nozzle, the jet dramatically expands near its exit section. The mixing zone, where a radial transfer of impulse and energy takes place, and where parameters of the plasma jet continuously change from their initial values to the values characteristic of the ambient atmosphere, forms in the peripheral region of the jet starting from the exit section of the nozzle. Therefore, the transition region of the jet, and then the basic one, forms outside the initial region to boundary $T-T$. The temperature and velocity of the plasma jet decrease as a result of its dilution with cold air, this deteriorating heating of the spraying material. The spraying material actively interacts with the atmosphere components (O_2, N_2) already in the initial region. For example, for standard plasmatron UMP-4 the concentration of argon in the jet at a distance of $(2-3)d_0$ is 50 %, and in the zone where the spraying particles interact with the workpiece surface at a distance of 70−100 mm $((10-15)d_0)$ the concentration of argon is 20 %. This leads to formation of oxide and nitride inclusions in the coatings, that deteriorate properties of the latter (porosity, cracking, exfoliation) [2, 3].

To prevent the processes causing admixture of the atmosphere components to the jet, plasma spraying is performed in normal-pressure shielding atmosphere (APS), in rarefied controlled atmosphere (VPS), under a layer of liquid (WPS) and in increased-pressure

Figure 1. Flow diagram of plasma spraying with free-expanding plasma jet
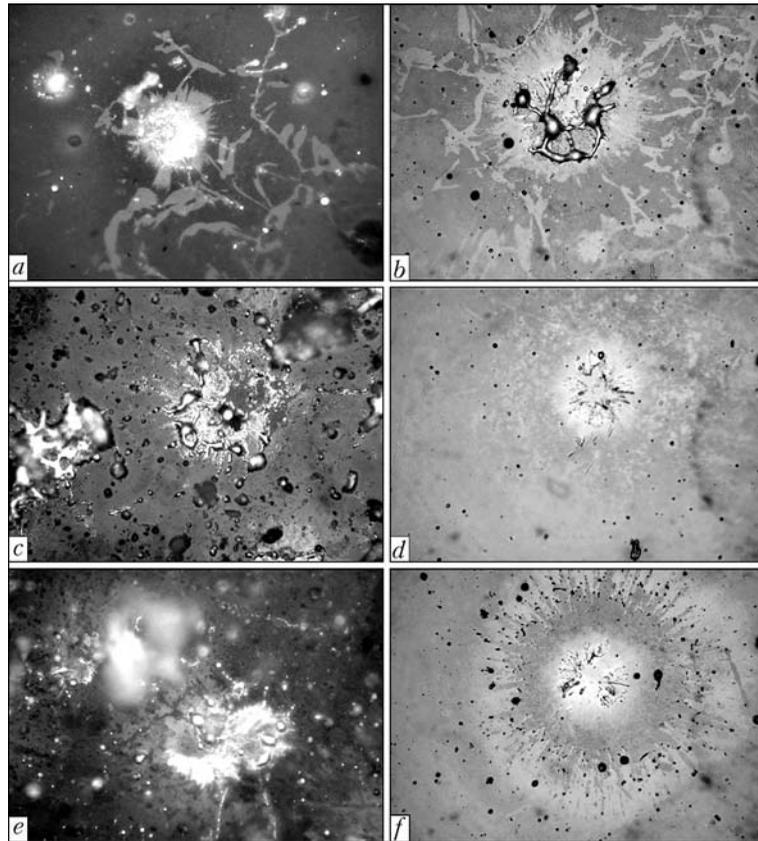
Figure 2. Splats of particles of powder PT-NA-01 sprayed by the plasma arc method without (*a, c, e*) and with extension (*b, d, f*) at currents of 300 (*a, b*), 400 (*c, d*) and 500 (*e, f*) A

controlled atmosphere (HPPS) [3–6], as well as by using systems with local shielding [3, 7–10].

The following tasks can be achieved by using the system of local shielding of the plasma spraying zone:

• increase in size of the high-temperature zone of the plasma jet (by restricting admixture of an ambient cold gas) and concentration of the spraying material in the central part, which leads to more efficient heating of the spraying material and more rational utilisation of the plasma jet energy;

• mitigation of the oxidation process caused by reaction of the spraying material with active components of the ambient atmosphere (O_2, N_2).

The purpose of this study was to evaluate the efficiency of the use of the protective extension in plasma spraying and its effect on improvement of the quality of coatings by upgrading heating and accelerating of the powder particles during spraying, as well as the protection of the spraying material from the ambient atmosphere (O_2, N_2).

The effect of the protective system on properties of the coatings was evaluated in the experiments on plasma arc spraying with and without the protective extension by using plasma spraying unit UPU-8M and a thermoreactive powder of the PT-NA-01 grade (95 wt.% Ni– 5 wt.% Al) with a particle size of $+40 - -60$ μm [11].

The efficiency of heating of the particles was determined by evaluating their appearance after solidification in collision with the surface of a glass plate (splat-test). Spraying was carried out with and with-

out the extension at different specific energies of the process

$$\varepsilon = \frac{UI\eta}{V_{p.g}},$$

where U is the voltage, V; I is the current, A; η is the efficiency of the plasmatron; and $V_{p.g}$ is the flow rate of the plasma gas, m^3/h.

The value of ε was varied by varying the current (300, 400 and 500 A). The plasma gas was argon with a flow rate of 1.38 m^3/h. Arc voltage was 30 V, and efficiency of the plasmatron was 53 % at a current of 300 A, 48 % at 400 A, and 47 % at 500 A (which was determined by using software CASPSP [12]). Under these conditions the specific energy of spraying was varied from 3.5 to 4.2 and to 5.2 $kW\cdot h/m^3$.

Spraying was performed on glass plates measuring $50 \times 30 \times 3$ mm. As seen from the appearance of the splats sprayed without the extension (Figure 2), at a current of 300 A the particles did not melt and rebounded from the surface, and at 400 A melting of the particles was incomplete (the shell melted, and the nucleus remained solid; increase in the amount of the incompletely melted particles in a coating leads to formation of coarse pores). At a current of 500 A the particles fully melted. In spraying with the extension, the particles fully melted already at a current of 400 A.

Therefore, the application of the extension allowed decreasing the required specific energy of the spraying

Table 1. Matrix of fractional (2^{4-1}) factorial experimental design

Experiment No.	I, A	$V_{p.g}$, m³/h	H, mm	Ar/N₂
1	+	+	+	+
2	+	+	−	−
3	+	−	+	−
4	+	−	−	+
5	−	+	+	−
6	−	+	−	+
7	−	−	+	+
8	−	−	−	−
9	0	0	0	0

Table 2. Boundary values of factors of plasma spraying of powder PT-NA-01

Level	I, A	$V_{p.g}$, m³/h	H, mm	Ar/N₂
+	500	1.50	160	0.7
−	400	1.26	100	1
0	450	1.38	130	0.85

process using powder Ni−5Al from 5.2 to 4.2 kW·h/m³ (by 20 %), this being a result of increasing the size of the high-temperature zone of the plasma jet.

Measurement of the velocity of the spraying particles in the plasma jet at a distance of 140 mm from the exit section of the nozzle by using instrument ISSO-1 showed that in spraying of powder PT-NA-01 with the extension the velocity of the particles was about 120 m/s, this being 25 % higher than the velocity of the particles in spraying without the extension (95 m/s).

Optimisation of the spraying parameters was performed by the method of mathematical experimental design [13], and the optimisation parameter was a material utilisation factor (MUF), which was determined in spraying on a flat surface (250 × 250 × × 1.2 mm) for each spraying variant (with and without the extension).

Weight of a sprayed coating and spraying powder was evaluated by using the KERN balance EMB 200-2 with a measurement accuracy of ±0.01 g.

Table 1 presents the matrix of the fractional (2^{4-1}) factorial experimental design for evaluation of MUF. Current, plasma gas flow rate, plasma gas composition and spraying distance which have the most substantial effect on the spraying process, were chosen as variable factors [14]. In addition to the variable spraying fac-

tors, the following factors were chosen as the constant ones: powder consumption − 32 g/min, spraying time − 15 s, and transporting gas flow rate − 0.21 m³/h.

The limits of variation of the factors were chosen on the basis of the experience of spraying using the said powder and characteristics of the spraying equipment. The boundary values of the factors are given in Table 2.

Table 3 gives the values of MUF in plasma arc spraying with and without the extension.

The regression equation was derived from the results of the experiment under conditions without the extension (Table 3) for the dependence of MUF on the spraying factors:

$$\text{MUF (\%)} = 48.1 + 0.045I - 6.46V_{p.g} - 2.08H + 1.8(\text{Ar}/\text{N}_2).$$

Parameters of spraying with the extension at a maximal value of MUF by using powder PT-NA-01 were determined in a similar way. In this case the regression equation for the dependence of MUF on the spraying factors has the following form:

$$\text{MUF (\%)} = 72.9 - 0.148I - 5.1V_{p.g} - 0.16H + 92.5(\text{Ar}/\text{N}_2).$$

As established as a result of analysis of the experimental results (Table 3), without the use of the extension the highest value of MUF was achieved in mode 6, which provides the maximal amount of the melted spraying particles and the lowest amount of the overheated particles, the presence of which leads to losses for evaporation and splashing of the particles melt.

Table 3. Values of MUF in spraying of powder PT-NA-01 with and without extension

Experiment No.	I, A	$V_{p.g}$, m³/h	H, mm	Ar/N₂	MUF without extension, %	MUF with extension, %
1	500	1.5	100	1	48	51
2	500	1.26	160	1	43	58
3	400	1.5	160	1	34	64
4	400	1.26	100	1	56	74
5	500	1.5	160	0.7	38	28
6	500	1.26	100	0.7	72	62
7	400	1.5	100	0.7	41	61
8	400	1.26	160	0.7	52	59
9	450	1.38	130	0.85	60	70
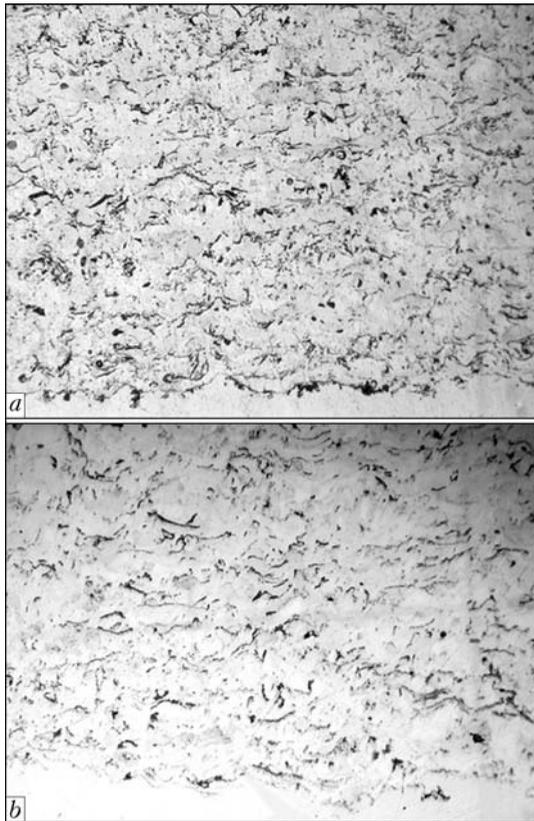
Figure 3. Microstructures (×200) of coatings sprayed by using powder PT-AN-01 without (mode 6, MUF = 72 %) (*a*) and with extension (mode 4, MUF = 74 %) (*b*)

Figure 4. Strength of adhesion of coatings produced by spraying without (*2*) and with (*1*) extension by using powder PT-NA-01

By using the extension, the maximal value of MUF was obtained in mode 4, which differed from mode 6 in a lower current (400 instead of 500 A) and in a composition of the plasma gas (pure argon instead of the Ar/N$_2$ mixture), this coinciding with the results of the above-described splat-test. This decrease in the specific energy of the spraying process for achieving the maximal value of MUF in the case of using the extension is attributable to increase in size of the high-temperature zone of the jet and in velocity of the particles.

The average value of MUF in spraying with the extension by using the Ar/N$_2$ mixture increased but insignificantly (from 51 to 53 %), whereas in the case of using argon as a plasma gas the average value of MUF in spraying with the extension grew from 45 to 62 %, compared to the average values of MUF achieved in spraying without the extension. This is related to the fact that in spraying without the extension the low-enthalpy (in case of argon used as a plasma gas) plasma is diluted with air, which leads to dramatic lowering of its temperature and decrease in size of the high-temperature zone. The use of the extension and the addition of N$_2$ as a high-enthalpy plasma gas make it possible to provide an extended high-temperature zone.

Figure 3 shows microstructures of the coatings sprayed with and without the extension by using powder PT-AN-01 at the parameters with the maximal value of MUF. Structure of the coatings consisted of the molten particles in the form of lamellae. In addition to pores, oxides uniformly distributed across the coating and being lighter in colour, compared to the pores, were located along the boundaries of the particles. This made it possible to distinguish them and evaluate the degree of oxidation of the coating material.

Analysis of structures of the coatings produced in modes with the maximal value of MUF allows a conclusion of the correspondence of the chosen spraying parameters to the process of deposition of coatings from the completely melted powder particles, which, upon colliding with the surface, form lamellae.

The coatings produced by spraying without the extension had porosity of 0.4 % and oxide content of 5 %. In case of using the extension, porosity of the coatings was 0.1 %, and oxide content was 4.5 %.

The coating to substrate adhesion strength was evaluated by the glue method according to GOST-14760–69 and ASTM C 633–79 by using tensile testing machine R-50 (maximal load — 50 kN). Spraying of four specimens at the spraying parameters with the maximal value of MUF was carried out simultaneously for each variant. Thickness of the coatings was 0.25 ± ± 0.03 mm.

Adhesion strength of the coatings sprayed without the extension was 30 ± 3.3, and that with the extension was 36 ± 2.8 MPa. The coatings produced with and without the extension differed in the character of fracture. The coatings sprayed without the extension fractured along the interface with the substrate, whereas the coatings sprayed with the extension fractured in the glue, this evidencing the really higher strength of adhesion of the coatings to the substrate, compared to the fixed value. Therefore, in spraying with the extension the coating to substrate adhesion strength increased not less than by 20 % (Figure 4).

CONCLUSION

The use of the protective extension increases the average velocity of spraying particles of powder PT-NA-01 by 25 %, improves heating of the powder particles, and decreases the required specific energy of the spraying process by 20 % due to increase in size of the high-temperature zone of the plasma jet. The

coatings produced by spraying with the extension contain 10 % less oxides (5.0 and 4.5 %, respectively), they have lower porosity (decreased from 0.4 to 0.1 %), and their strength of adhesion to the substrate grows by 20 % (from 30 ± 3.3 to 36 ± 2.8 MPa).

1. Donskoj, A.V., Klubnikin, V.S. (1979) *Electric plasma processes and units in machine building*. Leningrad: Mashinostroenie.
2. Dresvin, S.V., Donskoj, A.V., Goldfarb, V.M. et al. (1972) *Low-temperature plasma physics and technology*. Moscow: Atomizdat.
3. (1973) *Production of coatings by high-temperature spraying*. Ed. by I.K. Druzhinin, V.V. Kudinov. Moscow: Atomizdat.
4. Bobrov, G.V., Iliin, A.A. (2004) *Deposition of inorganic coatings*. Moscow: Intermet Engineering.
5. Lugscheider, E. (1988) The family of plasma spray processes — present status and future prospects. In: *Proc. of 1st Plasma-Techn. Symp.* (Lucerne, Switzerland, 1988), Vol. 1, 23—48.
6. Lugscheider, E., Rass, E., Nicoll, A.R. (1991) Underwater plasma spraying. In: *Proc. of 2nd Plasma-Techn. Symp.* (Lucerne, Switzerland, 5—7 June 1991), Vol. 1, 213—219.
7. Borisov, Yu., Chernyshov, A., Korzhyk, V. (1991) Structure and parameters of heterogeneous plasma jets shielded by water flow. *Ibid.*, 75—84.
8. Houben, J.M., Zaat, J.H. (1976) Shielded open air plasma spraying of reactive materials. In: *Proc. of 8th Int. Thermal Spray Conf.* (Miami Beach, USA), 78—85.
9. Baldaev, L.Kh., Borisov, V.N., Vakhalin, V.A. (2007) *Thermal spraying*: Manual. Moscow: Market DS.
10. Kudinov, V.V., Kosolapov, A.N., Pekshev, P.Yu. (1987) Extensions for formation of local shielding in plasma spraying. *Izvestiya SO AN SSSR. Series Technical Sciences*, 69—75.
11. Murashov, A.P., Demianov, I.A., Grishchenko, A.P. et al. (2009) Application of protective extension in thermal spraying of quasi-crystalline coatings. *The Paton Welding J.*, **4**, 46—47.
12. Borisov, Yu.S., Krivtsun, I.V., Muzhichenko, A.F. et al. (2000) Computer modelling of the plasma spraying process. *The Paton Welding J.*, **12**, 40—50.
13. Bondar, A.G. (1973) *Mathematical modelling in chemical engineering*. Kiev: Vyshcha Shkola.
14. Petrov, S.V., Karp, I.N. (1993) *Air-gas plasma spraying*. Kiev: Naukova Dumka.

AGGLOMERATED FLUXES
IN LOCAL WELDING PRODUCTION (Review)

V.V. GOLOVKO

E.O. Paton Electric Welding Institute, NASU, Kiev, Ukraine

USSR priority in development of agglomerated (ceramic) fluxes is noted. Stages of development of investigations on their improvement and widening of their application areas are described.

Agglomerated fluxes are a mechanical mixture of powder-like components made in the form of grit of appropriate granulation, cemented by a binder or sintering. Each granule of agglomerated flux consisting of strongly bound fine particles is characterized by a constant ratio of all ingredients. Granules of different size are close by specific weight that ensures absence of flux separation at its application. In this respect agglomerated fluxes differ favourably from other non-fused fluxes (mechanical mixtures).

A certain similarity in fabrication of granulated non-fused fluxes and ceramic products (material grinding, forming together with binder, subsequent heat treatment) formed the basis for calling these fluxes ceramic fluxes in Soviet scientific-technical and normative publications [1]. In foreign literature fluxes of this type are called agglomerated fluxes, and in IIW and ISO documents they are classified as bonded fluxes.

The priority of development of ceramic (agglomerated) fluxes belongs to the Soviet Union. A prerequisite for development of ceramic fluxes were experiments on automatic welding with feeding of non-fused flux into the arcing zone conducted as far back as in 1937 in the welding laboratory of N.E. Bauman MHTU [2]. As proposed by K.K. Khrenov granulated non-fused flux made from electrode coating charge was used in these experiments for the first time. Flux was fed in a small amount and open-arc welding was performed. This work was not taken further at that time, it, however, demonstrated the technological advantages of granulated flux compared to powder-like fluxes-mixtures.

More profound studies on development of ceramic flux composition for submerged-arc welding, investigation of metallurgical and technological features of this kind of welding consumables, development of the technology of their manufacture and application in the USSR were begun as far back as in 1948 by D.M. Kushneryov under the guidance of Prof. K.K. Khrenov in the Welding Production Chair of Kiev Polytechnic Institute, and starting from 1949 — in the Laboratory of Electrothermics of the Institute of Structural Mechanics of the Academy of Sciences of Ukr. SSR.

Registration Certificate of USSR Gostekhnika #2981-51-8 with priority of February 3, 1951 for ceramic fluxes was issued to K.K. Khrenov and D.M. Kushneryov.

Already the first works demonstrated the basic possibility of application in ceramic flux composition of ferroalloys, metals, carbon materials, carbonates, higher oxides of iron and manganese, alongside the regular slag-forming components [3, 4]. During the same period the broad possibilities offered by ceramic fluxes in terms of deposited metal alloying at application of low-carbon electrode wire, and improvement of weld resistance to porosity, were determined [4].

It should be noted that by the beginning of 1950s USSR already had centralized commercial production of fused fluxes which became widely accepted in many industries. However, the range of welding wires produced by local industry at that time was very limited, and did not satisfy the need of many users. In addition to limited possibilities of metallurgical impact on the weld metal, fused fluxes also featured a high sensitivity to the presence of moisture or rust on the edges being welded. Under the conditions, when low-carbon rimmed or semi-killed steel was the main material for welded metal structure fabrication, rust presence in the groove caused weld porosity [5].

Broad possibilities of variation of the composition of ceramic flux charge allowed successfully overcoming these problems. Moreover, at addition of various ferroalloys, alloying metal additives, and master alloys ceramic fluxes ensured an increase of weld strength, toughness, hardness and wear resistance, owing to weld metal alloying [6–9].

Submerged-arc welding was a new highly efficient process, which not only provided an increase of efficiency (by several times), but also guaranteed a high reproducibility of the results, while requirements to qualifications of workers-welders were significantly lowered. At the initial stage of development welding fluxes were regarded as a means for protection of the arcing zone from air and electrode metal losses, as well as for protection of the surrounding personnel from arc radiation.

Adequate realization of unique capabilities of the new welding process required an in-depth study, and conducting scientific research. Work performed in this direction, is systematized in a number of monographs [10–12]. Realization of fundamental postulates set forth in them, enabled development of ceramic fluxes increasing resistance to porosity by 2–3 times [13].

With improvement of steel quality the priorities in the field of welding consumables changed. It became necessary to develop fluxes with a low content of impurities, high refining ability, and rational alloying. The Academy of Sciences of Ukr. SSR deployed systematic studies of metallurgical features of welding with ceramic fluxes, allowing for increased requirements to welded joint quality and widening of the range of welded steels. As a result of this work, co-efficients of alloying element transition from the flux into the deposited metal were established experimentally, as well as the degree of influence of welding parameters on alloying element transition, that allowed calculation of the composition of flux alloying part by the specified composition of deposited metal with accuracy sufficient for practical purposes. Conducted studies showed that ceramic fluxes not only can alloy the deposited metal, but can also essentially lower its content of impurities, and improve the structure by modifying. These features are realized, for instance, at development of higher basicity fluxes, providing minimum oxidation of alloying elements in the weld pool, and improved cracking resistance of weld metal [14–16].

Mastering of the technology of mass production of increased and high-strength low-alloyed (HSLA) steels by local industry and widening of the scope of their application in welded metal structure fabrication brought to the forefront the problem of lowering of hydrogen content in the weld metal. Postulates defined by V.I. Dyatlov [17] on the predominant running of metallurgical reactions in the gas phase in submerged-arc welding were further elaborated in the field of development of fluxes designed for welding low-alloyed steels. As a result of investigation of the features of running of metallurgical reactions in welding with ceramic fluxes, systematized in the work by D.M. Kushneryov, it is established that application of a certain quantity of carbonates and higher iron oxides in the slag-forming base of the fluxes allows lowering both partial pressure of hydrogen in the arc atmosphere, and its content in the metal of welds and HAZ, and, due to that, ensuring a high resistance to cracking in thick steel welding. These developments were realized in practice in the form of fluxes for welding chromium-nickel stainless steels [18]. TsNI-ITMash under the guidance of K.V. Lyubavsky developed oxygen-free ceramic fluxes of FTsK type for welding high-alloyed steels [19], and at Zhdanov Metallurgical Institute K.V. Bagryansky developed a series of ceramic fluxes for surfacing parts of metallurgical equipment [20].

Beginning from 1960s, PWI deployed systematic investigations on development of ceramic flux compositions, technology of welding and surfacing with their application, as well as technology of mechanized commercial manufacture of fluxes of this type. Results of investigation in the field of metallurgy of welding with ceramic fluxes [21, 22], generalized in dissertation works of V.G. Svetsinsky [23], and V.M. Kiriakov, were realized at mastering of the technology of commercial production of ceramic fluxes at Nizhnedneprovsky Metalware Plant [24].

Appearance of new grades of low-alloyed steels, providing as a result of thermomechanical treatment ultimate tensile strength of not lower than 650 MPa and high impact toughness at low climatic temperatures, posed a new problem for the developers — producing cast metal of welds, which would be equivalent to base metal by the level of their mechanical properties. Solution of this problem required performance of investigations to study the possibility of controlling the weld metal structure by variation of welding flux composition. As a result of such work performance at PWI under the guidance of Prof. I.K. Pokhodnya, a new concept of structuring the ceramic flux composition was formulated, according to which the main alloying of weld metal should be performed at the expense of electrode wire (solid or flux-cored), while the flux has to fulfill the functions of providing the refining, microalloying and modifying of weld pool metal. The above approaches were used to develop ceramic fluxes for welding structures from low-alloyed steels in chemical engineering, at prefabrication of bridge metal structures [25, 26]. Volume of ceramic flux production in the USSR during this period of time was up to 2000 t per year.

An essential improvement of the quality of rolled stock for welded structure fabrication in the last quarter of the XX century led to the need of creation of new generation welding consumables developed on the basis of fundamental investigations of metallurgy of arc welding processes, physico-chemical processes in slag and metal systems, and metals science of low-alloyed steels. PWI staff performed a large scope of investigations aimed at elaboration of scientific approaches to solution of problems of formation of optimum structure of welded joint metal, required level of indices of weld metal formation, ensuring the specified characteristics of welded structures from low-alloyed steels of increased and high strength. As a result of performed research, generalized in dissertation works by V.V. Golovko and S.D. Ustinov, positive influence of certain non-metallic inclusions on initiation and development of ferrite components of metal of HSLA steels was established, providing an increase of both strength and toughness of welded joints [27–29]. Agglomerated fluxes, developed during this period, were accepted in welding in general and special shipbuilding, in fabrication of stationary and semisumbersible platforms for work performance on the World Ocean shelf [30].

Beginning from the end of 1990s PWI has conducted systematic investigations to study the possible influence of welding flux on the conditions of formation of weld metal microstructure. The possibility of forming non-metallic inclusions of specified composi-

tion in the weld metal by controlling the flux oxygen potential and alloying ability of welding consumable composition and ensuring strengthening of weld metal structure by solid solution alloying was shown.

In modern materials science non-metallic inclusions are regarded as active centers of formation of the required microstructure, without which it would be impossible to produce welded joints of HSLA steels with the level of mechanical properties equivalent to base metal. In foreign publications such a direction was called «oxide metallurgy», and technology of producing inclusions of a certain composition, morphology and size distribution in the metal — «inclusion engineering» [31, 32]. Performed thermodynamic calculations, numerical simulation of the processes of non-metallic inclusion formation both in the liquid metal of weld pool, and in the region of its solid-liquid condition, systematized in [33], allow taking development of modern local agglomerated fluxes to a new level, ensuring their high competiveness, compared to developments of leading world manufacturers of welding consumables.

Consideration of processes differing by their metallurgy, which are applied for manufacturing of welding fluxes, as one technological package, allowed suggesting a new process for flux manufacturing, which combined such advantages of fused fluxes, as lower susceptibility to atmospheric moisture absorption, high resistance of flux granules to breaking up during flux application with broad capabilities of controlling the metallurgical processes in the arcing zone and in the weld pool, characteristic for agglomerated fluxes [34]. The new technology envisages refining low-grade raw materials by their melting in open gas furnace with subsequent processing in electric-arc furnace and use as charge components in agglomerated fluxes. During flame processing as a result of high oxidation ability of gas medium an essential lowering of sulphur content in the slag is achieved, and features of metallurgical processes in electric-arc furnace allow refining the melt as to phosphorus. During agglomerated flux manufacture the charge materials, included into its composition, are not subjected to any heat treatment, which would allow performing such refinement, so that higher requirements are made to their composition as to impurity content. Application of higher purity synthetic slags in agglomerated flux composition widens the range of high-quality raw materials, and also improves such consumer characteristics of the flux, as resistance to atmospheric moisture absorption and granule breaking up during flux application due to presence of fused products in their composition. Here the possibility of flexible influence on welding process metallurgy, typical for agglomerated fluxes, is preserved. Introduction of such a technology of welding flux manufacturing in industry showed that local agglomerated fluxes, not inferior by their regulated characteristics to foreign analogs, are superior to them in terms of cost-effectiveness of application.

1. Khrenov, K.K. (1951) Ceramic non-fused flux for automatic welding. In: *Coll. dedicated to 80th anniversary of E.O. Paton*. Kiev: AN Ukr. SSR.
2. Nazarov, S.T., Chistyakov, A.N. (1939) Automatic arc welding with feed of granulated flux in arc. *Avtogennoe Delo*, **4**, 27—30.
3. Khrenov, K.K., Yarkho, V.I. (1940) *Technology of electric arc welding*. Moscow: Mashgiz.
4. Khrenov, K.K., Kushnerev, D.M. (1951) Ceramic non-fused fluxes for automatic welding. *Avtogennoe Delo*, **6**, 1—4.
5. Pidgaetsky, V.V. (1970) *Pores, inclusions and cracks in welds. Processes of formation and methods of prevention*. Kyiv: Tekhnika.
6. Kosmachev, I.G. (1952) *Automatic surfacing of multiblade tool*. Moscow, Leningrad: Mashgiz.
7. Khrenov, K.K., Kushnerev, D.M. (1953) Ceramic non-fused fluxes for automatic welding. In: *New methods of welding and cutting of metals*. Kiev: Gostekhizdat Ukr. SSR.
8. Khrenov, K.K., Kushnerev, D.M. (1954) *Ceramic fluxes for automatic arc welding*. Kiev: Gostekhizdat Ukr. SSR.
9. Bagryansky, K.V. (1955) Automatic surfacing of mill rolls. In: *Abstr. of Sci.-Techn. Conf. of Welders*. Moscow: Mashgiz.
10. (1948) *Automatic submerged-arc welding*. Ed. by V.V. Shevernitsky, B.I. Medovar. Kiev, Moscow: Mashgiz.
11. (1953) *Automatic electric arc welding*. Ed. by E.O. Paton. Kiev, Moscow: Mashgiz.
12. Frumin, I.I. (1961) *Automatic electric arc surfacing*. Kharkov: Metallurgizdat.
13. Kushnerev, D.M. (1959) About resistance of welds to formation of pores induced by rust in submerged-arc welding with ceramic flux. *Avtomatich. Svarka*, **4**, 25—27.
14. Khrenov, K.K., Gapchenko, M.M., Kushnerev, D.M. (1958) Automatic welding of cold-resistant steel 12N3 with ceramic flux. *Ibid.*, **12**, 19—22.
15. Khrenov, K.K. et al. (1959) Specifics of weld modification with titanium in automatic welding of medium-carbon steel. *Svarochn. Proizvodstvo*, **6**, 26—28.
16. Kushnerev, D.M., Grebelnik, M.P. (1960) Ceramic flux for automatic welding of stainless steel of 1Kh18N9T grade. *Ibid.*, **5**, 34—36.
17. Dyatlov, V.I. (1951) Specifics of metallurgical processes in submerged-arc welding. In: *Coll. dedicated to 80th anniversary of E.O. Paton*. Kiev: AN Ukr. SSR.
18. Khrenov, K.K., Kushnerev, D.M. (1961) *Ceramic fluxes for automatic arc welding and surfacing*. Kiev: Gostekhizdat Ukr. SSR.
19. Lyubavsky, K.V., Lvova, E.P. (1958) New fluxes for arc welding. *Svarochn. Proizvodstvo*, **10**.
20. Bagryansky, K.V. (1955) Automatic surfacing of steel rolls with ceramic flux. *Ibid.*, **5**, 37—41.
21. Podgaetsky, V.V. (1963) Reaction of hydrogen oxidation in arc atmosphere. *Avtomatich. Svarka*, **9**, 7—13.
22. Kushnerev, D.M., Golovko, V.V., Patrov, B.V. (1976) Effect of surface properties of contact phase on transfer of alloying elements from ceramic flux to deposited metal. *Ibid.*, **2**, 20—23.
23. Kushnerev, D.M., Svetsinsky, V.G. (1963) Investigation of automatic welding of high-strength cast iron with ceramic flux. *Ibid.*, **9**, 53—61.
24. Kushnerev, D.M., Svetsinsky, V.G., Lapchenko, V.A. (1971) Industrial production of ceramic fluxes. *Ibid.*, **4**, 66—69.
25. Kazakov, L.N., Dontsov, V.M., Shulepov, V.S. et al. (1984) Mechanical properties of welded joints of 09G2S steel made with ceramic flux ANK-47. *Ibid.*, **3**, 38—40.
26. Golovko, V.V., Grebenchuk, V.G. (1991) Weldability of 14KhGNDTs steel in different flux-wire combinations. *Svarochn. Proizvodstvo*, **5**, 13—15.
27. Pokhodnya, I.K., Golovko, V.V., Kushnerev, D.M. et al. (1990) Estimation of oxidizing ability of ceramic fluxes. *Avtomatich. Svarka*, **2**, 45—48.
28. Pokhodnya, I.K., Golovko, V.V., Denisenko, A.V. et al. (1999) Effect of oxygen on formation of acicular ferrite structure in low-alloy weld metal. *Ibid.*, **2**, 3—10.
29. Pokhodnya, I.K., Kushnerev, D.M., Ustinov, S.D. et al. (1987) Results of comparative tests of fused and ceramic fluxes applied in welding of 12KhN2MDF steel. *Ibid.*, **11**, 61—64.
30. Golovko, V.V. (2003) Application of agglomerated fluxes for welding of low-alloy steels (Review). *The Paton Welding J.*, **6**, 25—28.
31. Ogibayashi, S. (1994) Advances in technology of oxide metallurgy. *Nippon Steel Techn. Rept.*, 61(**4**), 70—76.
32. Ma, Z.T., Janke, D. (1998) Oxide metallurgy — its purposes and practical approaches. *Acta Met. Sinica*, 11(**2**), 79—86.
33. Golovko, V.V. (2004) Modelling of composition of non-metallic inclusions in weld metal of high-strength low-alloy steels. *Avtomatich. Svarka*, **5**, 3—7.
34. Golovko, V.V., Galinich, V.I., Goncharov, I.A. et al. (2008) Agglomerated fluxes — new products of OJSC «Zaporozhstekloflyus». *The Paton Welding J.*, **10**, 36—39.

REPAIR EXPLOSION CLADDING
OF THREADED CHANNEL OF CAR AXLES

L.M. LOBANOV[1]**, S.Yu. ILLARIONOV**[1]**, L.D. DOBRUSHIN**[1]**, N.A. PASHCHIN**[1]**, V.V. TISENKOV**[1]**, S.V. BONDAREV**[2]**,
S.A. GAVRILOV[2]**, N.A. SERGIENKO**[3] **and A.V. KUTISHENKO**[3]
[1]E.O. Paton Electric Welding Institute, NASU, Kiev, Ukraine
[2]Ukrainian Scientific-Research Institute of Car-Building, Kremenchug, Ukraine
[3]State Administration of Railroad Transportation in Ukraine «Ukrzaliznytsya», Kiev, Ukraine

The most common defect of axles of wheelsets of RU1-Sh type railway cars is damage or wear of threaded openings M20 for bolts that fix retainer plates of roller bearings. It is suggested that such threaded openings should be repaired by explosion cladding with a repair sleeve and subsequent cutting a new thread in it. Fatigue tests of the repaired openings showed that their life time is almost identical to that of the new axles.

Keywords: *explosion welding, explosion cladding, car axle, threaded channels, repair, fatigue test*

Increase of service life of rolling stock due to recover of working capacity of the worn parts for railway cars gains significant attention at modern stage of development of railway transport in Ukraine. Advanced technological processes characterized by high reliability with minimum prime cost and sufficiently easy realization under conditions of the car-repair enterprises of «Ukrzaliznytsya» are developed in particular.

The possibility of repair of the axles of wheelsets of RU1-Sh cars (ISO 1005-9–86 standard) has the large importance due to their high cost and significant metal intensity. This is in particular relevant since the car-repair enterprises of «Ukrzaliznytsya» have stored a significant amount of the damaged axles.

A damage or wear of threaded openings M20 for bolts that fix retainer plates of roller bearings is one of the most often and difficult to remove defects of the axles. The problem is that an insignificant mechanical damage of an element of the thread stops running of a bulky structure of critical application standard life time of which makes 8–15 years. A threaded opening has the high requirements on static strength, fatigue strength and accuracy of geometry.

Sealing using CO_2 welding or coated-electrode welding with subsequent drilling of an opening and cutting of a new thread is the most widespread method of repair of the threaded openings. However, given methods of repair have the disadvantages lying in high expenses on purchasing of new specialized welding equipment and consumables. It should be noted that A1, A2, A3 and A4 steel grades, from which the car axles are manufactured, refer to a class of limited weldability (GOST 1380–71), i.e. tend to crack formation in welding under standard conditions. This promotes a necessity in development of the special technological measures providing required quality of deposited metal. At that the geometry of plug type

welded joint results in complicated weld shrinkage that is an additional factor promoting crack formation in metal of an axle journal. The residual shrinkage shortenings promote deformation of geometry characteristics of the part and as a result inadmissible reduction of diameter of an axle location for roller bearing appears.

Alternative and simpler method is developed for car-repair enterprises of the Russian Federation. It is based on drilling out of the damaged opening, cutting of lager diameter thread in it with subsequent screwing of a cylinder sleeve with internal threaded opening M20. However, the specified method is characterized by low reliability since unscrew of the sleeve can take place under the effect of vibration loadings specific for operation of the axle of railway car during running.

The aim of the present work is a development of virtually new method for repair of the threaded openings M20 without disadvantages specific for methods mentioned above. The proposed method is based on application of the principles and procedure of explosion welding and has the following advantages:

• low cost of assembly equipment and consumables;

• strength of welded joint corresponding to specified mechanical characteristics;

• absence of heat effect typical for fusion welding and crack formation, respectively;

• elimination of formation and structural defects specific for fusion welding (pores, lacks of fusions, undercuts and slag inclusions);

• prevention of shrinkage shortenings and reduction of diameter of the axle journal location for roller bearing.

Materials and methods of investigation. An object for investigation was the damaged threaded channels M20-6N of axle journals RU1-Sh of 180 mm length (Figure 1). The axles with one damaged threaded opening per each end surface were used for adjustment of the repair technology to full-scale axles.
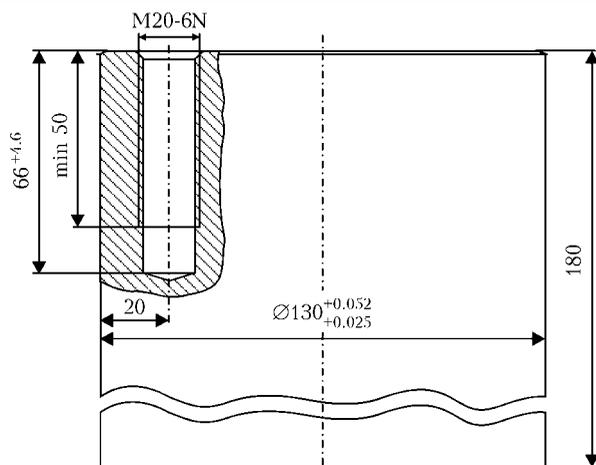
Figure 1. Scheme of axle journal

Figure 2. Scheme of internal explosion cladding using core charge: *1* — pipe being clad; *2* — cladding pipe; *3* — charge of explosive

It is impossible to deposit a repair coating directly over the rests of damaged thread using explosion welding method, therefore, the threaded opening was calculated to a diameter somewhat larger than 20 mm and then polished. The quality polishing was a necessary condition since explosion welding was carried out near a low border of area of welding (the minimum energy was applied for providing safety joint) due to impossibility of positioning of significant amount of explosive in the cladding sleeve and providing of a larger gap. A scheme of internal cladding using core charge (Figure 2), which is the most simple on technology of performance and easy for calculation of a mode of explosion welding, was used for explosion cladding of channels of 10—25 mm in diameter. A mixture of trotyl and ammonium nitrate was an explosive providing 2—3 km/s detonation rate and rate of contact point, respectively.

Steel 20 was selected as a material for cladding sleeve. This is conditioned by the fact that the cladding element is exposed to significant high-speed deformation in explosion welding, therefore, it should be sufficiently ductile and susceptible to cracking. The material with $\delta \geq 25$ % is the optimum for explosion welding if relative elongation in tension δ is used as an index of ductility. The charge with diameter close to critical was used in our case (if diameter of the charge is lower than critical, then a process of propagation of detonation wave does not take place). Therefore, a level of energy spent for plastic deformation of joining zone is to be minimized by means of selection of sleeve material with high ductility characteristics. Besides, the chemical compositions of sleeve and steel of axle should not have significant difference for preventing appearance of galvanic couple which can result in intensification of corrosion processes.

The materials of cladding sleeve and axle according to data of the quality certificate have the following mechanical characteristics: $\sigma_t = 420-425$ MPa, $\sigma_y = 274-286$ MPa, $\delta = 42-43$ %; and $\sigma_t = 520-560$ MPa, $\sigma_y = 300$ MPa, $\delta = 22$ %. Further investigations showed that small static strength of the sleeve in comparison
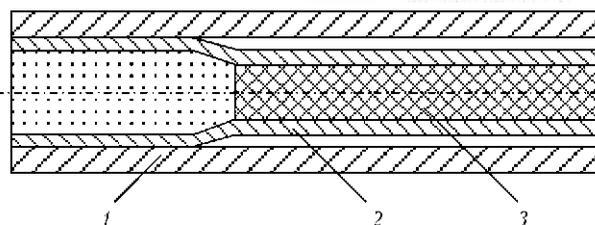
to that of steel of the axle is compensated by sufficient structural strength of a repaired thread whish is, first of all, should be resistant to small on level, but multiple loadings, taking place under conditions of real running of the axles. It should be noted that significant strengthening of sleeve metal takes place at high deformation rate in explosion welding that has positive effect on providing of the necessary structural strength of the thread joint.

Wall thickness of the cladding sleeve was equal 2.5 mm. The following factors were considered at that:
• inner diameter of the repaired surface should not exceed 17.3 mm;
• worn thread was bored to diameter somewhat larger than 20 mm;
• presence of some expansion of the opening at cladding due to effect of high pressure pulse;
• thinning of cladding sleeve due to its expansion in the process of throwing.

A banding was applied to the axle for preventing of significant expansion of opening channel in a process of explosion cladding as well as increasing diameter of axle journal (Figure 3). Nevertheless, at that the diameter of axle journal exceeded its nominal value (by 0.1—0.2 mm), therefore, further correcting turning was necessary.

A fatigue test was used as a method for evaluation of mechanical strength and service life of the repaired thread. The corresponding procedure and bench were developed by the specialists of SE «Ukrainian Scientific-Research Institute of Car-Building». Figure 4 shows a scheme of device providing performance of tensile test simultaneously for two threaded openings at $P_{max} = 98$ kN (10 tf) and $P_{min} = 49$ kN (5 tf) with
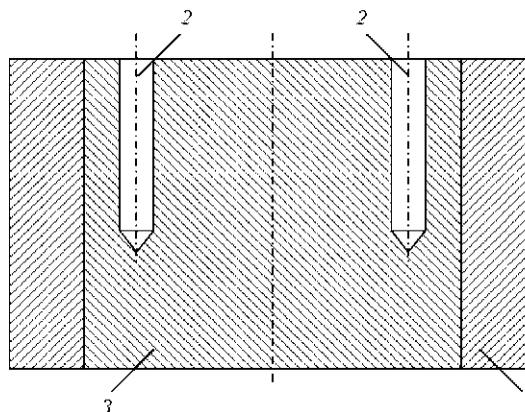
Figure 3. Scheme of banding of axle journal: *1* — tread ring; *2* — repaired openings; *3* — axle journal
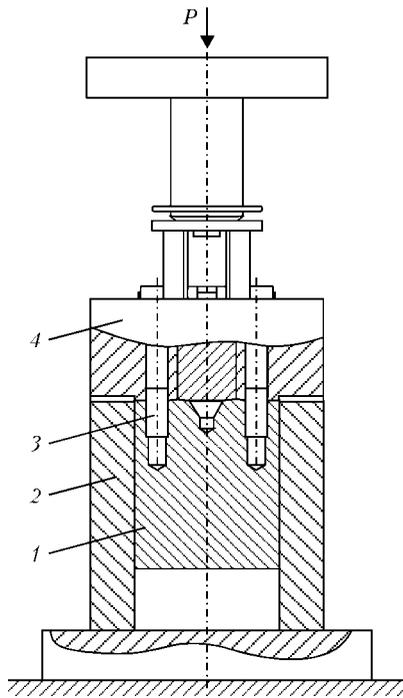
Figure 4. Scheme of device for axle journal testing: *1* — axle journal; *2* — cup; *3* — bolt; *4* — holder

loading frequency 5 Hz. The journals of new axles served as the base samples for comparison. Geometric characteristics of threaded openings M20-6N were verified before the test using Go–No-Go thread gage. Only two first screw threads were loaded, i.e. a bolt was twisted per two screw threads that made the test tougher since the bolt is to be twisted at minimum per 16 screw threads under the real situation of axle running. Loading of more screw threads resulted in break-away of a head or thread part of the bolts and provided no possibility for carrying the thread in the opening to full failure.

Figure 5 shows a cross-section of repaired threaded opening along the channel axis. A lack of penetration of 5 mm length is taking place close to the channel bottom that is character during realization of the process of explosion welding. The screw thread of only 45 mm length is to be cut according to Figure 1, therefore, presence of such a lack of penetration is insignificant and acceptable.

Figure 6 shows the microstructures of joints of steel of axle and repair sleeve along the opening axis at 3, 15 and 45 mm distance from its beginning.

Figure 5. Macrosection of repaired threaded opening
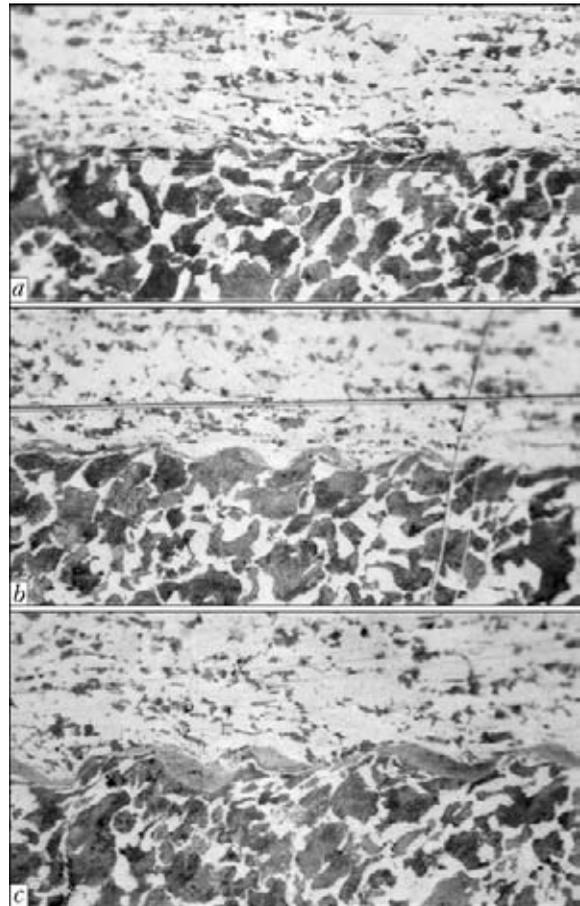
Figure 6. Typical microstructures (×400) of the joint metal of repair coating (steel 20 upwardly) and metal of axle journal at 3 (*a*), 15 (*b*) and 45 (*c*) mm distance from the beginning

Boundaries of the joining zone have mainly wave-like form and characterize by sufficient stability that indicate the presence of quality welded joint. At that dimensions of the wave are very small: excursion (two amplitudes) makes 2 μm and length is 6 μm. This is evidence of the fact that explosion welding was performed at low limit of welding parameter range. No changes of the metal structure outside the joining zone were found.

Results of fatigue tests of the samples of new axle journals of RU1-Sh type and journals with repaired threaded openings are given in the Table. Figure 7 shows the photos of the new and repaired openings of axle journals after the tests.

The minimum life time of the thread $N_p^{\min}$ (minimum number of cycles before failure with probability 0.95) was found by formula

$$\lg N_p^{\min} = \lg N - Z\alpha S_{\lg N},$$

where $\lg N$ is the logarithm of life time average value; $Z\alpha$ is the quantile of normal distribution for specified one-sided probability α at $\alpha = 0.95 Z\alpha = 1.645$; $S_{\lg N}$ is the root-mean-square deviation of the life time logarithm.

The minimum values of life time $N_p^{\min} = 127{,}000$ cycles of loading for samples of journals manufactured from the new axles and $N_p^{\min} = 122{,}000$ cycles of load-

Figure 7. General view of the openings in new (base) (*a*) and repaired (*b*) journals of axle after the tests

Figure 8. General view of repaired axles RU1-Sh

Figure 9. Repaired channel for thread cutting

ing for samples of the axle journals with threaded openings repaired using explosion welding method were obtained after processing of the test results.

Repair welding of threaded openings M20 on RU1-Sh full-scale axles. Two axles with damaged threaded openings (one per each edge) were represented for adjustment of the developed technology to RU1-Sh full-scale axles and further route tests of SE «Ukrspetsvagon». Figures 8 and 9 show a general view of the repaired axles and threaded channel. Reproducibility of explosion welding mode on full-scale axles and their models (quality of joint was controlled using metallographic investigations) was determined based on similarity of radial deformation of the clad channel. Diameter of the channel after cladding made 17.4−17.5 mm that is quite acceptable for cutting of thread M20-6N.

Repaired axles as a part of one car truck were put under the special car designed for transportation of mineral fertilizers in March 2011 and being used by SE «Ukrzalisnytsya» till present time. Current monitoring of repair welded joints was carried out. The car with repaired axles have already run 23 thou km without a damage and wear of the repaired threaded opening M20 as for October 2011.

Presented technology after insignificant modification can be recommended for implementation at car-repair enterprises of «Ukrzalisnytsya», first of all at «Ukrspetsvagon». One of the variants of practical realization lies in organizing of coming of the mobile teams of engineers from PWI to «Ukrzalisnytsya»

Results of fatigue tests of threaded openings of axle journals

Sample No.	Life time N_p, cycle	
	New axles	Axles with repaired threaded openings
1	156,000	145,000
2	134,000	124,000
3	142,000	145,000
4	165,000	150,000

enterprises for performance of repair work applying explosion cladding at working areas of a customer.

CONCLUSIONS

1. It is shown that the method of explosion cladding allows depositing of repair coating in the damaged threaded opening M20 of the axle journal of wheelsets for RU1-Sh type cars. At that the cracks in the journal metal and zone of joining with repair coating as well as shrinkage shortenings and reduction of diameter of location of the axle journal for roller bearing are absent.

2. It was determined that minimum values of fatigue life of the axles with threaded openings repaired by explosion welding method made 122,000 loading cycles that only 4 % lower of the base value for the new axles.

3. Two full-scale axles with repaired threaded openings M20 were route tested and showed no damage or unallowable wear after running of 23 thou km according to their condition in October 2011.

4. The developed technology has a perspective to be used at car-building enterprises of «Ukrzalisnytsya».

FEATURES OF PRODUCING SOUND WELDS IN ELECTRON BEAM WELDING OF THICK HIGH-STRENGTH STEELS

V.Ya. BELENKY, D.N. TRUSHNIKOV, G.M. MLADENOV and **T.V. OLSHANSKAYA**
Perm National Research University, Perm, RF

Features of formation and solidification of weld metal in electron beam welding of high-strength steels with deep penetration were investigated. Both the possibility of increasing the degree of structural inhomogeneity and prevention of appearance of specific defects in welding with electron beam oscillation are shown.

Pearlitic class high-strength alloyed steels 34KhN1M, 38Kh2NM, 40KhN2MA are widely used in manufacture of critical products for heavy and transportation engineering (axles, shafts and other heavy-duty parts). However, their poor weldability at application of arc welding processes greatly limits the possibilities of welded product design.

At present EBW is becoming widely accepted. It allows not only producing welds with high values of weld height-to-width ratio, but also provides minimum dimensions of the HAZ and high level of mechanical characteristics of welded joints. Statistical and numerical simulation is applied for EBW mode prediction [1–3]. At the same time EBW has a number of disadvantages: formation of specific defects in the weld root, instability of penetration depth, complexity of reproduction of electron beam focusing mode.

This work is a study of the features of producing sound welds at EBW of thick high-strength steels.

At the first stage of investigations cylindrical samples of 38Kh2NM steel with 30 mm wall thickness were welded in EB installation with ELA 60/60 power unit at 12 kW power and 14 m/h speed.

Figure 1. Macrostructure (×2) of weld metal in the transverse (*a*) and longitudinal (*b*) sections

Parameters of electron beam focusing were monitored and reproduced using a method developed by the authors, which is based on recording the high-frequency component of current of a non-self-maintained discharge in plasma. This discharge is excited in plasma, formed in the zone of application of high power density electron beam to the metal, through an electron collector located above the welding zone, and having a positive potential of 20–30 V relative to the product being welded [4, 5]. During experiments a component of 10–20 kHz frequency was singled out of the current spectrum of non-self-maintained discharge in plasma. Extreme values of this component amplitude were used to establish the «sharp» focusing of the electron beam providing the maximum depth of penetration at specified values of accelerating voltage and beam current.

Figure 1 shows macrosections of penetration zone obtained in welding by static electron beam. Macrosection clearly shows the keyhole penetration shape with a widened upper and narrowing middle and root parts of the weld, characteristic for welding mode with «sharp» focusing. The longitudinal section has specific root defects — peak formation and voids in the root part of the penetration zone.

Results of investigation of primary structure of weld metal established the presence of four characteristic zones, located along weld height, which are characterized by different dimensions and geometrical shape of primary crystallites (see Figure 1, *b*).

First zone (weld bead) consists of large polyhedral crystallites. Average diameter of crystallites, determined by the secant method, was equal to 0.25 mm in the cross section, and 0.32 mm in the longitudinal section, the depth of this zone being 1.5–2.0 mm.

The first and second structural zones form in the upper widened part of the weld. Macrostructure of these zones differs only slightly from the structure formed in arc welding processes.

The second zone consists of columnar crystallites directed normal to the fusion line in the weld cross-section, and practically vertically to its surface in the
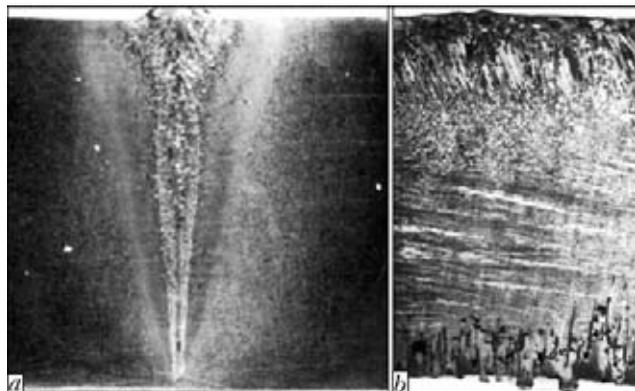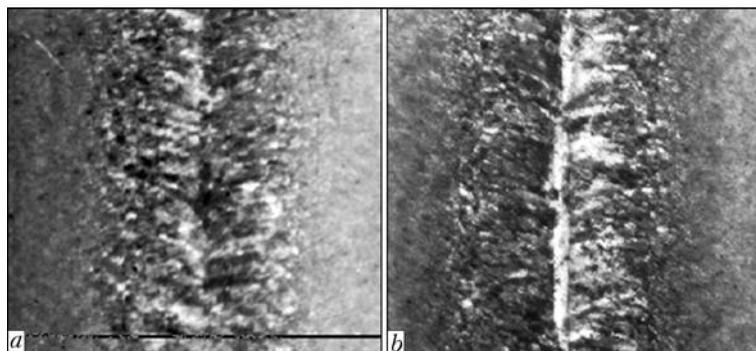
Figure 2. Nature of intergrowing of crystallites (×7) in the third (*a*) and fourth (*b*) zones

longitudinal direction. Average size of crystallites in the weld cross-section is equal to 0.9 × 0.3 mm, and in the longitudinal direction — 2.5 × 0.3 mm, second zone depth is 3.5−5.5 mm.

Third zone in weld cross-section consists of columnar crystallites, which intergrow in the weld center. Their axes are parallel to weld surface and normal to the fusion line. In the longitudinal section these crystallites have polyhedral structure (Figure 2, *a*). Average crystal diameter is equal to 0.15 mm, its length is about 0.66 mm, and angle of convergence of solidification fronts is minimum from both sides. Thus, intergrowing of crystallites in the weld center, reduction of their dimensions compared to crystallites of the first and second zones show that the solidification rate in this part of the weld is much higher. Increase of solidification rate is, certainly, related to more intensive heat removal, dependent on molten metal volume in different zones of the weld. Depth of the third zone is equal to 3.75−4.75 mm.

Difference of the fourth zone from the third zone consists in that in addition to columnar crystallites having the same orientation, in the central part of this zone fine polyhedral crystallites appear in the cross section (Figure 2, *b*). In the longitudinal section in the weld center these crystallites have columnar structure, being long and narrow with maximum length of up to 15 mm in the welding direction. Crystallite axes are practically parallel. In the fourth zone a considerable refinement of structure along the weld height was found. So, in the weld lower part in the cross-section crystallite length and width change from 0.97 to 0.27 and from 0.13 to 0.08 mm, respectively. In the longitudinal section crystallite length decreases

from 15 to 1.6 mm, and their width changes from 0.41 to 0.12 mm along the weld center. Depth of this zone is equal to 12.5−15.0 mm. Thus, the given results are indicative of the fact that solidification rate increases with increase of zone depth.

Specific defects (peak formation and cavities) were found in welds, which form only in the fourth zone, and the largest of them — on the boundary of the third and fourth zone.

Investigations of weld metal showed that its structure is a finely-dispersed ferrite-carbide mixture with a fringe of proeutectoid ferrite along the dendrite boundaries. Primary structure along the weld zones is also greatly different. In the widened upper part of the weld the metal structure is of a pronounced dendritic nature with a rather wide ferrite net (Figure 3, *a*). In the weld middle its metal structure is cellular-dendritic, grain size decreases practically two times (Figure 3, *b*). A fine-grained structure forms in the weld root part, which is close to cellular structure by its type (Figure 3, *c*).

Measurements of grain size (width of dendrites and cells) by weld height showed that no significant refinement of dendrites was found in the first three zones. Average value of dendrite width in these zones is in the range of 21−24 μm. An abrupt refinement of the structure occurs along the fourth zone depth — from 6 to 20 μm.

On the whole it can be noted that in EBW by a static sharply focused electron beam, weld metal is characterized by a considerable structural and mechanical inhomogeneity. In addition, specific defects form in the weld root part, markedly lowering the welded joint service properties.
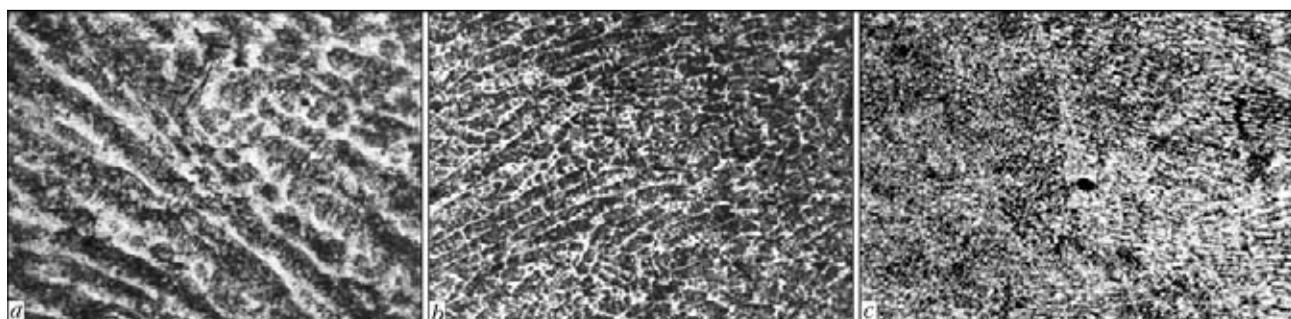
Figure 3. Microstructures (×300) of metal in the upper (*a*), middle (*b*) and lower (*c*) parts of the weld
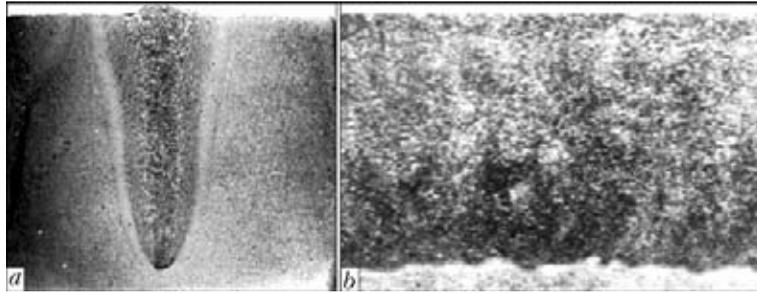
Figure 4. Macrostructures (×1) of weld produced in the transverse (*a*) and longitudinal (*b*) sections in EBW with X-shaped oscillations

The second stage included investigation of welded joint formation at EBW of 38Kh2NM steel with electron beam oscillation, which was performed in order to make a controlling impact on metal solidification processes and produce more sound welded joints. At selection of oscillation parameters (scanning frequency and amplitude) theoretical estimates proposed in [6] were used.

Studying welds made in welding with electron beam oscillation across and along the weld, as well as with electron beam rotation, showed that the above paths of electron beam scanning do not ensure any essential increase of structural homogeneity of weld metal, while absence of root defects is achieved only at large oscillation amplitude, leading to an essential lowering of penetration depth and increase of weld width.

Electron beam oscillation along the X-shaped path is of considerable interest in terms of formation of welds with a uniform structure and absence of root defects at optimum configuration of penetration zone [7]. In this connection formation of welds in EBW of 38Kh2NM steel with electron beam scanning along an X-shaped path was studied.

Welding was performed with mode parameters similar to those used in experiments on welding this steel by a static electron beam. Electron beam focusing, similar to experiments with a static beam, was optimized by parameters of high-frequency component of current of non-self-maintained discharge in the plasma formed in the beam impact zone.

Electron beam was scanned along the X-shaped path by changing phase shift φ of harmonic beam oscillations in two planes normal to each other by the following law:

$$\Delta\varphi = \frac{\pi}{2}\left[1 - \text{sign}\left(\sin \frac{1}{2}\,\omega t \right) \right],$$

where $\text{sign}(U) = \begin{cases} 1 \text{ at } U \geq 0 \\ -1 \text{ at } U > 0 \end{cases}$; ω is the oscillation frequency; *t* is the time.

Scanning frequency was selected in keeping with theoretical estimates taken from [6], and was equal to 600 Hz, and scanning amplitude, proceeding from the conditions of ensuring an optimum configuration of penetration zone with minimum increase of weld width, was 1.8 mm.

Investigation of macrostructure of a weld made at EBW with X-shaped oscillations showed an essential change of penetration zone configuration that is manifested in reduction of widening in the weld upper part, and formation of penetration zone of practically constant width. Penetration zone has the same characteristic zones, as in welding without electron beam oscillation, but here the level of penetration depth variation is markedly decreased, specific root defects are completely absent, and structure of the third and fourth zone changes (Figure 4). In the third zone the crystallites take an oval shape, which is almost polyhedral, and in the fourth zone the central section with polyhedral crystallites is increased. Columnar crystallites of this zone change their shape and become oval. Crystallite dimensions decrease along the entire weld length (Figure 4, *b*).

Thus, at EBW of high-strength steels an effective technique is electron beam oscillation along the X-shaped path at «sharp» focusing of the beam. In this case, production of weld metal with a high level of structural and mechanical homogeneity is ensured, and specific defects in weld root are absent.

1. Mladenov, G., Vutova, K., Wojcicki, S. (1998) Experimental investigation of weld depth and thermal efficiency during electron beam welding. *Vacuum*, **51**, Issue 2, 231–233.
2. Koleva, E. (2005) Electron beam weld parameters and thermal efficiency improvement. *Ibid.*, **77**, Issue 4, 413–421.
3. Erofeev, V.A., Logvinov, R.V., Nesterenkov, V.M. (2010) Specifics of application of equivalent heat source taking into account the strains and stresses in electron beam welding. *Svarka i Diagnostika*, **4**, 22–26.
4. Yazovskikh, V.M., Trushnikov, D.N., Belenky, V.Y. (2004) The mechanism of secondary emission processes in electron beam welding with electron beam modulation. *Welding Int.*, **18**, Issue 95, 724–729.
5. Trushnikov, D.N., Belen'kii, V.Ya., Yazovskikh, V.M. et al. (2007) Formation of a secondary-emission signal in electron beam welding with continuous penetration. *Ibid.*, **21**, 384–386.
6. Belenky, V.Ya. (1989) Estimation of optimal frequency of electron beam oscillation in welding. *Fizika i Khimiya Obrab. Materialov*, **1**, 106–111.
7. Belenky, V.Ya. (1986) Electron beam scanning along X-shaped trajectory as means of root defect refinement during electron beam welding. *Avtomatich. Svarka*, **9**, 35–37.

NEW TYPE OF PULSE STABILIZER
OF ALTERNATING CURRENT WELDING ARC

I.I. ZARUBA[1], **V.V. ANDREEV**[1], **A.F. SHATAN**[1], **G.N. MOSKOVICH**[1] and **V.A. KHALIKOV**[2]

[1]E.O. Paton Electric Welding Institute, NASU, Kiev, Ukraine
[2]Institute of Electrodynamics, NASU, Kiev, Ukraine

Peculiarities of the methods used for pulse stabilization of welding arc are considered. The fundamentally new approach and design of the pulse stabilizer of AC welding arc are offered.

Instability of arcing is observed in consumable and non-consumable (tungsten) arc welding using AC of commercial frequency (50 Hz) during change of electrode polarity. The various type pulse stabilizers of arcing are often used in practice for elimination of this disadvantage. Their operation is based on a transfer of additional pulse of energy in a discharge gap during transition of voltage and current through zero value. It results in a delay of gas deionization in the gap and facilitation of further arc ignition [1].

The pulse energy in many pulse stabilizers is pre-stored in the capacitors which are charged by special current sources. These sources can be self-contained or manufactured in a form of additional windings on magnetic circuit of the main welding transformer. Storage capacity (capacitor) and power source is the main assemblies of pulse stabilizers of arcing applied in industry at present time. They determine the structure and cost of these devices.

Meanwhile, the pulse stabilization of welding arc can be provided without application of the charge devices and storage capacities using the energy of welding circuit and at that making no damage to manufacturing process. Basis of such a method is an application of EMF of self-induction which appears during breakage of the welding circuit with quick-break switchboard and agrees in direction with voltage of the main power source and sums with it providing the arc discharge between the electrode and part and supporting stable arcing.

For the first time, verification of the proposed principle and device [2] was performed by the E.O. Paton Electric Welding Institute applicable to excitation of low-amperage arc in microplasma welding.

Vacuum electromagnetic relay *4*, winding of which with stabilitron *5* and dinistor *6* were in series connected to the output terminals of a rectifier bridge was connected to the power source for microplasma welding consisting of transformer *1*, rectifier bridge, *2* and smoothing supply choke *3* (Figure 1). Contact *7* of the electromagnetic relay is connected in parallel

to arc gap *8*. If there is no arcing, voltage in discharge gap *8* and contact *7* equals an open-circuit voltage of the power source. This voltage is not enough for a gap breakdown. A voltage pulse will be obtained if contact *7* is closed for some time and then rapidly opened. EMF of self-induction formed at that and having the same direction as voltage of the power source sums with the latter. The voltage pulse providing breakdown and arc ignition appears in the discharge gap (between the electrode and part). Resistor *10* regulates a value of high-voltage pulse. Capacitor *9* promotes keeping the contacts of relay from burning that increase life time of the device. Stabilitron *5* and dinistor *6* automatically switch on and off relay *4* depending on voltage at the output of power source. Voltage at the output of rectifier *2* will be equal the open-circuit voltage during the arc extinction that resulted in switching on of stabilitron *5* and dinistor *6*. Relay *4* switches on and closes contact *7*. Current, value of which depends on resistance of resistor *10*, will appear in the circuit. Voltage at the output of rectifier *2* will be reduced to the value providing opening of relay *4* which in turn opens contact *7*. Voltage pulse appearing at contact opening causes breakdown of discharge gap *8*. Ignition of the welding arc, feeding from transformer *1* and rectifier *2*, reduces the voltage in the discharge gap to value, at which relay *4* cannot switch on. A cycle will be automatically repeated at welding arc extinction.

Efficiency of the proposed principle of pulse stabilization of welding arc and appropriateness of its
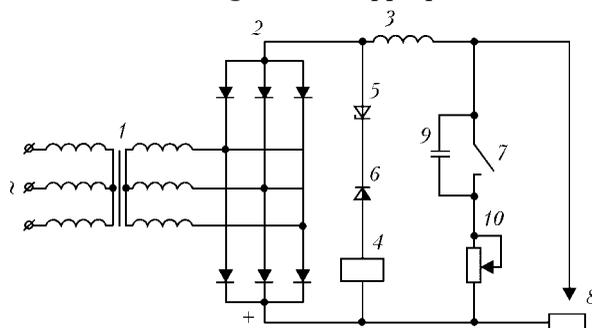
Figure 1. Scheme of device for pulse stabilization of arcing [2] (for designations see the text)

practical application, for example, at microplasma welding, i.e. DC welding, were verified by experimental results. Safe initial arc ignition and its re-ignition at accidental extinction were provided. Secure initial ignition and re-ignition of the arc gains meanwhile particular importance in welding on AC of commercial frequency (50 Hz) when arc ignites and extinct 100 times per second. Described device cannot be used for AC welding since a reaction on electrode polarity change was not provided for in it. Besides, the pulse voltage does not reach the required value because of insufficient rate of opening of electric circuit by the relay contacts in many cases.

The authors of this work had a task to develop a device for stabilization of welding arc of 50 Hz AC, for which no special power sources with charging capacitor was necessary, and transfer of sufficiently powerful energy pulse in the discharge gap was provided at the moments of initial excitation of the arc, change of electrode polarity and at random arc extinctions.

A key was developed for this, which can respond (open and close secondary circuits of the transformer) in several microseconds and provide necessary rate of current change during opening. The key is developed based on high-voltage transistor of BU508DF type with high response speed. Since EMF of self-induction, appearing in the secondary circuit of the transformer, achieves several kilovolts, the two suppressors (1.5E440A) limiting the voltage value on power transistor to 880 V are connected in parallel to the latter for protection from a surge. Current protection of the transistor is also provided. If specified value 1.4 V of voltage drop on the resistor in transistor circuit is exceeded then the power transistor would be forcedly closed by the controller. Besides, the controller allows also regulating and selecting the whole range of device parameters (amount of ignition and stabilization pulses, duration of the first or the second, time gap period between them and others).

The main point of new device [3] for initial ignition and re-ignition of AC welding arc and stabilization of its arcing lies in an additional switching unit, embedded in its scheme, providing switching on and off of the transistor after previously specified period of time. The device is actuated during the polarity change. The pulse being transmitted in this moment is followed

by a repeated pulse generated after previously determined time interval.

Figure 2 shows a structural scheme of the device being connected in parallel to welding transformer *1* and discharge gap — welding arc *8*. The scheme includes rectifier bridge *2*, high-voltage power transistor *3* and control unit *4* consisting of pulse former *5*, delay unit *6* and synchronization unit *7*. Additional elements of the scheme (surge protection, pulse current regulation, its duration and others) are not given here. The scheme provides a voltage control in the discharge gap and delivers a controlling signal for switching on and off of the high-power transistor at the moment of polarity change. The signal consists of two parts following one after another with a time gap determined by operator. It makes one fourth of a period of 50 Hz AC in our case.

Functioning of the high-voltage power transistor (switching on and off during several microseconds) takes place for the period of controlling signal activity that results in voltage surge in the discharge gap, its breakdown and welding arc ignition. If voltage of the power source increases to the required value (ignition voltage U_{ign}) at that, then secure arcing will proceed during the whole part of semi-period. Otherwise, the arcing is established by the second pulse which follows after one fourth of the period and almost equals the maximum value of voltage of the power source, due to which secure excitation and further arcing are provided.

Switching on of welding transformer *1* provides appearance of open-circuit voltage $U_{o.-c}$, changed according to a sine law, at the output terminals of the transformer as well as in discharge gap *8*. Control unit *4* switches in use high-voltage transistor *3* at the moment of reaching of zero value ($U_{o.-c} = 0$) that results in appearance of the surge, breakdown of discharge gap *8* and arc ignition. If pulse energy or voltage of the power source at this moment of time are not sufficient for support of arc discharge, then the stable arc ignition is provided by the second pulse, which will appear at the moment close to maximum voltage of the power source. Monitoring of arc voltage and feeding of the energy pulses in the discharge gap during polarity change are continuously performed by the control unit.

Instability of the welding process can be caused by polarity charge as well as arc extinctions and other reasons. The proposed device also allows performing re-ignition in these cases. Time of re-ignition depends on the moment of arc extinction. Switching on of the transformer at the beginning of the process takes place in any moment of the period, however, the switching unit is actuated only during the polarity change. Excitation of the arc may not take place at once since sufficient amount of energy is not yet stored in the welding circuit at the beginning of the process. The discharge gap has no residual ionization at that and
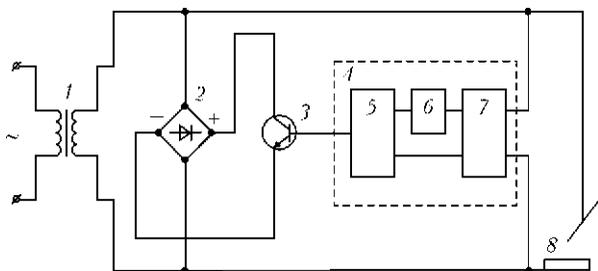
Figure 2. Structural scheme of device connected to welding transformer for excitation and stabilization of AC welding arc (for designations see the text)
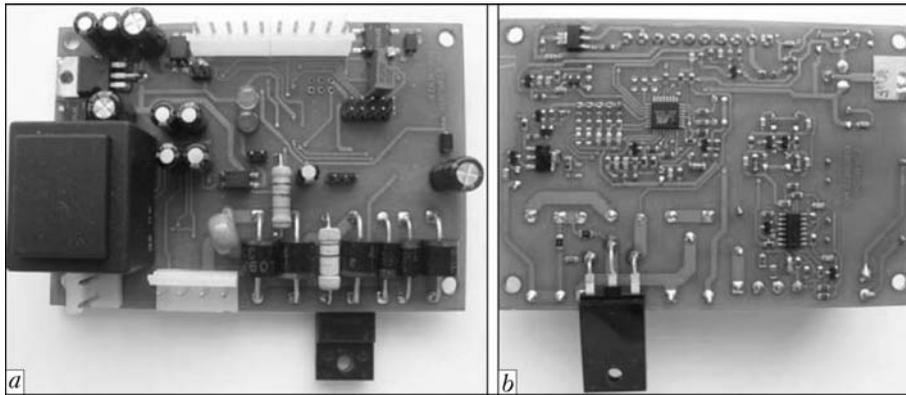
Figure 3. General view of front (*a*) and rear (*b*) side of board for pulse stabilizer of AC welding arc

voltage in it can be equal zero in this moment. However, the second pulse coinciding with the maximum value of open-circuit voltage and summing with the latter follows the first one after one fourth of the period (the time is stated by operator) and provides safe arc ignition. It should be noted that appearance of the energy pulse during arcing will make no notable influence on the process of welding due to short-term activity of the pulse.

If the arc extinction takes place during the first fourth of the period it can be easily ignited due to pulse following the first after one fourth of the period and coinciding with the amplitude value of open-circuit voltage. Arc ignition will take some time if its extinction takes place during the part of the period

with sine drop of voltage. There can be no arc ignition at polarity change but it will be ignited by second pulse also summing with the maximum of open-circuit voltage.

New pulse devices (Figure 3) have already find commercial application as AC arc stabilizers and oscillators for argon-arc welding and other cases.

1. Paton, B.E., Zaruba, I.I., Dymenko, V.V. et al. (2008) *Welding power supplies with pulsed stabilization of arc burning*. Kiev: Ekotekhnologiya.
2. Lobachev, V.M., Zaruba, I.I., Shelyagin, V.D. et al. *Device for exciting and supply of low-power arc*. USSR author's cert. 427805. Prior. 15.02.1971. Publ. 15.05.74.
3. Paton, B.E., Zaruba, I.I., Andreev, V.V. et al. *Device for ignition and re-ignition of AC welding arc*. Pat. 62596 Ukraine. Publ. 12.09.2011.

ELECTRODE COMPRESSION DRIVE FOR RESISTANCE SPOT MICROWELDING

Yu.N. LANKIN, V.F. SEMIKIN, P.P. OSECHKOV and **E.N. BAJSHTRUK**
E.O. Paton Electric Welding Institute, NASU, Kiev, Ukraine

Electrode compression drive for resistance spot microwelding was developed on a base of a step motor for spring dosing of the compression force. The drive allows implementation of complex cyclograms of compression of electrodes and programmed variation of their feed speeds.

K e y w o r d s : *resistance spot microwelding, electrode compression drive, microcontrol*

The electrode compression drive for resistance spot welding should provide displacement of the upper electrode relative to the fixed lower one and compression of the workpieces welded at a preset force. In resistance spot welding machines the stroke of the movable electrode is usually 5–20 mm, and the electrode compression force is adjustable from 1 to 80 N [1].

Based on the peculiarities of the process of resistance spot welding, its optimal cyclogram should correspond to that shown in Figure 1 [2]. The cyclogram has three stages: *I*, *II* and *III*. In stage *I*, preliminary reduction F_r serves to remove gaps between the work-

pieces and provide the required values of electrode–workpiece contact resistances in the cold state. Monotonous growth of F_w in stage *II* allows maintaining the stable pressure between the workpieces, despite increase in the contact area and liquid nugget diameter. Two regions *a* and *b* can be distinguished in stage *III*: F_w in a small first region is kept constant (usually for 0.03–0.10 s) to provide some cooling of the external metal layers of the workpieces and prevent deep dents in forging; and forging force F_f is applied and maintained in the second region to decrease tensile stresses and buckling of the joints, and to prevent hot cracks and cavities. However, in practice the force cyclogram is made simpler depending on the thickness, properties, configuration and degree of criticality of
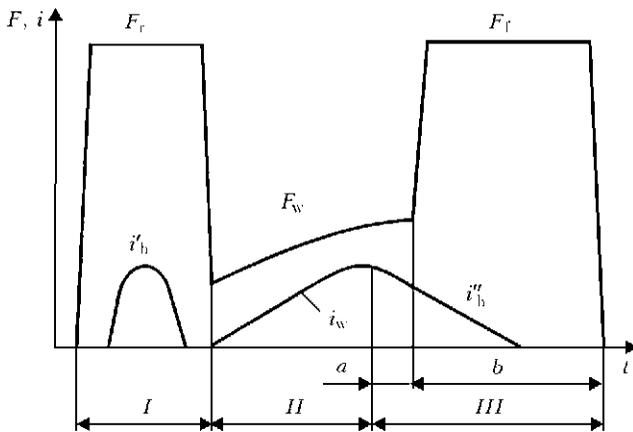
Figure 1. Optimal spot welding cyclogram: i_w — welding current; i_h' — heating current; i_h'' — postweld heating current

the joints, quality of fit-up, as well as real capabilities of the welding equipment.

The following drives are used in resistance spot microwelding machines to displace the movable electrode and generate the compression force for the workpieces welded: pedal-load, spring, pneumatic, hydraulic, electromagnetic and pneumatic-hydraulic. Spring drives received wide acceptance in the machines for resistance spot microwelding of small thicknesses [1]. These drives generate the force due to compression of springs, which is provided by pressing the foot pedal by a welder using a separate pneumatic drive, electromagnet or electric drive with eccentric.

Below we describe the spring drive for displacement and compression of electrodes, based on a linear
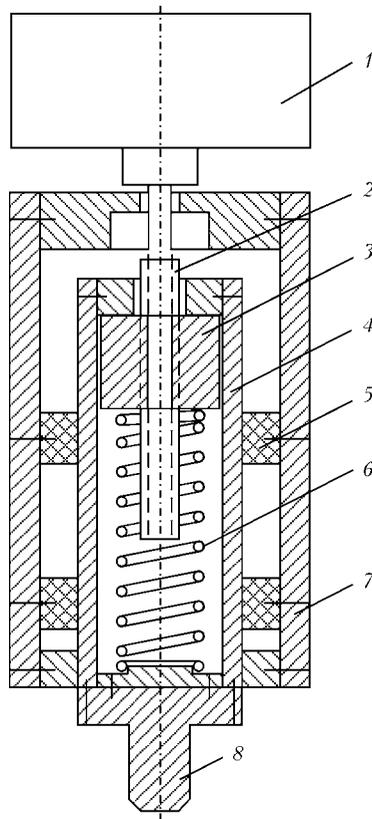
Figure 2. Kinematic diagram of spring mechanism of electrode compression drive with step motor (for designations see the text)

drive with a step motor (SM). Kinematic diagram of the drive is shown in Figure 2. Casing 7 of the electrode displacement and compression drive is immovable and fixed to the frame of the resistance spot microwelding machine. Electrode 8 together with cup 4 is moved along fluoroplastic guides 5 with respect to casing 7. Prior to welding, electrode 8 together with cup 4 is located in the upper position, i.e. the electrode is lifted. When motor 1 is switched on «to rotation», screw 2 connected to the shaft starts rotating. As a result, nut 3 is moved down along the screw. Through spring 6 the nut affects cup 4 and electrode 8 connected to it. The latter is moved down to touch the workpiece surface. Spring 6 is not practically compressed because of a low sliding friction force in contact between polished cup 4 and fluoroplastic guides 5.

The electrode stops moving after it touches the worpiece surface, and nut 3 while moving down starts compressing spring 6. The force of compression of the spring is transferred to electrode 8, thus generating the welding force. The value of this force is proportional to the force of compression of the spring, i.e. the stroke of the nut, and can be easily adjusted by the quantity of steps of SM 1 after touching the workpiece by the electrode.

To provide sound welded joints in microwelding of wire to sheet, wire to wire, etc., it is required that the compression mechanism be characterised by a low time lag [1]. The drive developed meets in full this requirement. The mass of the movable part in it is determined only by masses of electrode 8 and cup 4, i.e. it is minimal.

The use of SM makes the control system much simpler, as no displacement sensors are required to determine displacement of the electrode and compression of the spring. Structural diagram of control of the electrode compression drive is shown in Figure 3. «Microchip» microcontroller 3 performs all the main control functions. Signals from control panel 2 and sensor 1 of touching a workpiece by the electrodes are fed to its inputs. Microcontroller 3 feeds control signals to SM controller 4. Output signals of controller 4 control full-bridge driver 5, which SM 6 is connected to. Acyclic four-winding SM with permanent electromagnets DShI-200-2 provides torque of 0.225 N·m at an acceleration frequency of 1000 Hz.

The angle of rotation of the motor shaft in perormance of one control pulse is 1.8° (200 ppr). Microcontroller 3 feeds a series of pulses to motor controller 4, the frequency of which determines the speed of the motor, and the quantity of which — the angle of rotation of the shaft and, hence, the length of displacement of nut 3 (Figure 2). In addition, the microcontroller sets the direction of rotation and length of step of the motor. Controller 4 allows decreasing the step of the motor two times (from 1.8 to 0.9 deg/step) to provide a smoother motion of the motor.
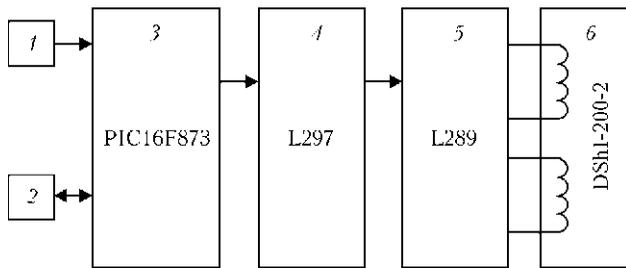
Figure 3. Structural diagram of control of electrode compression drive (for designations see the text)

Figure 4. Cyclogram of operation of the electrode displacement and compression drive: h — electrode displacement length

The mode setting and welding switch on buttons, as well as the alphanumeric display of parameters are located on control panel *2*.

The maximal acceleration frequency of DShI-200-2 (the maximal control frequency, at which the unloaded motor can be started up and stopped without step skipping) is 1000 Hz. A smooth acceleration by gradually increasing the control frequency is used to achieve a higher rotation speed. The smooth acceleration for our drive allowed doubling the frequency of steps of SM compared to the acceleration frequency.

Owing to the use of SM and microprocessor control the developed drive makes it possible to implement any algorithm of displacement and compression of electrodes, e.g. indicated in study [1]. Figure 4 shows implementation of optimisation of the electrode displacement and compression force cyclogram similar to that shown in Figure 1. The electrode compression force is set by the quantity of steps of SM. The maximal compression force equal to 60 N is varied at discreteness of 0.07 N and maximal speed of 120 N/s.

Like the electrode compression force, the electrode displacement length is determined by the quantity of steps of SM by feeding a preset quantity of control pulses to it from the microcontroller, and the displacement speed is determined by the frequency of these pulses. The said parameters can be varied over wide ranges. The maximal stroke of the electrode is 10 mm, discreteness of setting of the displacement is 0.07 mm,

and the maximal displacement speed is 14 mm/s. The drive allows performing the shock-free operation of the electrodes by using the programmed decrease of speed of SM before touching the workpiece by the electrode. This provides decrease in mechanical wear of the electrode tip, increase in sharpening intervals, rise in productivity and extension of service life of the electrodes.

CONCLUSION

The developed electrode compression drive for resistance spot microwelding machines provides precise performance of setting of the displacement and variations in the electrode compression force following the any complexity programs. The drive is characterised by compactness, relative simplicity and low time lag of its movable part. Its drawback is a lower operation speed compared to pneumatic and hydraulic electrode compression drives.

1. Moravsky, V.E., Vorona, D.S. (1985) *Technology and equipment of spot and projection capacitor-discharge welding*. Kiev: Naukova Dumka.
2. Orlov, B.D., Chakalev, A.A., Dmitriev, Yu.V. et al. (1986) *Technology and equipment for resistance welding*. Moscow: Mashinostroenie.

IMPROVEMENT OF METHOD OF PLASMA SURFACING WITH SIDE FEEDING OF FILLER WIRE

K.P. SHAPOVALOV[1], **N.A. MAKARENKO**[2] and **L.A. GRANOVSKAYA**[3]

[1]PC «NKMZ», Kramatorsk, Ukraine
[2]Donbas State Machine Building Academy, Kramatorsk, Ukraine
[3]OJSC «SIS-Soda», Slavyansk, Ukraine

A method of plasma surfacing with side feeding of solid and flux-cored wires was improved. A feature of this method is an alternating pulse nature of burning of straight polarity arcs between plasmatron nonconsumable electrode−item and plasmatron nonconsumable electrode−wire that increases surfacing efficiency and decreases base metal penetration depth.

K e y w o r d s : *plasma surfacing, filler wire, magnetic blow, straight polarity plasma arc, alternating mode of arcing, increase of surfacing efficiency, penetration of base metal*

Several methods of plasma surfacing with side feeding of filler wire [1−3] were developed for commercial application:

• plasma jet surfacing with current-carrying filler wire at electrically neutral item (Figure 1, *a*);

• plasma arc surfacing with neutral filler wire (Figure 1, *b*);

• twin-arc surfacing at which plasmatron, wire and item are alive (Figure 1, *c*)

An analysis shows that each of the methods have its advantages and disadvantages. Plasma arcing takes place between the filler wire and plasmatron nonconsumable electrode in surfacing with neutral item. Efficiency of surfacing increases in this case, however, there is a possibility of appearance of lacks of fusion in the base metal due to low heat input. Small process efficiency is the main disadvantage of the second method of plasma surfacing with neutral filler wire. The most widespread is the third method providing for twin arcing: one arc burns between plasmatron nonconsumable electrode and item and second one — between plasmatron nonconsumable electrode and filler wire. At that, regulation of heat input into the

wire as well as item can be performed during change of current of two arcs.

However, magnetic blow is observed in simultaneous burning of two arcs and their electromagnetic coupling, thus, current of the arc of plasmatron nonconsumable electrode−filler wire is to be limited. Its maximum value can be taken from relationship [4] $I_a = 0.266I + 90$ (A).

Surfacing efficiency of more than 10 kg/h [4] as well as reduction of depth of penetration in the base metal cannot be obtained at that resulting in increase of surfacing costs.

Thus, the known methods of plasma surfacing with side feeding of the filler wire have one or another disadvantages and problem of increase of technical and economical indices of this process is still relevant.

The aim of the present study lies in improvement of efficiency of the process of plasma surfacing with filler wire by increase of the heat input in the filler wire at controlled heat input into the base metal.

The effect of magnetic blow appearing during an interaction of two arcs is to be reduced to a minimum for achievement of the indicated aim. A method of plasma surfacing with alternating burning of straight polarity arc was developed to solve this task. The method provides for burning of only one arc at each
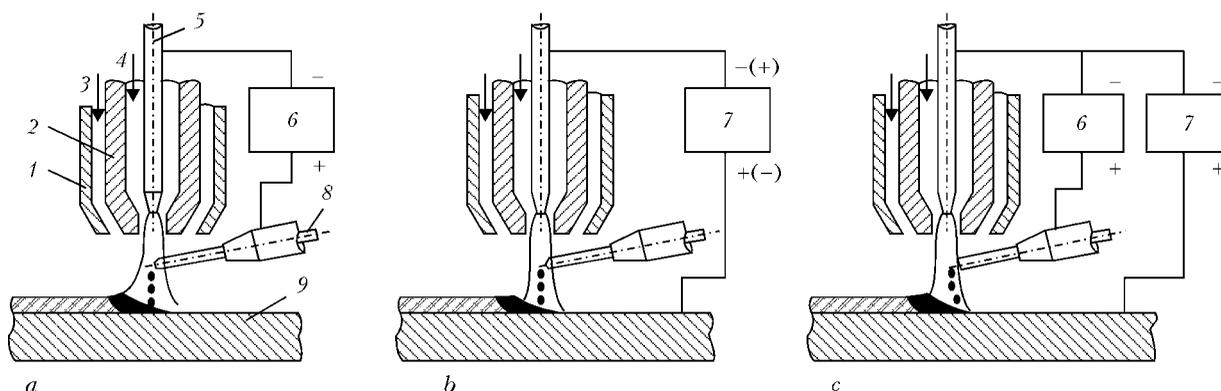
Figure 1. Scheme of plasma surfacing with side feeding of filler wire by plasma jet with current-carrying filler wire (*a*), by plasma arc with neutral filler wire (*b*) and by twin arc (*c*) [3]: *1, 2* — shielding and plasma-shaping nozzles, respectively; *3, 4* — shielding and plasma gases; *5* — electrode; *6, 7* — power source of indirect and direct arcs; *8* — wire; *9* — item
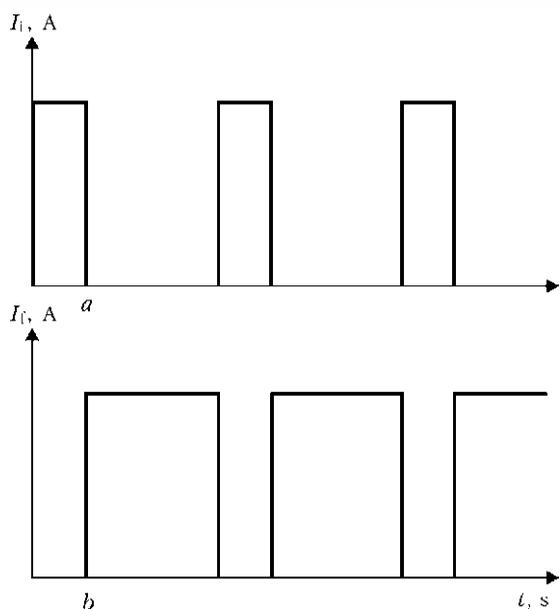
Figure 2. Diagram of operation of TOR-350 unit: *a* — current of arc of plasmatron nonconsumable electrode–item; *b* — plasmatron nonconsumable electrode–filler wire

Figure 3. Simplified principle scheme of power source for TOR-350 unit: $T1$ — power transformer; $T2$ — transformer of arc exciter; $VD1-VD3$ — diodes; $K1$, $K2$ — contactor switches; $R1$, $R2$ — ballast rheostats; $R3$, $R4$ — resistors

moment of time: plasmatron nonconsumable electrode–item or plasmatron nonconsumable electrode–filler wire (Figure 2) that allows eliminating the mutual electromagnetic influence of the arcs.

Amount of heat input, which is put in the filler wire and item, can be easily changed by regulation of current pulse duration achieving at that the necessary surfacing efficiency and reducing penetration depth of the base metal. In a number of cases reduction of penetration depth of the base metal allows multilayer surfacing be replaced by one-layer that makes significant influence on a prime cost of the surfaced parts.

Unit TOR-350 for plasma surfacing of the flat parts was developed for realization of the developed technology. Figure 3 shows a principle scheme of unit power source.

The power source operates in the following way. A pilot arc is excited by the arc exciter. The pulse transformer $T2$ of the latter is switched in series into a circuit of plasmatron nonconsumable electrode. Contactor switch $K2$ is closed at that and current of the pilot arc is limited by resistor $R3$ and makes around 60 A. The main arc is excited at filler wire contact with the item and the contactor switch $K2$ is opened at that and current of the pilot arc is additionally limited by resistor $R4$ to 20–25 A. A control circuit (CC) switches in turn the groups of thyristors $VS1-VS3$ or $VS4-VS6$ supplying the filler wire or item. It should be noted that the thyristors operate in switching mode and current regulation of each arc is performed by the ballast rheostats. Figure 4 shows general view of the power source of the unit.

The unit operates in mode with neutral item at switched on thyristors $VS1-VS3$ and switched off thyristors $VS4-VS6$, and mode with neutral filler wire is used in the case of constantly switched on
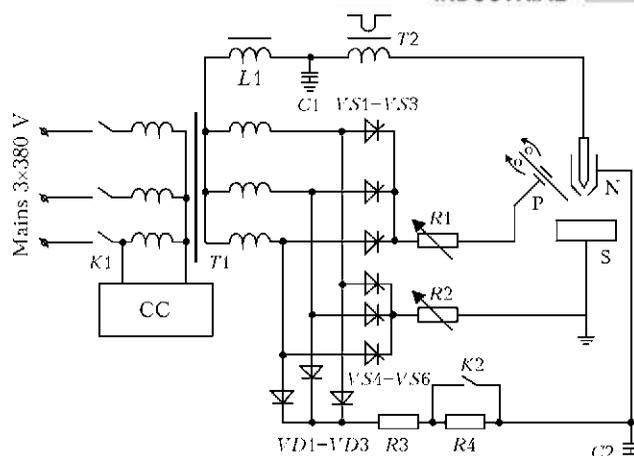
thyristors $VS4-VS6$ and switched off thyristors $VS1-VS3$. The unit woks in normal mode of plasma surfacing with current-carrying filler wire at constantly switched on thyristors $VS1-VS3$ and $VS4-VS6$. A self-contained cooling system of the plasmatron is switched on by the power source.

Preliminary investigations showed that the efficiency can be increased up to 16 kg/h applying plasma surfacing with alternating arcing, and penetration depth of the base metal at that makes not more than 2 mm.

The unit is used for surfacing of iron-based high-chromium alloy resistant to abrasive wear on plates under commercial conditions. Surfacing of the plates from steel 20 of 40 mm thickness is carried out with preliminary heating up to 600 °C in furnace, furnace soaking at the same temperature during 20 min after surfacing and there cooling. The following mode of surfacing was used at that: current of the arc pulse of
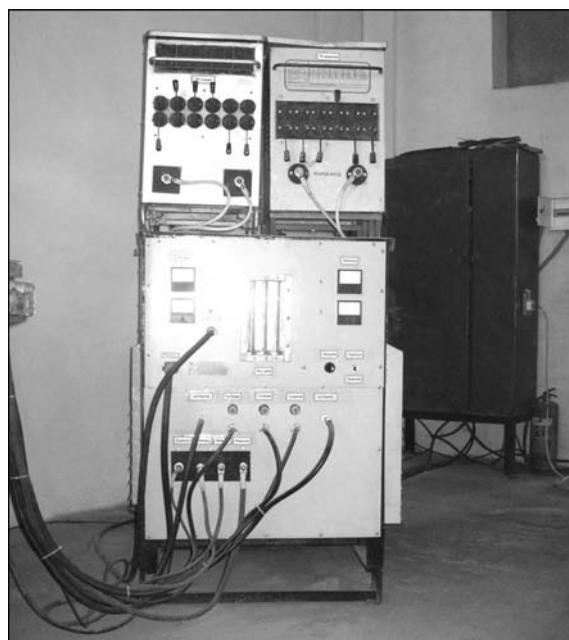
Figure 4. Power source of TOR-350 unit for plasma surfacing of flat parts using antiphased pulse current

plasmatron nonconsumable electrode–item made 160 A, of plasmatron nonconsumable electrode–filler wire was 210 A; duration of pulse of the arc current being 0.1 s for plasmatron nonconsumable electrode–item and 0.3 s for plasmatron nonconsumable electrode–filler wire; surfacing rate made 8.72 m/h, consumption of plasma argon showed 4 l/min and 18 l/min of argon for shielding.

Degradation of quality of formation of the deposited bead at pulse duration increase should be noted.

CONCLUSIONS

1. It is shown that efficiency is increased and penetration depth of the base metal is reduced at plasma twin-arc surfacing with side feeding of filler wire and alternating burning of straight polarity pulse arc.

2. It is determined that duration of the current pulses should not exceed 0.3 s for providing good formation of the deposited metal.

3. The unit for plasma surfacing by filler wire with alternating burning of pulse arc was developed. The unit is universal since other methods of plasma surfacing can also be realized.

1. Vajnerman, A.E., Shorshorov, M.Kh., Veselkov, V.D. et al. (1969) *Plasma surfacing of metals*. Leningrad: Mashinostroenie.
2. Sidorov, A.I. (1987) *Recovery of machine parts by spraying and surfacing*. Moscow: Mashinostroenie.
3. Gladky, P.V., Pereplyotchikov, E.F., Ryabtsev, I.A. (2007) *Plasma surfacing*. Kiev: Ekotekhnologiya.
4. Hiroya, T., Misuaki, M., Shaji, I. et al. (1978) Characteristics of plasma arc welding with wire addition. *Transact. of JWS*, **1**, 35–40.

Memorable dates

AT THE ORIGINS OF INTEGRATED DEVELOPMENT OF WELDING PRODUCTION

80 years ago Evgeny O. Paton for the first time in the world put forward an idea about integrated development of the theory and practice of welding and started forming specialized research and design organization with the purpose of solving various tasks in the path of progress of welding production

In 1929 academician Evgeny Oskarovich Paton, known bridge-builder, takes a decision to apply welding in bridge construction, and organizes an electric welding laboratory. The scientist rather quickly designed rational welded assemblies of span structures, machines and boilers, developed methods of strength testing and analysis of welds, began designing the bridge decking, started consulting designers and production specialists. Welding was already applied in bridge repair and construction in the USSR and other

countries, but many specialists were unwilling to eliminate riveting and bolted joints, fearing failures which occurred in bridges across the Albert channel in Belgium. For three years E.O. Paton with several associates performed a large scope of work to study strains, developed a number of welded structures and proved that the designers did not take into account the features of welding and simple replacement of technology lead to catastrophies. He came to the conclusion that the success of welding development and introduction depends on solving a number of problems, lying in metallurgical, electrical engineering and many other planes. Having made sure that weld quality depends on welder's qualifications, E.O. Paton poses the task of developing a reliable process of welding with automatic machines.

In 1932 in the All-Ukrainian Academy of Sciences off-site sessions in Kharkov (at that time capital of Ukr. SSR) and in the cities of Donbass region, E.O. Paton made presentations to production teams and general public on the problems and advantages of welding production. His article «Paths of electric welding development during the Second Five-Year Plan period» was published in specialized journals and as individual brochures in Russian and Ukrainian. It gives a comprehensive analysis of the condition of

E.O. Paton among the participants of 1st All-Union Conference on submerged-arc welding (1940)

arc and resistance welding, proves the need for wide application of advanced technologies, sets forth the idea of the decisive role of welding mechanization and automation, and outlines the ways to solve the defined problems.

In 1933 the level of scientific work, which was performed by the laboratory led by E.O. Paton, already corresponded to the requirements for an academic institute. Establishment of such an institute was approved by the Presidium of the All-Ukrainian Academy of Sciences on January 3, 1934. In keeping with the government act the Institute was granted the official status of Electric Welding Institute (EWI), and E.O. Paton remained its director to the end of his life. He established the world's first specialized welding research institute, with a structure which ensures fast performance of the entire work cycle from scientific-technical idea and special research up to creation and introduction of technologies and equipment. Design Department continued designing apparatuses, feeding electrode wire with different coating systems. At the same time, the Institute intensively developed various processes for welding zone protection and weld quality improvement. Meanwhile, E.O. Paton continued designing welded structures and providing consultations for their production. In 1930 welding began to be used for manufacture of sugar plant equipment and seeders. In 1932 «Leninskaya Kuznitsa» plant in Kiev welded the first ship from the river ship series. In 1933 welding of steam boilers was mastered in «Krasny Kotelshchik» plant in Taganrog.

In 1935 EWI developed A-66 welding head, providing welding fire feed rate depending on arc voltage drop. By the end of 1930s Technology Department performed metallurgical investigations, developed the compositions of USSR's first fused fluxes, silicon-manganese wire and technology of high-speed semi-submerged arc welding of structural steel with bare wire.

In June 1940 single-pass automatic welding of a butt weld of 13 mm sheet at 30 m/h speed was demonstrated at a conference at EWI. The new welding process made a great impression on production specialists — it turned out to be 11 times more efficient that manual arc welding.

On December 20, 1940 an Act of the USSR Soviet of People's Commissars and CC of AUCP(b) on introduction of automatic submerged-arc welding during a six month period at 20 major plants of the country was published. E.O. Paton was appointed member of the Council on Machine-Building at USSR SPC; he was entrusted with fulfillment of this Act. At the same time he was charged with the functions of Head of Electric Welding Department at TsNIITMash (in Moscow), while remaining to be EWI Director. In January 1941 E.O. Paton's dream was implemented at V.M. Molotov Plant of Metal Structures — automatic welding of beams of span structure of a bridge across the Dnieper was set up. Evgeny Paton was awarded Stalin Prize of the first degree.

A.N. Kornienko, Dr. of Sci. (Hist.)

EFFECT OF THE SHAPE OF TUNGSTEN CARBIDE PARTICLES ON THEIR MICROHARDNESS, CHEMICAL HETEROGENEITY AND WEAR RESISTANCE OF THE COMPOSITE DEPOSITED METAL

A.P. ZHUDRA and **V.I. DZYKOVICH**

E.O. Paton Electric Welding Institute, NASU, Kiev, Ukraine

Results of investigations of spherical and non-spherical particles of tungsten carbides $WC-W_2C$ produced by the method of thermal centrifugal spraying are described. Chemical and energy-dispersive spectral analyses of the particles were carried out. Wear resistance of clad samples was investigated. It was shown that part of the non-spherical particles can be used for deposition of composite coatings.

Keywords: *tungsten carbides, thermal centrifugal spraying method, spherical particles, non-spherical particles, composite deposited metal*

In production of granulated tungsten carbide powders by different technologies [1] the finished material contains certain amounts of non-spherical particles, the presence of which leads to substantial deterioration of flowability of the powders. This violates stability of operation of feeding devices in plasma powder, laser and other cladding methods.

Table 1. Data of X-ray spectral microanalysis of different shapes of powder particles

Shape of particles	Content of elements, wt.%		
	C	Fe	W
Non-spherical	3.70	–	96.30
	13.24	0.60	86.16
	9.27	0.73	90
Spherical	4.85	–	95.14
	4.79	0.31	94.90
	4.93	0.10	94.97

The special vibration table was developed, which can be used to separate particles of the non-spherical shape from total mass of the granulated powders, as well as to produce powders with their much lower content [2]. However, even the vibration table fails to fully separate particles of the non-spherical shape.

The task of the authors was to investigate chemical heterogeneity of tungsten carbide particles of different shapes produced by the thermal centrifugal spraying method and effect of the non-spherical particles on wear resistance of the composite deposited metal.

Samples of tungsten carbide powders of spherical and non-spherical shapes (particle size composition — 100−250 μm) produced by the thermal centrifugal spraying method were taken for the investigations.

Chemical heterogeneity of different shapes of the tungsten carbide powder particles was studied by using scanning electron microscope CAM SCAN 4 with LINK ENERGY 2000 system (energy-dispersive analyser) [3]. Figure 1 shows distribution of tungsten, carbon and iron in the investigated particles, and Table 1 gives results of the elemental analysis conducted at different local points.

It should be noted that the point analysis may involve the probability of deposition of carbon on the
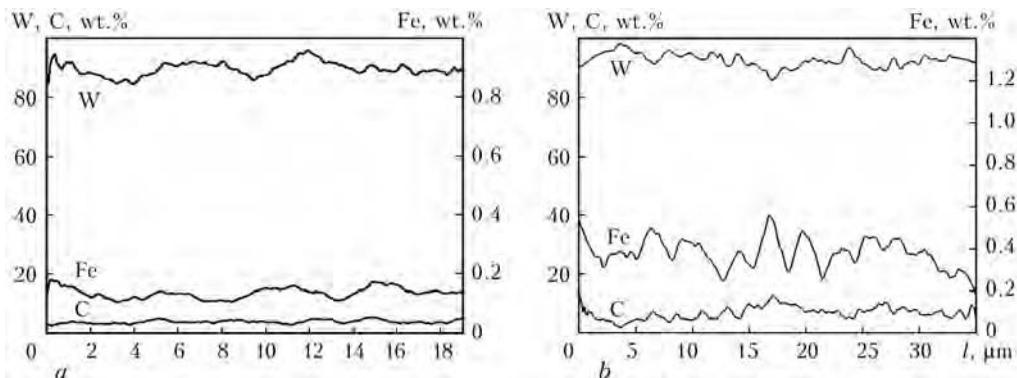
Figure 1. Curves of distribution of elements in non-spherical (*a*) and spherical (*b*) particles: *l* — length of a secant

Table 2. Content of carbon in particles and their microhardness

Shape of particles	Content of carbon, wt.%	HV100, MPa
Non-spherical	4.12	2764 ± 187
Spherical	3.96	2914 ± 254

Figure 2. Diagram of wear resistance (A) of samples clad with composite alloys with different contents of non-spherical tungsten carbide particles: 1 — 100 % of spherical particles; 2 — 80 % of spherical particles + 20 % of non-spherical particles; 3 — 50 % of spherical particles + 50 % of non-spherical particles; 4 — 100 % of non-spherical particles; 5 — 100 % of crushed tungsten carbide particles; 1–4 — powders produced by thermal centrifugal spraying

surface of a particle being investigated. In this case the carbon indicators become overstated. These results will be much more accurate if a bigger surface area of the particle is scanned. However, the data obtained in determining the carbon content by the chemical analysis method should be considered most reliable (Table 2).

The investigations showed that particles of the spherical shape have more consistent values in terms of chemical composition and microhardness. The St3 steel samples with a diameter of 10 mm and 20 mm long were clad to study wear resistance of the composite coatings produced by using the tungsten carbide powder as a wear-resistant component. Nickel silver of the MNMts60-20-20 grade was used as a binder alloy for all the samples. Cladding of the samples was performed in graphite crucibles by the plasma arc method. Three samples each with a different content of particles of the non-spherical shape were clad.

Wear resistance was investigated by using unit NK-M [4]. According to this procedure, the semi-fixed abrasive was applied to cause wear, the quartz sand being used as the abrasive. The samples of annealed steel 45 served as a reference. To compare, the tests were also conducted on the samples clad with crushed tungsten carbide.

As shown by the investigations results (Figure 2), wear resistance of the clad samples, the reinforcing phase of which contains up to 20 % of particles of the non-spherical shape, was only 10–12 % lower than that of the samples with the spherical reinforcing phase. Thus, some content of non-spherical particles in the composite deposited metal with the tungsten carbide-base reinforcing phase is quite tolerable.

Therefore, the tungsten carbide particles of the spherical shape produced by the thermal centrifugal spraying method have a more homogeneous chemical composition with regard to carbon and tungsten, while wear resistance of the clad samples, the reinforcing phase of which contains up to 20 % of the non-spherical particles, is only 10–12 % lower compared to the samples with the spherical reinforcing phase, which is acceptable for the composite deposited layers.

1. Dzykovich, V.I., Zhudra, A.P., Bely, A.I. (2010) Properties of tungsten carbide powders produced by different technologies. *The Paton Welding J.*, **4**, 22–24.
2. Bogatyreva, G.P., Ilnitskaya, G.D., Petasyuk, I.D. (2010) Increase in quality of tungsten carbide powders. Rock cutting and metal working tools: technique and technology of their production and application. In: *Transact of ISHM*, Issue 13.
3. Dzykovich, V.I. (2010) *Study and development of materials for wear-resistant hard-facing on the base of spheroidized granules of tungsten carbides*: Syn. of Thesis for Cand. of Techn. Sci. Degree. Kiev.
4. Yuzvenko, Yu.A., Gavrish, V.A., Marienko, V.I. (1979) Laboratory machines for estimation of wear resistance of deposited metal. In: *Theoretical and technological principles of surfacing*. Kiev: PWI.

THESIS FOR A SCIENTIFIC DEGREE

E.O. Paton Electric Welding Institute of the NAS of Ukraine

B.F. Stefaniv (PWI) defended thesis for Candidate degree in December, 22, 2011 on the subject «Development of cadmium-free brazing alloys and technology of brazing for mining extracting tool with diamond-hard-alloy plates».

The thesis is devoted to the problem of creation of cadmium-free brazing alloys based on the system Ag−Cu−Zn and creation of updated highly efficient rock-destroying tool for drilling wells for methane production.

The influence of tin within the range of concentrations of 3−10 wt.% on the structure, ranges of melting and chemical heterogeneity of alloy of the system Ag−Cu−Zn, the area of spreading of brazing alloys on hard-alloy plates and stainless steel as well as strength of brazed joints were determined. It was established that investigated brazing alloys with content of tin of up to 5 wt.% can be applied as a replacement of known cadmium brazing alloys for brazing of steels, but they can not be recommended for brazing of hard alloys.

The peculiarities of structure formation and properties of alloys of the system Ag−Cu−Zn−Sn in alloying by nickel and manganese were studied. Suggested are the compositions of brazing alloys, which according to their properties of wetting hard alloys and stainless steels are not inferior than the best cadmium brazing alloys, for example PSr-40, but considerably surpass them in relation of strength of brazed joints (up to 400−450 MPa).

The influence of palladium on the structure, ranges of fusion and chemical heterogeneity of alloy of the system Ag−Cu−Zn−Ni−Mn was investigated, area of spreading of brazing alloys on hard-alloy plates and stainless steel as well as strength of brazed joints was determined. It was established that palladium has a great influence on structure formation and properties of alloys of Ag−Cu−Zn−Ni−Mn system and at the content of 5 wt.% it increases strength properties of brazed joints from 250 to 350 MPa.

As a result of generalization of complex of tests the conclusion was made that the most perspective are the systems of brazing alloys Ag−Cu−Zn−Sn−Ni−Mn and Ag−Cu−Zn−Ni−Mn−Pd. The technical conditions on production of brazing alloys of the system Ag−Cu−Zn−Ni−Mn−Pd were composed. The obtained pilot batches were used for manufacturing of full-scale products.

Much attention was paid to evaluation of efficiency of diamond layer of diamond-hard-alloy cutters (DHAC) after heating for brazing by gouging of specified rock. It was shown that offered technology of DHAC brazing with cooling of diamond layer allows applying brazing alloys with temperature of brazing of more than 700 °C without losses of efficiency of the layer.

The technology of brazing of DHAC into a blade was created, according to which all cutters, as compared to known solutions, are brazing into a blade simultaneously. It excludes secondary heating of a cutter and decreases risk of degradation of diamond layer.

The modern technology for manufacturing of drill bits using DHAC and design of bits of domestic production (V.N. Bakul Institute for Superhard Materials of NASU) was developed. As a result of application of new technology the drifting on a bit increased from 80−120 to 400−500 m. This is a good result for mentioned DHAC, though it was considerably lower than values of foreign analogues.

The values of drifting at the level of foreign analogues (up to 2000 m) at transition to DHAC of foreign production and optimization of design of bits and calibrators were obtained. The corresponding patents were granted for the design of the last ones.

The technology of production of drill bits and calibrator developed in the E.O. Paton Electric Welding Institute was implemented for underground drilling of degasification wells at the A.F. Zasyadko Mine (Donetsk).

THESIS FOR A SCIENTIFIC DEGREE

E.O. Paton Electric Welding Institute of the NAS of Ukraine

I.S. Gakh (PWI) defended thesis for Candidate degree in December, 22, 2011 on the subject «Physical and technological peculiarities of electron beam welding of high-nickel heat-resistant alloys with a single-crystalline structure».

The thesis is devoted to the solution of the problem of producing of permanent joints of single crystals of heat-resistant nickel alloys at repair of working blades of GTE and enlargement of single crystals.

The state-of-the-art of the problem of weldability of heat-resistant nickel alloys was considered and reasonability of work fulfillment was grounded. The criteria of quality of welded joints were determined and methods for control of weldability of this class of material were determined. It was offered to consider the weldability of single crystals from the point of view degradation degree of perfection of single-crystalline structure.

The peculiarities of formation of structure of welded joint depending on crystallographic conditions on the front of pool crystallization and technological parameters of EBW process were studied. The regularities were established which are used during control of structure formation of weld metal.

It is shown that crack formation in weld can be prevented at welding speed of 10−15 m/h; preheating up to 350−450 °C allows its increase up to 20−25 m/h. The influence of location of weld pool relatively to crystallography of substrate on formation of random orientation grains was found. The favorable crystallographic conditions of weld metal formation with single-crystalline structure were determined. It was shown that during joining, when the surface of fusion is close to the plane {111}, a number of grains of random orientation in a weld can reach 80 %. At the surface of fusion {100} and direction of welding <001>, the number of grains of random orientation is decreased down to 5−10 %, and during fusion {100} in direction <011> — to 2−4 %.

The orientation conditions of weld pool solidification were determined, at which the formation of single-crystalline welded joint is achieved. It was established that producing of single-crystalline welded joint is achieved at coincidence of direction of maximal temperature gradient with direction of easy growth d along the front of pool crystallization with disorientation of not more than 15°.

The scheme of adaptation of shape of a pool to crystallographic orientation of welded joint is presented. The conditions of welding and modes of their performance, which allow controlling of solidification of weld pool both in welding as well as in surfacing of filler material, were grounded and proposed.

The principal problems of welding of heat-resistant nickel single crystals were solved, which exclude probability of formation of grains of random orientation in the structure of weld metal and cracks. It was shown that level of long-time strength at 900 °C is $\sigma_{50} \geq 300$ MPa which remains 85 % of this value for the base metal. The tensile and yield strengths within the range of temperatures of 500−1000 °C are at the level of values for the base metal.

The principal technology of repair EBW of working blades of JS32 alloy for GTE D18T was developed.

SUBSCRIPTION
FOR «THE PATON WELDING JOURNAL»

If You are interested in making subscription directly via Editorial Board, fill, please, the coupon and send application by fax or e-mail.

The cost of annual subscription via Editorial Board is $324.

Telephones and faxes of Editorial Board of «The Paton Welding Journal»:

Tel.: (38044) 200 82 77, 200 81 45

Fax: (38044) 200 82 77, 200 81 45.

«The Paton Welding Journal» can be also subscribed worldwide from catalogues of subscription agency EBSO.

Subscription to the electronic version of «The Paton Welding Journal» can be done at site: *www: rucont.ru*

РУКОНТ
национальный цифровой ресурс

We offer for the subscription all issues of the Journal in pdf format, starting from 2009. You can subscribe to individual issues or to the entire archive including all issues over a period of 2009–2011. The subscription is available for natural persons and legal entities.

ADVERTISEMENT
IN «THE PATON WELDING JOURNAL»